# Alma Mater Studiorum - Università di Bologna

## DOTTORATO DI RICERCA IN CHIMICA

### Ciclo XXVI

Settore Concorsuale di afferenza: 03/C2

Settore Scientifico disciplinare: CHIM04

## Development of innovative catalysts for the hydrodechlorination to fluoroethers

Presentata da:   **Manuel Gregori**

Coordinatore Dottorato

**Prof. Aldo Roda**

Relatore

**Dott.ssa Stefania Albonetti**

Correlatori

**Prof. Giuseppe Fornasari**

**Dott. Stefano Millefanti**

**Esame finale anno 2014**

Hydrodechlorination

Ruthenium

Palladium

Copper

Activated carbon

MCM

# Summary

# Abstract

In this work the hydrodechlorination of $CF_3OCFClCF_2Cl$ to produce unsaturated $CF_3OCF=CF_2$ was studied over a series of supported metal catalysts. Currently this molecule is produced from the precursor $CF_3OCFClCF_2Cl$ by dechlorination with zinc powder. An important cost on the economic and environmental balance is represents by the large amount of $ZnCl_2$ produced and to be disposed of. A new approach, based on gas-phase hydrodechlorination over supported catalysts can lead to a new sustainable process.

During the feasibility step of this project, substantially two kind of materials were studied: metals supported over activated carbon and Pd/Cu species supported over MCM-41 mesoporous silica.

Observed catalytic performances were strongly dependent on the metal and support used.

All carbon-supported Ru, Pd, and bimetallic catalysts are fairly active and yielded the target product $CF_3OCF=CF_2$, the higher selectivity being obtained with ruthenium- and palladium-based materials. Nevertheless, Ru-based catalysts showed poor stability and this deactivation may be attributed to the deposition of chlorinated organic species blocking the active sites. On the other hand, palladium-containing catalysts showed high stability. Ru/Pd and Pd/Cu bimetallic catalysts exhibited long-term selectivity and stability, highlighting the possibility for these materials to be employed in the $CF_3OCF=CF_2$ production process.

During the second part of this thesis, a series of bimetallic meso-structured Pd/Cu MCM-41 catalysts were studies to overcome possible mass transfer limitations. The materials were obtained by different synthesis methods. The incorporation of Pd and Cu during MCM-41 synthesis, did not destroy the typical hexagonal array and ordered pore system of MCM-41. However, the calcination for the removal of the template provoked significant segregation of oxides. The impregnation leads to pore-occlusion and formation of Cu particles and large bimetallic PdCu species. Larger metal particles leads to lower $CF_3OCFClCF_2Cl$ conversion, while the monometallic particles can decrease the selectivity to $CF_3OCF=CF_2$, fostering the dehalogenation to $CF_3OCH=CF_2$.

# Chapter 1

## 1   Aim of the work

The environmental sustainability of industrial production is a growth engine for develop new plant technologies and substitute old processes introducing a new production philosophies, focused on the optimum use of all the available chemicals, maximizing the process efficiency but taking into strongly account the intrinsic hazards of the used chemicals.

One of the acts of awareness historically higher in the impact to the chemical manufacturing was certainly to be considered as the Vienna Convention for the Protection of the Ozone Layer and thus, the consequent Montreal Protocol. Indeed, after a period of great development and application of these organic compounds containing chlorine, fluorine and bromine, known by various commercial brands and with an extremely high worldwide production, the proven harmful effects on the stratospheric ozone layer of these compounds imposed their elimination. The huge amount of CFCs produced up to 1995 in the world (240.000 ton/year) represent a strong impetus to chemical research aimed at destruction, substitution and transformation of these molecules and the conversion of the systems and technologies dedicated to the production and use of these chemical compounds. In this area has assumed growing importance the reaction of hydrodechlorination of chlorofluorocarbons, in particular directed to the production of unsaturated fluorinated hydrocarbons that show interesting characteristics for the production of polymers with specific properties of mechanical strength, thermal and chemical resistance.

Within our collaboration with SOLVAY SPECIALTY POLYMERS ITALY, the desire to transfer the knowledge, developed on the CFCs hydrodechlorination reaction, leads to this investigation focused on the study of innovative catalysts for the production of perfluoromethylvinyl ether (indicated by the abbreviation MVE) according to the reaction:

$$CF_3OCFClCF_2Cl + H_2 \rightarrow CF_3OCF=CF_2 + 2HCl$$
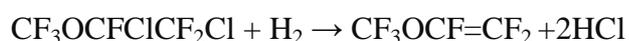
Currently the trifluoromethyltrifluorovinyl ether ($CF_3OCF=CF_2$) commercial production process, based on $CF_3OCFClCF_2Cl$ precursor dechlorination, is carried out using the

## 1. Aim of the work

reprotoxic dimethylformamide as solvent and stoichometric amount of Zn, produces large quantities of by-products such as $ZnCl_2$ and exhausted solvent, resulting in a significant cost to be calculated in the economic and environmental balance. A new approach, investigated into this work, based on $H_2$-assisted gas-phase dechlorination over metal-supported catalysts, may lead to a new sustainable process, where the unique stoichometric co-product, hydrogen chloride, could be reused on chlorination processes.

Specifically, the work was carried out according to the points:
• Preparation and characterization of noble metals-based carbon supported catalysts.
• Survey of the catalytic performance.
• Study of the deactivation phenomena.
• Optimization of the synthesis of mesoporous support MCM-41.
• Preparation and characterization of PdCu/MCM-41 catalysts.
• Test in the hydrodechlorination reaction of PdCu/MCM-41 catalysts.

Finally, the success in the catalyst design for the hydrodechlorination of $CF_3OCFClCF_2Cl$ (ADM) led to the filing of patent and publications, in addition to the scale-up of the industrial plant nowadays in progress.

2

# Chapter 2

## 2 Introduction

### 2.1 Fluoropolymers

Since their discovery, sixty years ago, fluorinated polymers are still in growing, providing solutions and new possibilities to an incredible various areas of technology such as energy storage and transformation, optical data transmission in addition to the best-known application as coating, piping, membrane, wire and cable, thanks to their crucial, outstanding and flexible properties. Despite of the lucky laboratory observation which evidenced the first sample of this new family of materials (PTFE), nowadays, the valuable answers to several industrial and technological requests come from difficult tasks of optimization and formulation of these polymers, where the presence of fluorine confers unique properties. Indeed, as well as the physical and chemical properties of organic compounds are strongly affected by the introduction of fluorine, the basic characteristics of this nobel gas and of the carbon-fluorine bond could be considered as a guidelines to understand the unique combination of properties of this class of polymers [1].

First of all, fluorine atoms form the strongest bond among all the single bonds involving carbon. The C-F bond has high ionic character and is strongly polarized by the most electronegative element, but has extremely low degree of polarizability. These evidences are directly connected to the weak intermolecular forces between fluorinated molecules responsible of the reduced cohesive energy of the materials.

Moreover, fluorine has not only the higher value of electronegativity, but has a relatively small size. These properties ensure the absence of steric problems leading to a possible total substitution of hydrogen in a molecule, and taking into account this, is clearly intelligible how the outstanding chemical resistance evidenced by highly fluorinated organic molecule is due to a protective shield of fluorine atoms over the carbon skeleton.

The stiffness of the fluorine containing molecule was due to an extended repulsive forces between fluorine atoms and fluorinated groups, which increase rotational energy around carbon-carbon bonds.

## 2. Introduction

Furthermore, because of its small size, fluorine can be added to replace hydrogen in a preformed polymer crystal framework, resulting in the formation of many structurally disordered polymers and copolymers of fluoroethylenes, even with random stereochemistry.

Nevertheless, the research in this field is still very much present, because this unique combination of properties leads to advantageous and disadvantageous behaviors. As above mentioned, the first and more pleasing properties are related to the chemical and thermal stability. Furthermore, in front of highly technological requests, this class of materials are excellent in providing dielectric characteristics, particularly low refractive index, UV resistance, flame resistance, solvent resistance and also low coefficient of friction, good lubricant and releasing characteristics and oleo- and hydro-phobicity.

However, the very weak cohesive energy hits some physico-mechanical properties of highly fluorinated materials, leading to a limitation in their creep resistance, strength, and dimensional stability. Obviously, these disadvantages reached the maximum negative effect when the fluorination degree of materials is high or total, in fact, an excellent example of this is the PTFE, which since his application has been subjected to changes that could make it more workable and melt processable.

The pathway taken in the innovation of fluorinated polymers, introducing partially or totally non-fluorinated monomers has on the one hand improved some properties of the final polymer, in particular the physico-mechanical properties, thanks to the interactions increased between C-H and C-F bonds and groups. On the other hand the presence of bonds C-H has reduced some of the properties about chemical and thermal stability of the final material. For this reason, the development and formulation of various fluorinated polymers are strongly influenced by the purpose of use, and are evolving along with the emerging technologies, leading to a large number of products with apparently identical constituent monomers, but radically different in terms of final properties.

As above mentioned, since his development, PTFE was subjected to changes in order to improve the processability of these highly fluorinated materials. The behavior sought, led to the definition of a family of thermoplastic fluoropolymers [2].

Within this family, the use of perfluorovinylethers, has assumed more and more importance allowing to "break" the polymer cristallinity, improving the melt-processability of the materials. Obviously, the modification investigated are numerous, in fact, some are fully fluorinated polymers, obtained by copolymerizing tetrafluoethylene with small amounts of some other perfluorinated monomer; some are homopolymers of other fluoro-

4

olefins, while others are copolymers of a fluoro-olefin with ethylene. However, as a class these materials display some common characteristics, namely thermal and chemical stability, solvent resistance, flame resistance, dielectric properties, surface properties, which are of critical value in the very numerous application sectors.

## 2.2   Survey of hydrodechlorination technologies

Since its introduction, the Montreal Protocol has represented and still represent a strong motivation for the enactment of legislation on substances harmful to the ozone layer. Obviously, all the positive results in terms of greenhouse gas emissions have been achieved thanks to the development of methodologies for the management and disposal of CFCs, HCFCs and HFCs.

The treatment technologies for these substances are divided into two categories: conversion and destruction. The conversion is a treatment aimed at the transformation of these compounds in others with lower environmental impact and in several cases products of industrial interest. Among the treatments of conversion, what is more applied in the industrial field is definitely the hydro-dehalogenation reaction that allows the removal of the halogens, with production of hydrogen halide and formation of hydrocarbons (fluorocarbons or other molecules of industrial interest).

On the other hand, the treatments of destruction consist in a conversion of the chlorofluorocarbons compounds in hydrogen halide and $CO_2$. The developed technologies for this purpose consist in :

1 . Irradiation with UV rays , $\gamma$ and ultrasound;

2 . Oxidation with supercritical $H_2O$;

3 . Heat treatment such as incineration and pyrolysis;

4 . Catalytic destruction.

Nowadays the used methodology is the destruction by heat, while the other technologies are still under study. From an industrial point of view, the treatments of incineration are conducted at high temperatures in the presence of oxygen, maintaining condition of extremely high pressure due to the flame inhibition properties of CFCs.

## 2. Introduction

This type of technology is designed to be resistant to the corrosive phenomena, caused by the presence of hydrogen halides and elemental halogen formed during the treatment, in addition to the produced $CO_2$.

Furthermore, a valid alternative to incineration, consists in the pyrolysis treatment using high temperature plasma (between 10000 and 30000 K). The Ar-plasma is formed by monovalent ions of argon accelerated by a high frequency electric field, where the CFCs are transported with the aid of an oxidizing gas such as oxygen or water steam. The use of the latter allows minimizing the formation of secondary products such as $CF_4$ and $CF_3Cl$, which are characterized by particularly high values of half-lives.

However, it must be remarked that both technologies are proposed as energy- consuming , in the sense that use large amounts of energy for their operation [3].

In fact, the biggest problem in the technologies of destruction is the energy consumption related to the high temperatures required. On the other hand, considering the conversion technologies, the problem is on the effectiveness of the conversion, which can be improved by implementing the use of a catalyst. Obviously, the development of a catalytic system capable of ensuring high catalytic performance, resistance to deactivation and to the aggressive conditions of the reaction environment, is not an easy task.

The process most commonly used today consists in a catalytic oxidation of CFCs, in the presence a catalyst of the type $BPO_4$, $PO_4$-$ZrO_4$, $V_2O_5$ and $W_2O_5$, which show high catalytic activity, even if affected by deactivation phenomena.

### 2.2.1 Hydrodechlorination reaction

Regarding the techniques of conversion, is certainly one of the most important the hydrodechlorination reaction, which provides the possibility of converting a CFC compounds into a dechlorinated compounds and hydrogen chloride, less dangerous for the environment and of strong industrial interest [3]. The products that are usually achieved by these processes are HFC and unsaturated fluorocarbons: the first compounds are not harmful to the ozone layer because is completely dechlorinated (lack of radical initiator), while fluorinated olefins are used as monomers for the synthesis of highly technological fluoropolymers.

In the process of dechlorination, the halogenated substrates react with a hydrogen donor, generally $H_2$, forming a mixture of hydrocarbons, halogenated organic substances and hydrogen halide. Chlorine atoms contained in the molecule are extracted and replaced by hydrogen, leading to the formation of HCl [4].

6

The dehalogenation reaction is selective for the chlorine atoms because the energy of C-Cl bond is lower than the C-F bond, with the result that the fluorine atoms are not involved in this mechanism, if not in negligible percentages. The values of the energy of C-F bond in CFCs ranging from 500 to 540 KJ/mol, while the values for the C-Cl bond in the same molecule are reported to be around 320 KJ/mol.

The hydrodechlorination reaction is generally carried out at temperatures between 200 and 300°C [5] and allows to obtain mixtures of compounds in which the chlorine has been eliminated (unsaturated) or substituted by hydrogen. The use of suitable catalysts allows to obtain significant yields even at moderate temperatures, with high selectivity to the products of interest. The choice of the active phase plays an important role in obtaining mixtures of mono-and poly - hydrogenated compounds. Indeed, studies performed until now have identified as best catalyst's active phase all metals of VIII transition group having the best activity and selectivity. In particular Pd finds great applicability thanks to its Cl/H exchange high selectivity and to its good resistance to deactivation induced by acids produced by the reaction [6]. Other metals, such as Pt, Ni, Ru and Rh, showed interesting catalytic properties due to their ability in promote adsorption of hydrogen for homolytic rupture of the covalent bond; however what is not still clear is the interaction mechanism between the active phase and halogenated substrates [7].

### 2.2.1.1 *Hydrodechlorination to unsaturated product*

As above mentioned, the hydrodechlorination reaction is one of the processes of CFCs conversion, most interesting when products of commercial interest such as olefins are generated, also because they are particularly used in the production of polymeric fluorinated materials.

The formation of an unsaturated fluorinated product involves the removal of two chlorine atoms bound on two adjacent carbon atoms, with subsequent formation of a double bond and hydrogen chloride [8]. However, the reaction cannot be completely selective towards the removal of chlorine and therefore could be formed several defluorinated compounds through the elimination of HF.

The typical reaction of hydrodechlorination is the following:

$$R_1\text{-CFCl-CFCl-}R_2 + H_2 \rightarrow R_1\text{-CF=CF-}R_2 + 2HCl$$
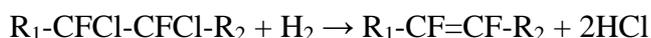
## 2. Introduction

Usually in this type of processes a secondary reactions producing partially hydrogenated by-products can occur, by substitution of one or more chlorine atoms, to give a mixture of various saturated or unsaturated compounds. The key factors that contribute to the formation of the expected product with high selectivity could be summarized as the operative conditions, the relationship between the reagents fed and the type of catalyst used. The catalysts which contain metals with a high affinity for hydrogen, show high catalytic activity and at the same time a propensity toward hydrogenated products. As example platinum atoms, as found in literature, have a great affinity with $H_2$ in gas-phase (as well as the Rh, although in lesser amount), which makes it very active in the hydrodechlorination, especially for the formation of molecules totally dechlorinated (saturated). On the other hand, ruthenium shows a significant activity towards reactions that lead to unsaturated fluorinated molecules, at the same time it's possible incurring in deactivation phenomena, due to the formation of oligomers on the catalyst surface [9]. Nickel shows a good selectivity for the reaction of hydrodechlorination with formation of unsaturated molecules, but the activity is much lower than Pt or Pd-based catalysts, if not mantaining temperatures above 300°C and higher $H_2$/CFC molar ratio with respect to the noble metals containing catalysts.

In literature, mixed catalysts containing Pd and Ni which have shown a good activity toward unsaturated products mono-substituted (R-CF=CFH) have been reported [10]. Moreover, catalysts containing Ni and P, in the form of $Ni_2P$ , $Ni_3P$ and $Ni_{12}P_5$, have shown good catalytic results at moderate temperatures (200°C), with conversion values around 65%, with the possibilities of reaching values around 95% by increasing the operating temperature (300°C). These mixed systems, show a greater catalytic activity than the monometallic catalysts, caused by a higher affinity toward the hydrogen molecule [11].

### *2.2.1.2 Reaction behaviors*

The hydrodechlorination reaction is generally carried out at temperatures between 200 and 300°C at atmospheric pressure. The literature shows several assumptions concerning the reaction mechanism. According to the proposed mechanism, the reaction of hydrodechlorination is composed of two stages: the first step is the CFCs molecule adsorption on the surface through C-Cl bond cleavage, resulting in the formation of metal-carbon and metal-chlorine bonds. These species, chemically bound to the active phase, react with the activated hydrogen chemisorbed on the catalyst surface, with the formation of a hydrofluorocarbon and HCl (Figure 1).

8

The by-products formation depends on the speed ratio between the dehalogenation and the hydrogenolysis reaction [8].

In fact, at the beginning a molecule will be adsorbed on the surface due to one C-Cl bond cleavage (with formation M-C bond) and subsequently the intermediate can react with activated hydrogen on the catalyst surface, forming a Cl/H mono-substituted product, or in the case of a second C-Cl bond cleavage, a carbene complex. The Cl/H mono-substituted product is obtained when the hydrogenolysis speed is greater than the C-Cl cleavage speed. On the contrary, the formation of poly-hydrogenated species could indicate a strong interaction between active sites and intermediates, making a hydrogenolysis reaction necessary for breaking the M-C formed bonds [7].

In the case of a reaction that favors the formation of fluorinated unsaturated molecules, the mechanism provides an adsorption of CFC through two carbon atoms: the desorption of the molecule of interest is no longer due to hydrogenolysis, but to a rearrangement of the substrate, with double bond formation. The hydrogen adsorbed in this case has only the function of eliminating the halogen from the surface through the formation of the corresponding hydrogen halide [7].
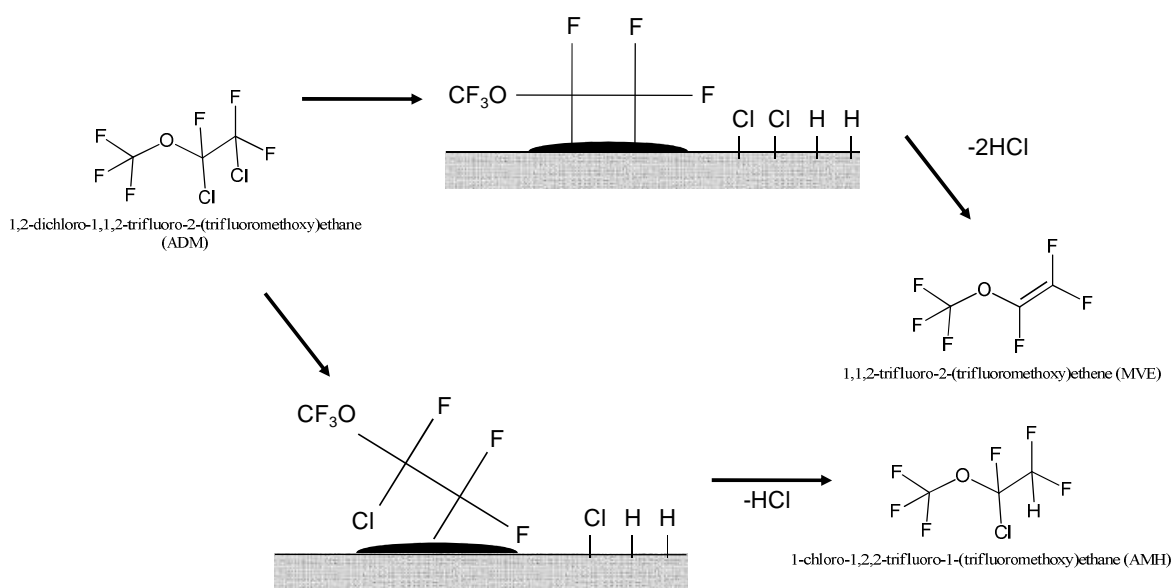


*Figure 1. Different intermediates formed during the gas-phase hydrogen-assisted dechlorination.*

According to the theories developed, the completely hydrogenated products are formed by consecutive extractions of chlorine atoms from the substrate, with the formation of carbine-like intermediates, which are then hydrogenated.

## 2. Introduction

As previously expressed, nowadays the trifluoromethyltrifluorovinyl ether ($CF_3OCF=CF_2$) commercial production process, based on $CF_3OCFClCF_2Cl$ precursor dechlorination [12], is carried out using the reprotoxic dimethylformamide as solvent and stoichometric amount of Zn, produces large quantities of co-products such as $ZnCl_2$ and exhausted solvent, resulting in a significant cost to be calculated in the economic and environmental balance. With the aim of investigating a new approach, the starting point of this work will be to design a metal-supported catalysts for the $H_2$-assisted gas-phase dechlorination, leading to a new sustainable process, with HCl as unique co-product [13].

## References

[1] D. Sianesi, *La Chimica e l'Industria* **79** (1997) 17-21.

[2] G.G. Hougan, P.E. Cassidy, K. Johns, T. Davidson, *Fluoropolymers 1: Synthesis, (Topics in Applied Chemistry)*, **1**, Springer, 1999.

[3] H. Yu, E.M. Kennedy, A.A. Adesina, B.Z. Dlugogorski, *Cat. Surf. From Asia* **10** (2006) 40-54.

[4] T. Mori, J. Kubo, Y. Morikawa, *Appl. Cat. A: General* **271** (2004) 69-76.

[5] E.J. Shin, A. Spiller, G. Tavolaris, M. A. Keane, *Phys. Chem. Chem. Phys* **1** (1999) 3173-3181.

[6] A. Weirsma, A.T. Cate, E.J.A.X. Van de Sandt, M. Makkee, *Ind. Eng. Chem. Res.* **44** (2007) 4158-4165.

[7] T. Mori, T. Yasuoka, Y. Morikawa, *Cat. Today* **88** (2004) 111-120.

[8] C. Baird, *Chimica Ambientale*, Zanichelli, **1997**.

[9] V. I. Avdeev, V. I. Kovalchuk, G. M. Zhidomirov, J. L. d'Itri, *J. Struct. Chem.* **48** (2007) S171-S180.

[10] A. Srebowata, W. Juszczyk, Z. Kaszkur, K. Karpinski, *Cat. Today* **124** (2007) 28-35.

[11] X. Liu, J. Chen, J. Zhang, *Ind. Eng. Chem. Res.* **47** (2008) 5362-5368.

[12] V. Tortelli, P. Calini, A. Zompatori, E. Antenucci, **US Patent 203368** (2007) assigned to Solvay Solexis Spa [IT/IT].

[13] M. Gregori, G. Fornasari, G. Marchionni, V. Tortelli, S. Millefanti, S. Albonetti, *Appl. Catal. A: General* **470** (2014) 123-131.

# Chapter 3

## 3 Materials and Methods

### 3.1 Activated carbon supported catalysts

Activated carbon is an industrially well-known name for a class of carbonaceous products derived from procedures of oxidation, carbonization or pyrolysis of various materials. Mainly applied in the impurities removal treatment for gases and liquids, activated carbons are especially suitable because of their high surface area and high adsorptive properties (Table 1). In fact, the surface of activated carbons can trap impurities through physical van der Walls interactions, and the presence of a high surface area can be directly related with a high adsorptive power [1].

| | Impregnation | | |
|---|---|---|---|
| Chemicals | Quantity, wt% | Activated carbon[a] | Examples for applications |
| Sulfuric acid | 2–25 | F 1–4 mm Ø | ammonia, amine, mercury |
| Phosphoric acid | 10–30 | F 1–4 mm Ø | ammonia, amine |
| Potassium carbonate | 10–20 | F 1–4 mm Ø | acid gases (HCl, HF, $SO_2$, $H_2S$, $NO_2$), carbon disulfide |
| Iron oxide | 10 | F 1–4 mm Ø | $H_2S$, thiols, COS |
| Potassium iodide | 1–5 | F 1–4 mm Ø | $H_2S$, $PH_3$, Hg, $AsH_3$, radioactive gases/radioactive methyl iodide |
| Triethylenediamine | 2–5 | F 1–2 mm Ø<br>G 6–16 mesh | radioactive gases/radioactive methyl iodide |
| Sulfur | 10–20 | F 1–4 mm Ø, G | mercury |
| Potassium permanganate | 5 | F 3 + 4 mm Ø | $H_2S$ from oxygen-lacking gases |
| Manganese IV oxide | | G 6–16 mesh | aldehyde |
| Silver | 0.1–3 | F 3 + 4 mm Ø | F: phosphine, arsine |
| | 0.05–0.4 | G 8–30 mesh | G: domestic drinking water filters (oligodynamic effect) |
| Zinc oxide | 10 | F 1–4 mm Ø | hydrogen cyanide |
| Chromium–copper–silver molybdenum salts | 10–20 | F 0.8–3 mm Ø | civil and military gas protection |
| | | G 12–30 mesh | phosgene, chlorine, arsine |
| | | G 6–16 mesh | chloropicrin, sarin, and other nerve gases |
| Mercury (II) chloride | 10–15 | F 3 + 4 mm Ø | vinyl chloride synthesis, vinyl fluoride synthesis |
| Zinc acetate | 15–25 | f 3 + 4 mm Ø | vinyl acetate synthesis |
| Noble metals | 0.5–1.0 | F, G, P | organic synthesis, hydrogenation |
| (palladium, platinum) | 0.5 | G 2–5 mm | purification of terephthalic acid |

[a]F = pelletized activated carbon, G = granulated activated carbon, P = powdered activated carbon, Ø = pellet diameter.

*Table 1. Summary of the major industrial applications of activated carbon [2].*

Thanks to their excellent performance in purification purpose, world demand for activated carbon will rise around 10% annually, especially considering the biggest growing markets of China and India, where the factory emissions should be checked more frequently. On the Table 2 are reported the main fields of use, and their evolution in the last decade [3].

## 3. Materials and Methods

| US ACTIVATED CARBON DEMAND (million pounds) | | | | | |
| --- | --- | --- | --- | --- | --- |
| | | | | % Annual Growth | |
| Item | 2004 | 2009 | 2014 | 2004-2009 | 2009-2014 |
| Activated Carbon Demand | 430 | 565 | 1175 | 5.6 | 15.8 |
|    Liquid Phase Applications | 328 | 360 | 505 | 1.9 | 7.0 |
|    Gas Phase Applications: | 102 | 205 | 670 | 15.0 | 26.7 |
|       Industrial Air Purification | 39 | 150 | 585 | 30.9 | 31.3 |
|       Motor Vehicles | 34 | 20 | 44 | -10.1 | 17.1 |
|       Other Gas Phase | 29 | 35 | 41 | 3.8 | 3.2 |

*Table 2. Activated carbon demand, estimated by a statistic US agency [3].*

The chemistry of adsorption phenomena over activated carbons can be simplified by considering several factors:

- the graphitic cross-linked structure gives to the activated carbons an irregular porous structure.

- the kinetics of adsorption can be dramatically affected by pore size distribution.

- the outer layer of carbon atoms contains unsaturated groups, which are important sites for chemical adsorption.

- the activation process governs the final porosity of carbons by clearing the pores from disorganized carbons and by producing surface groups containing oxygen, hydrogen, nitrogen and sulfur.

- likewise, through the residual non-graphitizable carbons content, the activation process governs the surface propensity for oxygen chemisorptions and then the surface oxidation.

- the surface degree of oxidation, is influenced by activation process, raw materials and ash content. It can be generally associated with functional groups (carboxyl, carbonyl, phenolic and quinonic) leading to an amphoteric character in aqueous solution.

- The ash content depends on the raw materials and, its components (calcium, magnesium, iron, potassium, sodium, zinc, lead, tin, copper, vanadium, etc.) may change adsorption process modifying the interaction of activated carbons with the molecules to be removed.

The use of activated carbons is specially diffused, by considering the catalytic purpose, when is necessary a significant resistance to the aggressiveness of reaction conditions, and when is required an extremely high specific surface area.

On the other hand, the great surface area and microporosity showed, can significantly limit uses of the activated carbons, to gas-phase reactions that involve small molecules and in the case of liquid-phase reaction, to low-viscosity operative conditions.

Obviously, the introduction of the active phase, which is generally constituted by noble metals, is performed by incipient or wet impregnation methods and by ion-exchange depositions.

**Catalysts Preparation**

In this work, ruthenium, palladium, palladium/ruthenium, palladium/gold, palladium/silver and palladium/copper catalysts with different metal content were prepared by incipient wetness impregnation ($RuCl_3$, $PdCl_2$, $HAuCl_4$, $AgNO_3$ and $CuCl_2$ supplied by Sigma-Aldrich) using activated carbon (surface area 1320 $m^2/g$) as support. Catalysts were dried overnight at 120°C, then activated with pure $H_2$ at 330°C for 1 h.

## 3.2   Mesoporous silicate MCM-41

The mesoporous silicate MCM-41, certainly the best known member of the molecular sieve family M41S, was first discovered and reported at the beginning of the nineties, following (but also encouraging) a strong development in the field of the self-assembled microstructure serving as a structure-directive agents. Indeed, the extremely high surface areas and the precise tuning of pore sizes achievable have focused the interest of the researchers in this field, leading to a great number of publications about synthesis, catalytic properties and innovative applications which are related to the their structure [4].

With the aim of exploiting the particular structural and morphological properties, a large number of investigation were proposed about the inclusion of dopants, partly shown in Table 3. The great number of studied systems also has evidenced that other mesoporous ordered oxides were found to be possible for such metals as Sb, Fe, Zn, Pb, W and Mo. However, most mesophase not yield porous materials and collapse when the template is removed, both by conventional heating and ion exchange.

The interest in doping the MCM-41 with other metals primarily comes from the intention of conferring catalytic properties to this highly ordered structure, but despite of the relevant

number of possible mechanism proposed, the amount of the incorporation, the reproduction of the mesophase, the stability of the prepared structure and the shape of the mesoporous phase frequently cannot be predicted. On the other hand, it must be remarked that, into the first publication reported by the Mobil researcher, the mesophase MCM-41 has been considered in order to introduce dopants (in that case aluminium) [5]. The huge amount of publications in this field represents the direct consequence to the great synthetic flexibility of these materials, in addition to the appreciable fine-tuning possibilities.

| Authors | Metal dopant | Si/dopant molar ratio | Synthesis route[a] |
|---|---|---|---|
| Beck et al.[1b] | Al | 15 | $S^+I^-$ |
| Corma et al.[41] | Ti | 56 | $S^+I^-$ |
| Reddy et al.[42] | V | 60 | $S^+I^-$ |
| Tanev et al.[43] | Ti | 100[b] | $S^0I^0$ |
| Sayari et al.[44] | B | 6.25[b] | $S^+I^-$ |
| Luan et al.[45] | Al | 10 | $S^+I^-$ |
| Fu et al.[46] | Al | ≈ 1[b] | $S^+I^-$ |
| Zhao, Goldfarb[47] | Mn | 11 | $S^+I^-$ |
| Abdel-Fattah, Pinnavaia[48] | Sn | 99 | $S^0I^0$ |
| Cheng et al.[49] | Ga | 30 | $S^+I^-$ |
| Cheng, Klinowski[50] | Ga, Al | 57, 57 | $S^+I^-$ |
| Koyano, Tatsumi[51] | Ti | 80 | $S^+I^-$ (MCM-48) |
| Tuel, Gontier[52] | Al | 6 | $S^0I^0$ |
| | Ga | 31 | $S^0I^0$ |
| | Fe | 55 | $S^0I^0$ |
| | B | 17 | $S^0I^0$ |
| Tuel et al.[53] | Zr | 17 | $S^0I^0$ |
| Ulagappan, Rao[54] | Cr | 30[b] | $S^+I^-$ |
| Zhang, Pinnavaia[55] | Ti | 50[b] | $S^+I^-$ (MCM-48) |
| | Cr | 50[b] | $S^+I^-$ (MCM-48) |
| | V | 50[b] | $S^+I^-$ (MCM-48) |
| Zhang et al.[56] | Ti | 277, 76 | $S^+X^-I^+$, $S^0I^0$ |
| | V | 434, 131 | $S^+X^-I^+$, $S^0I^0$ |
| | Cr | 163, 70 | $S^+X^-I^+$, $S^0I^0$ |
| | Mn | 3332, 118 | $S^+X^-I^+$, $S^0I^0$ |
| | Mo | 95, 199 | $S^+X^-I^+$, $S^0I^0$ |
| Echchahed et al.[57] | Fe | 40 | $S^+I^-$ (MCM-48) |
| He et al.[58] | Fe | 52 | $S^0I^0$ |
| Jones et al.[59] | Zr | 25 | $S^+I^-$ |
| Zhang, Ying[60] | Nb | 10 | $S^+I^-$ |
| Wong et al.[61] | Zr | 5 | $S^+X^-I^+$ |

[a] MCM-41 structure, unless otherwise noted. [b] Molar ratio values of precursor mixture, not of calcined materials.

*Table 3. Authors and the reported elements introduced into the silica framework, following the suggested synthesis route [4].*

### 3.2.1 Proposed formation mechanism

*LCT mechanism:* Following the similarity between lyotropic phases and the M41S family of mesoporous molecular sieve, the Mobil researchers proposed "a liquid crystal templating mechanism" based on two possible mechanistic pathways of synthesis (Figure

1). The first one, postulated that the silicate precursors (or other dopants precursors) occupied the space between a previously formed hexagonal array, deposing on the micellar rods. Indeed, this liquid crystal phase denoted as LC, is typical for the lyotropic phases.

On the other hand, in the second proposed mechanism, the inorganic precursors interact with the template, favoring the formation of the hexagonal arrangement. However, no explanation of this role of the inorganic precursors was suggested. Taking into account the synthesis conditions in terms of pH (high pH value was proposed) the organic template could be considered as a positive center, interacting with the inorganic precursors which finally condense into a solid, and the obtained mesoporous materials could be viewed as a continuous silica framework with encapsulated organic compounds [5].

The subsequent treatment for the template removal produced the typical MCM-41 opened mesopores.
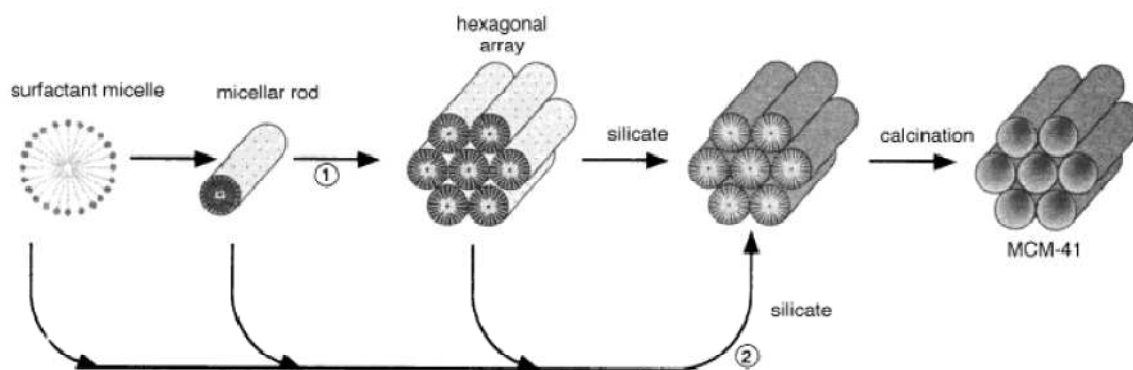


*Figure 1. LCT mechanism, proposed by the Mobil researchers.*

Furthermore, as it is now known, the synthesis conditions, used for preparing the mesophase following the method proposed by Beck et al., in particular in terms of template concentration, are far below to the critical micelle concentration excluding the required hexagonal LC formation necessary to the first proposed pathway 1 [4].

Indeed, an alternative study, carried out with the aim of further investigating the molar ratio between silica source and organic template, at high template/silica source molar ratio have reported the formation of different ordered arrays, classified and labeled as MCM-48, MCM-50 and so on (Figure 2) [6].

# 3. Materials and Methods
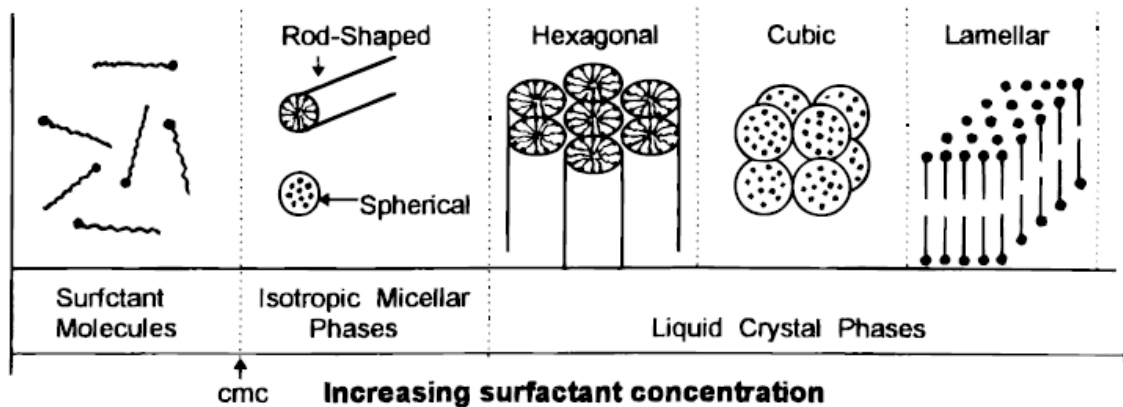


*Figure 2. Phase sequence of template-water binary system [6].*

Despite to the significant number of proposed synthetic methodologies, in this moment have been advanced no definitive explanations which can indicate a formation mechanism prior to another, but has took strength the hypothesis that the interaction between the inorganic precursors and the template is critical for the synthesis success.

Several mechanism, based on the general idea that the silicate species interact with the template favoring the LC formation, were proposed.

*Silicate rod assembly.* Carrying out a ^{14}N NMR study of the LC formation mechanism, Davis and coworkers have proposed that the formation of MCM-41, under the Mobil conditions, began with the deposition of multiple layer of silicate over the micellar rods.

The final steps of hydrothermal treatment and aging favor the complete condensation of the silica source, leading to the ordered MCM-41 phase, previously constitute of disordered silicate-encapsulated rods (Figure 3) [7].
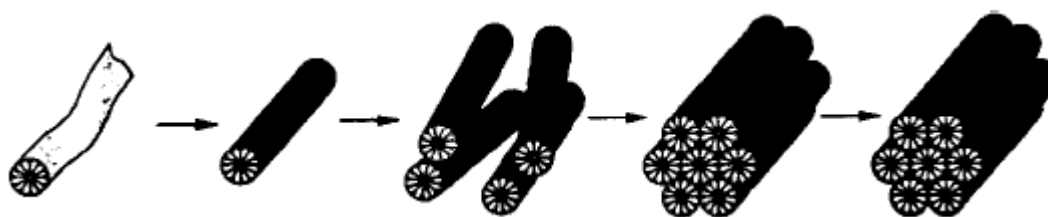


*Figure 3. Silicate-encapsulated rods, ordered in the hexagonal array [4].*

*Silicate layer puckering.* Realizing the same ^{14}N NMR study of the LC formation mechanism, Steel and coworkers reached a different interpretation, advancing the possibilities that the LC phase, prior to became an hexagonal array, was constituted of silicate layer intercalated with cylindrical rods. In this case, the aging treatment favor the puckering around the rods, leading to the well-known MCM-41 structure (Figure 4) [8].

16
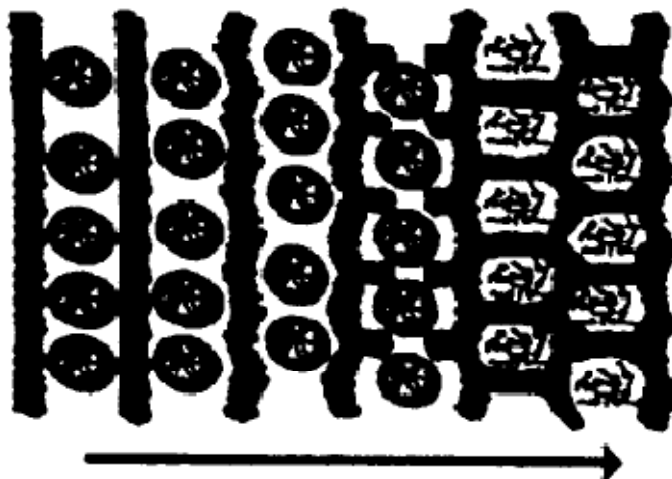
*Figure 4. Puckering of silicate layers proposed by Steel et al. [8].*

*Charge density matching.* Starting from a similar arrangement, Monnier and Stucky have proposed that the intercalated template was not shaped in cylindrical rods, but in a complete lamellar phase induced by the electrostatic interaction between the anionic silicates and the cationic template. When the silicate layer began to condense, the anionic charge associated with the silica source was reduced and, in order to maintain the charge balance, the silicate layer collapse transforming the lamellar structure into the hexagonal MCM-41 structure (Figure 5) [9,10].
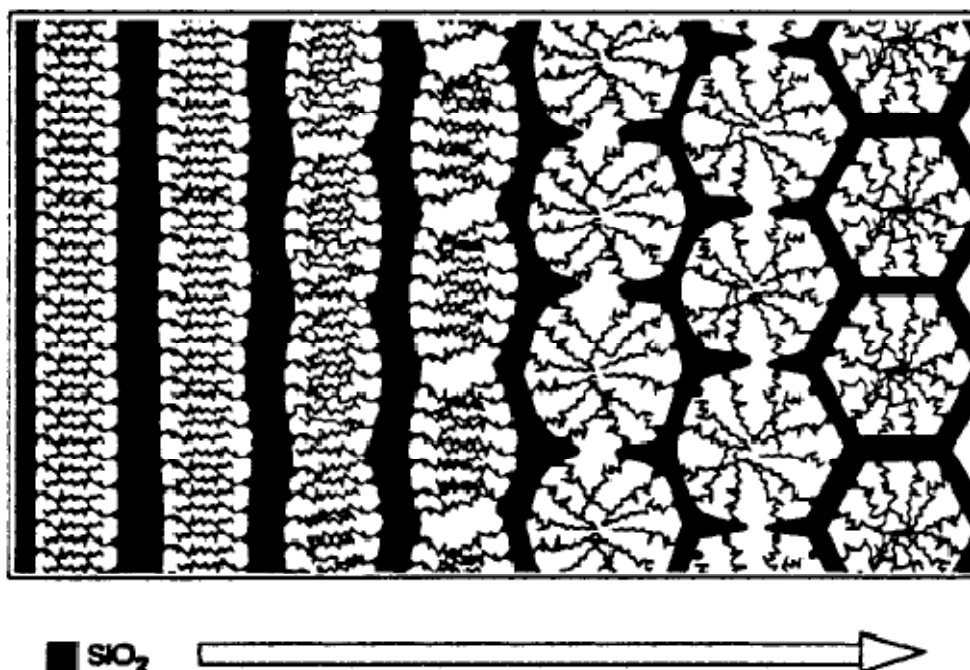


*Figure 5. Charge density matching mechanism [9].*

Similarly, the formation of the mesoporous material called FSM follows the same intercalation mechanism that cause a lamellar-to-hexagonal phase transformation.

## 3. Materials and Methods

After introducing the template by ion-exchange into mineral kadenite, its structure swells to a final product very similar to MCM-41 (Figure 6) [11].
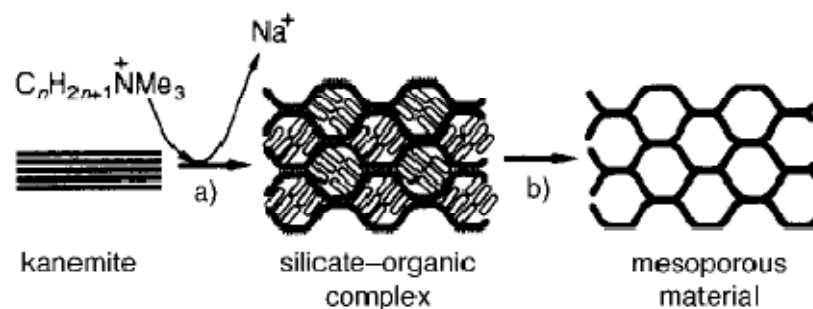


*Figure 6. Folding sheet of kanemite, intercalate with an organic template [11].*

Firouzi and coworkers have reported an interesting study, carried out with $^2$H and $^{29}$Si NMR spectroscopy, suggesting a true cooperative self-assembly of the silicates and template molecules at low temperature and high pH (about 14). Under these conditions, that prevented condensation of the silicate species, a hexagonal phase was found, in agreement with the effect of electrolytes on micellar phase transformation to hexagonal. When this silicatropic liquid crystal, called SLC, was heated the silicates has began to condense, forming the known MCM-41(Figure 7) [12].
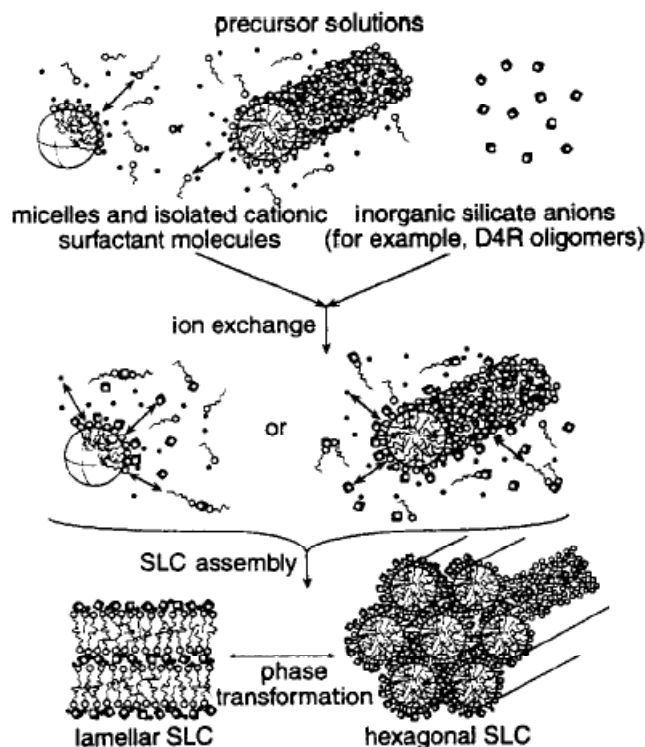


*Figure 7. Silicatropic liquid crystal template based mechanism, suggested by Firouzi et al. [12].*

### 3.2.2 MCM-41 synthesis

Since their discovery on 1991, a several number of synthetic procedures were reported based on sodium silicate, tetraethylorthosilicate, fumed silica and colloidal silica precursors. Because of this on the beginning of the investigation different procedures and silica source were evaluated. In this work, MCM-41 supports were prepared by using sodium silicate and tetraethylortosilicate as silica source and cetyltrimethylammonium bromide as templating agent. The synthetic procedures involved the preparation of the gel, hydrothermal treatment and calcination.

*Preparation of the gel*

*Sodium silicate MCM-41 (Sil):* The synthesis was performed according to the procedure reported by Beck and co-workers [5]. CTABr (cetyltrimethylammonium bromide, 99%, Sigma-Aldrich) and deionized water were stirred at room temperature until the mixture became homogeneous. Then sodium silicate (27% $SiO_2$, Sigma-Aldrich) was added to the mixture under vigorous stirring and aged for an hour. In order to favor the silicate poly-anions condensations the pH was adjusted by adding carefully a diluted aqueous solution of $H_2SO_4$ (96%, Sigma-Aldrich). The acid solution must be slowly added to the gel in order to avoid any local decrease in pH, which could results in a fast and disordered condensation of the silanols. Indeed, a typical acid addition involves at least 2 hours, depending on the batch volume. The obtained molar composition of gel mixture was 1.0 $SiO_2$: 0.55 CTABr: 0.14 $H_2SO_4$: 73 $H_2O$. The sample was labeled Sil.

*Tetraethylorthosilicate MCM-41 (TEOS):* The synthesis was performed according to the procedure reported by Cassiers and co-workers [13]. CTABr and deionized water were stirred at room temperature until the solution became clean. Then the tetramethylammonium hydroxide solution (TMAOH, 25 wt.% aqueous solution, Sigma-Aldrich) and the tetraethylorthosilicate (TEOS, 99.9%, Fluka) were added to the mixture, maintaining a vigorous stirring at 70°C for 2 hours. Because of this, the treatment at 70°C and the consequent vaporization of ethanol (formed by the condensation of silanols) could increase the viscosity of the gel, which should be controlled by closing the container, stopping the condensate. The obtained mixture, with a molar composition equal to 1.0 $SiO_2$ : 0.25 CTABr : 0.20 TMAOH : 35 $H_2O$, was aged at room temperature for 24 hours and labeled TEOS.

## 3. Materials and Methods

### *Hydrothermal treatment*

*Traditional hydrothermal treatment (HT):* The gels prepared according with the Beck and Cassiers methods were treated at 100°C for 144h in a PTFE-lined stainless-steel autoclave. Materials treated as above mentioned were indicate with the label HT (p.e. Sil-HT or TEOS-HT)

*Microwave-assisted hydrothermal treatment (MW):* The treatment was performed in a Milestone StartSYNTH microwave oven. The pressure and temperature was kept under control at 1.6 bar and 125°C [14]. The gel mixtures were reacted on 75 ml PTFE® autoclaves for 7 hours at 125°C. The obtained materials, were denoted as Sil-MW or TEOS-MW.

### *Calcination*

The slurries were filtered, washed with deionized water, and dried overnight at 60°C. The solids were calcined at 540°C for 6 hours in static air to degrade and remove the organic template and its residuals. In order to preserve the structure, a heating ramp of 1°/min was utilized [15].

### 3.2.3  Pd/Cu containing MCM-41 samples preparation

*Incipient wetness impregnated catalysts (i-PdCu-SHT or i-PdCu-THT).* After template removal, MCM-41 supports were impregnated with Pd and Cu species by incipient wetness impregnation of an appropriate $PdCl_2$ and $CuCl_2$ aqueous solution (molar ratio 1:1). The catalysts, were dried overnight at 120°C and finally treated with pure hydrogen flow at 330°C for an hour.

*"Direct introduction" catalysts.* Pd and Cu were incorporated in the course of MCM-41 synthesis using silicates, by adding the $PdCl_2$ and $CuCl_2$ aqueous solution (molar ratio 1:1) to the template solution. The pH was optimized to avoid metal hydroxides precipitation, and then was finally added the silica source. The gel mixtures prepared were treated by microwave irradiation at 125°C for 7 hours, as above mentioned for purely siliceous MCM-41. Filtered and dried powders, after the air-treatment at 540°C, were reduced with hydrogen flow at 330°C. The synthesized catalysts were labelled d-PdCu-SMW or d-PdCu-TMW.

## 3.3   Characterization methods

### 3.3.1   X-ray diffraction analysis

Powder X-ray diffraction analysis (XRPD) were widely used in catalysis to obtain information about chemicals on samples, investigate the evolution of crystalline phases but also to acquire morphological information in the case of MCM-41 silicate materials.

XRPD analysis could provide a large range of information, such as:

> - qualitative indication about crystallinity degree
>
> - qualitative identification of sample's chemical phases
>
> - quantitative analysis (introducing an internal standard)

Bragg's Law constitutes the cornerstone of diffractogram elaborations, providing a relation between diffraction angle and the spacing of crystalline planes, like a fingerprint for crystalline phases [16].

$$n\lambda = 2d \, sin\theta$$

where:

n = diffraction order

$\lambda$ = radiation wavelength

d = spacing of crystalline planes

$\theta$ = incident radiation angle

Furthermore, especially considering the formation of alloys, the Vegard's Law has been used to calculate the solid solution composition from the distortion onto crystalline unit cell parameters.

$$a_{AB} = xa_A + (1-x)a_B$$

where:

$a_{AB}$ = solid solution's unit cell parameter

$a_A$, $a_B$ = unit cell parameters for A and B components respectively

x = molar fraction

XRPD measurements were carried out in different diffractometer (Philips PW1710 and PANalytical X'PertPro) based on Bragg/Brentano geometry basically equipped with a proportional detector, using a Ni-filtered Cu K$\alpha$ radiation ($\lambda$=1.5418 Å) at 40 mA and 40 kV. For all catalysts, the first diffraction pattern in the 5-80° 2$\theta$ range was collected with a step size of 0.1° and time for step of 2 seconds. In a second time, specific methods were used to refine the information quality, decreasing the step size to resolve close reflections

or decreasing the acquisition velocity to magnify reflections intensity. Metals alloying were investigate in specific range using a high performance detector with a step size of 0.05° and time for step comparable to 800 seconds. Moreover, in the case of MCM-41 based materials, the small angle diffractogram was collected over the 1.6-15 °2θ range, 0.1° step size and 10 counting time and the wide angle diffractogram was collected over the 25-50 °2θ range, 0.1° step size and 5 counting time.

### 3.3.2 Transmission electron microscope analysis

Transmission electron microscope analysis (TEM) could be considered one of the most reliable and flexible analytical technique, that could provide information about particle distribution, composition, dimension and shape. High resolution images, formed from the interaction between the transmitted electrons through a thin-layer of dispersed sample are just one of the obtainable results, just one of the detectable radiations. In fact:

- diffraction patterns can be used to identify phases and space groups
- high resolution images can be used to measure particle size and structure formation, such as the hexagonal arrangement of the MCM-41 channels [16].

With the aim of revealing the particle composition, an EDS micro-probe can be used, which is based on the elaboration of emitted x-ray from an irradiated sample (similarly to X-ray fluorescence analysis). When in a inner core level a vacancies are created trough an incident high-energy radiation, an electron transition from the outer level to the vacancies, leads to an emission of characteristic radiations. The intensity of the emitted radiations can be linked to the energy difference between the electron levels, that identifies it as typical for each element. In fact, every element produce a complex spectrum, resulting from a wide range of possible electron transitions. In particular, emitted radiation can be classified according to the shell from which the electron is ejected (K, L and M from the inner one) and the width of the electron transition (α as one level, β e γ respectively two and three levels). Moreover, the presence of sublevels contributes to create a spectrum complicated and unique for each element.

TEM analysis were performed on a TEM/STEM FEI Tecnai F20 working at 200 KeV. The samples were prepared by dispersion of the powder in alcohol (ethanol or isopropanol) and deposition in a holey-carbon film supported with a titanium grid.

### 3.3.3 Thermo-gravimetric analysis

Thermo-gravimetric analysis are usually and fruitfully used to evaluate the thermal stability of materials but also to observe the weight loss of samples subjected to a progressive increase of temperature. Observing variations on the slope of this weight loss, is possible to recognize the precise temperatures where degradations and substances' evolution occur. In fact, the above mentioned weight loss can be attributed to the evolution of adsorbed substances  or to a thermal degradation of materials and templates in the case of porous catalysts preparation. The temperature at which substances are desorbed from the surface of a heated solid reflects the strength of the surface bond, and this analytical methods is clearly interesting for analyze exhaust catalysts.

### 3.3.4 Temperature programmed desorption, reduction and oxidation analysis

Determining the strength of surface bonds and interaction between metal phases and materials surface is fundamental for catalysts performance understand. Temperature programmed analysis can provide red-ox information about materials and following specific reagent diffusion model can provide information about metals particle size and homogeneity:

- reduction and oxidation behavior can be compared between materials

- profile areas could be used for quantitative analysis

- maximum temperature can be related to metal particle dimension

Temperature Programmed Analysis (TPDRO; desorption, reduction and oxidation) were carried out in a Thermo Scientific TPDRO 1100 working with a 5% $H_2$/Ar reduction mixture and 5% $O_2$/He oxidation mixture.

### 3.3.5 Nitrogen adsorption analysis

A typical adsorption/desorption measurement versus relative pressure $p/p^0$ over a solid provide several information about the morphological properties of samples. Considering that progressively higher pressure are used during nitrogen adsorption, capillary condensation occurs in pores increasingly larger, making it possible to evaluate the pore size distribution. The Kelvin equation shows how is possible to observe the nitrogen condensation in pores at pressures lower than the saturation pressure, indeed, when a capillary condensation occurs, the vapor pressure is lowered in concave meniscus of liquid [17].

## 3. Materials and Methods

$$ln\frac{P}{P^0} = \frac{-2\gamma V_L}{RT}\frac{1}{r_m}$$

where:

$r_m$ is the radius of curvature

$\gamma$ is the surface tension

$V_L$ is the molar volume

Moreover, applying computational models and equations (NLDFT, BJH, t-plot, HK and BET) to the obtained isotherms is possible to measure interesting parameters such as the pore size distribution, the attributable volume for each type of pores, the specific surface area and many others. It must be remarked that, any set of models is suitable for calculated parameters for a class of materials, but in other case, the introduction of alternative models could be more suitable [18]. Similarly, the analysis conditions should be specific for each class of materials.

$N_2$ adsorption/desorption isotherms (-196°C) were performed in a Micromeritics ASAP 2020 instrument. Samples were previously outgassed for 30 minutes at 150°C and 30 µmHg, and then heated for 120 minutes at 350°C.

## References

[1] F. Rodríguez-Reinoso, M. Molina-Sabio, M.T. González, *Carbon* **33** (1995) 15-23.

[2] K.D. Henning, H. von Kienle, *Ullmann's Encyclopedia of Industrial Chemistry*, WILEY-VCH, UK, **2013.**

[3] *www.freedoniagroup.com*

[4] J.Y. Ying, C.P. Mehnert and M.S. Wong, *Angew. Chem. Int. Ed.* **38** (1999) 56-77.

[5] J.S. Beck, J.C. Vartuli, W.J. Roth, M.E. Leonowicz, C.T. Kresge, K.D. Schmitt, C.T-W. Chu, D.H. Olson, E.W. Sheppard, S.B. McCullen, J.B. Higgins and J.L. Schlenker, *J. Am. Chem. Soc.* **114** (1992) 10834-10843.

[6] X.S. Zhao, G.Q.(Max) Lu, G.J. Millar, *Ind. Eng. Chem. Res.* **35** (1996) 2075-2090.

[7] C.-Y. Chen, S.L. Burkett, H.-X. Li, M.E. Davis, *Microporous Mater.* **2** (1993) 27-34.

[8] A. Steel, S.W. Carr, M.W. Anderson, *J. Chem. Soc. Chem. Commun.* **117** (1994) 1571-1572.

[9] A. Monnier, F. Schüth, Q. Huo, D. Kumar, D. Margolese, R.S. Maxwell, G.D. Stucky, M. Krishnamurty, P. Petroff, A. Fizouri, M. Janicke, B.F. Chmelka, *Science* **261** (1993) 1299-1303.

[10] G.D. Stucky, A. Monnier, F. Schüth, Q. Huo, D. Margolese, D. Kumar, M. Krishnamurty, P. Petroff, A. Fizouri, M. Janicke, B.F. Chmelka, *Mol. Cryst. Liq. Cryst.* **240** (1994) 187-200.

[11] S. Inagaki, Y. Fukushima, K. Kuroda, *J. Chem. Soc. Chem. Commun.* **8** (1993) 680-682.

[12] A. Fizouri, D. Kumar, L.M. Bull, T. Besier, P. Sieger, Q. Huo, S.A. Walker, J.A. Zasadsinski, C. Glinka, J. Nicol, D. Margolese, G.D. Stucky, B.F. Chmelka, *Science* **267** (1995) 1138-1143.

[13] K. Cassiers, T. Linssen, M. Mathieu, M. Benjelloun, K. Schrijnemakers, P. Van Der Voort, P. Cool and E.F. Vansant, *Chem. Mater.* **14** (2002) 2317-2324.

[14] A.N. Ergun, Z.O. Kocabas, M. Baysal, A. Yurum, and Y.Yurum, *Chem. Eng. Comm.* **200** (2013) 1057-1070.

[15] F. Kleitz, W. Schmidt, F. Schüth, *Micropor. Mesopor. Materials* **65** (2003) 1-29.

[16] J.M. Thomas, W.J. Thomas, *Principles and Practice of Heterogeneous Catalysis*, VCH, NY(USA), **2008.**

[17] S. Kulprathipanja, *Zeolite in Industrial Separation and Catalysis*, WILEY-VCH, UK, **2013.**

[18] M. Thommes, *CHemie Ingenieur Technik* **82** (2010) 1059-1073.

# Chapter 4

## 4 Activated carbon supported catalysts

### 4.1 Introduction

Several heterogeneous metal catalysts supported on activated-carbon were prepared following the previously explained procedures and studied on the hydrodechlorination of $CF_3OCFClCF_2Cl$ (ADM) in the presence of hydrogen. The hydrodechlorination activities of catalysts containing Ru, Pd, Ru/Pd, and Pd/IB element were investigated at different metal content, different contact time and also at different molar ratio in the case of bimetallic active phases. The main purpose of this part of the investigation was to define the best metal components for the active phase. Thus, the minimum characterization of the materials used, necessary for the understanding, have been reported. In a large number of catalytic trials using different catalysts the main product detected was the expected product, $CF_3OCF=CF_2$ (MVE). All the possible products were reported on the following scheme [1].
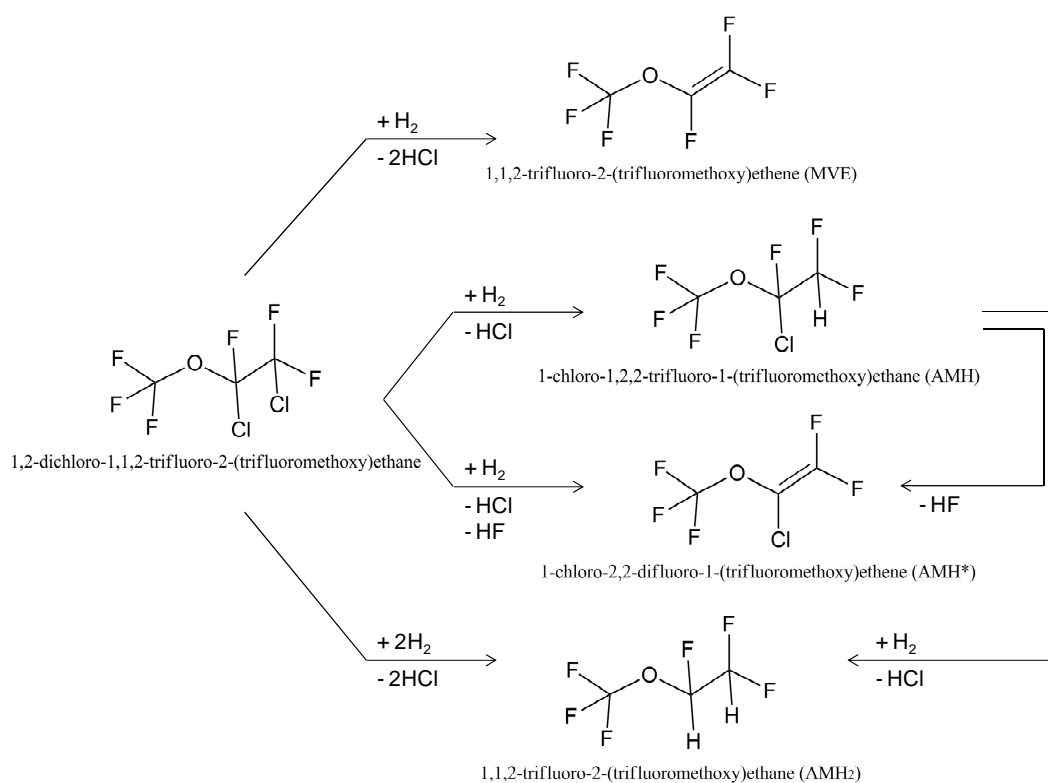


*Scheme 1. Reaction pathway proposed for the hydrodechlorination of $CF_3OCFClCF_2Cl$ [1].*

## 4.2 Monometallic catalysts

### 4.2.1 Catalytic performance of Ru-based catalysts

The hydrodechlorination of $CF_3OCFClCF_2Cl$ was performed over Ru-based catalysts summarized on Table 1. At the very beginning of this investigation, an accurate literature research was carried out in order to enrich the knowledge in this reaction, which needs a catalysts able to interact with halogenated species, but also activate hydrogen without hydrogenate the formed double bond.

When the hydrodechlorination was performed over 1%Ru catalysts, which is also commercially available, different operative conditions such as temperature, contact time and ADM feeding rate were used to investigate further the effects on catalytic performance [2].

| Sample | Description | Metal Content [%wt] | Precursors |
|--------|-------------|--------------------|------------|
| 0,5 Ru | IWI[a] on Activated Carbon (AC1) | 0,5 | $RuCl_3$ |
| 1,0 Ru | IWI[a] on Activated Carbon (AC1) | 1,0 | $RuCl_3$ |
| 1,5 Ru | IWI[a] on Activated Carbon (AC1) | 1,5 | $RuCl_3$ |

[a] Incipient Wetness Impregnation

*Table 1. Materials and composition of Ru-based catalysts involved in the hydrodechlorination study.*

### 4.2.1.1 Effect of Ru content on catalytic activity

Figures 1 and 2 show the activity of Ru-based catalysts with different metal contents. In particular, Figure 1 shows the evolution of $CF_3OCFClCF_2Cl$ conversion with the time on stream (TOS). On the other hand, on Figure 2 are compared MVE selectivity with the time on stream for each catalysts. The hydrodechlorination of ADM over the ruthenium reported catalysts generated MVE as the main product and traces amount of $CF_3OCFClCF_2H$ (AMH) and $CF_3OCFHCF_2H$ (AMH$_2$) molecules, especially at the beginning of the reaction. Firstly, has appeared interesting that all these materials showed high values of $CF_3OCFClCF_2Cl$ conversion, on the range of the industrial request, but at the same time a high loss of activity must be highlighted, particularly prevalent in the case of materials with higher Ru content (1.5%wt.).

When 0.5%Ru catalyst was used on reaction, the target product was formed with very high selectivity (98% after 9 h on stream), and by-products like Cl/H mono-substituted products ($CF_3OCFHCF_2Cl$ or $CF_3OCFClCF_2H$) were produced in trace amount. The increase of noble metal content to 1% wt. didn't lead to an activity increase, but Cl/H mono-

27

## 4. Activated carbon supported catalysts

substituted products formation increased slightly, as it was related to the amount of hydrogen activated by ruthenium active sites. In order to reveal a possible trend on by-product formation, another Ru-catalyst was prepared with a higher metal loading, equal to 1.5% wt. The obtained results showed unexpected values of conversion and selectivity. Indeed, the expected $CF_3OCFClCF_2Cl$ conversion enhancement was really interesting but considering this behavior, is also true that deactivation trend appeared worse with respect to the lower Ru-content catalysts. On the contrary, unexpectedly, over this catalyst, a decrease in the $CF_3OCFClCF_2H$ production was observed concomitant with a small formation of the di-hydrogenated product $CF_3OCFHCF_2H$. Nevertheless, considering the cumulative amount of "hydrogenated" products, which appeared higher ($CF_3OCFHCF_2Cl$ or $CF_3OCFClCF_2H$ and $CF_3OCFHCF_2H$), a relationship between MVE selectivity, hydrogen coverage and noble metal content could be theorized.
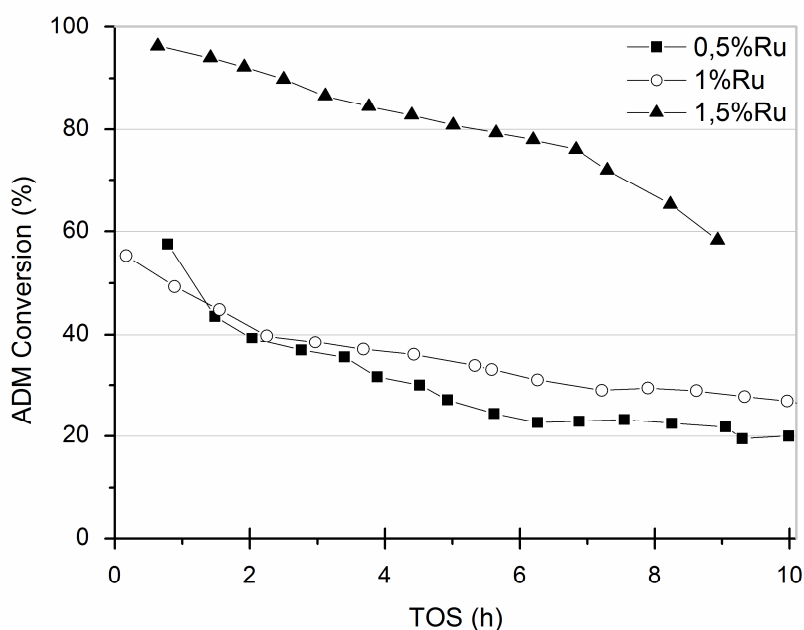


*Figure 1. Ru-based catalysts performance in terms of $CF_3OCFClCF_2Cl$ conversion. Reaction conditions: ADM = 16%v/v, contact time 10s, ADM/H$_2$ molar ratio = 1, reaction temperature 250°C.*

For all ruthenium-supported catalysts, a transient time to achieve the steady-state on the selectivity to perfluorinated olefin (MVE) has been reported during the earliest five hours of reaction (Figure 1). This behavior was concomitant with a general decrease in hydrogenated side-products formation such as the Cl/H replacement product $CF_3OCFClCF_2H$ (AMH) and di-hydrogenated product $CF_3OCFHCF_2H$ (AMH$_2$).

28

| By-products Selectivity at 8h | | |
|---|---|---|
| Sample | AMH | AMH2 |
| 0,5%Ru | 2,3 | n.d. |
| 1,0%Ru | 2,4 | n.d. |
| 1,5%Ru | 0,5 | 4,1 |
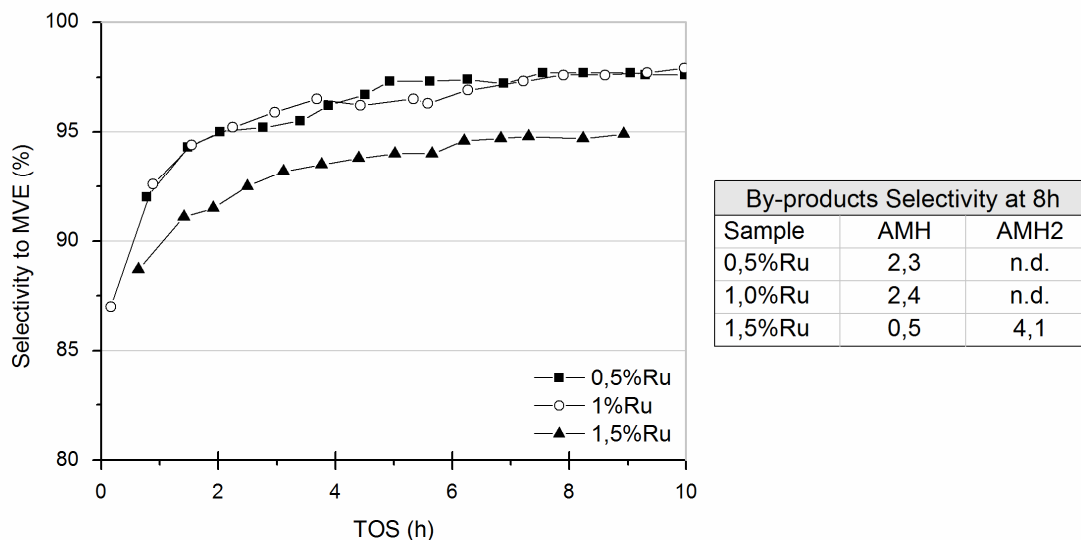
*Figure 2. Ru-based catalysts performance in terms of selectivity to MVE. Table reports the selectivity of the main by-products at the steady state.*

The observed decrease in formation of the Cl/H substitution products with time on stream, could be attributed to different interpretations. The activation reductive procedures to fundamental state of the active phase, generate a high hydrogen coverage over ruthenium species at the beginning of the reaction. Due to possible competitive adsorption of chlorine, which is formed by the dissociative absorption of $CF_3OCFClCF_2Cl$, the hydrogen coverage decreases with the time on stream. Again, a poor activity on hydrogen activation at reaction temperature can lead to a decreased hydrogen coverage, and thus, a decrease in production of mono-hydrogenated molecules; however, the decrease in formation of Cl/H substitution species, might also be due to a crystallites modification on the active phase that favors multiple interaction with active sites, leading to others molecules. At the same time, is equally possible that these mono-hydrogenated products were produced on a chemically different active sites that could be affected by deactivation, also caused by the hydrochloric acid formed during the reaction.

Nowadays, the reaction mechanism is not well defined yet, but a previously reported mechanism in hydrodechlorination reactions, suggested by Mori and co-workers [3], theorizes the possible interactions between active sites and reactive species in hydrodechlorination of trichloroethane. Some of the explained considerations could be extend to different possible reaction pathways associated with ADM hydrodechlorination, as shown in Figures 3 and 4.

# 4. Activated carbon supported catalysts
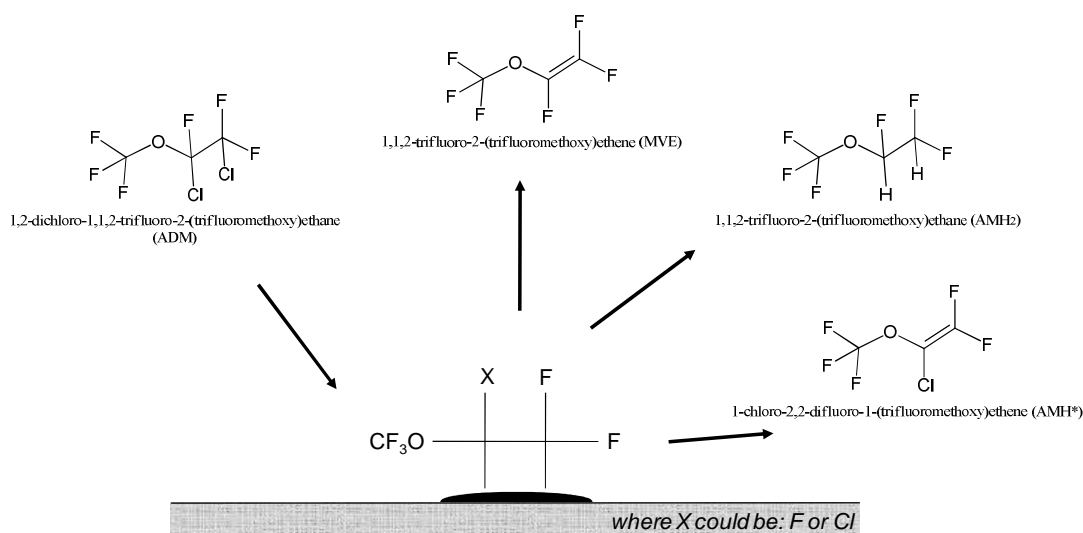


*Figure 3. Reaction products associated with bi-dentate intermediate.*
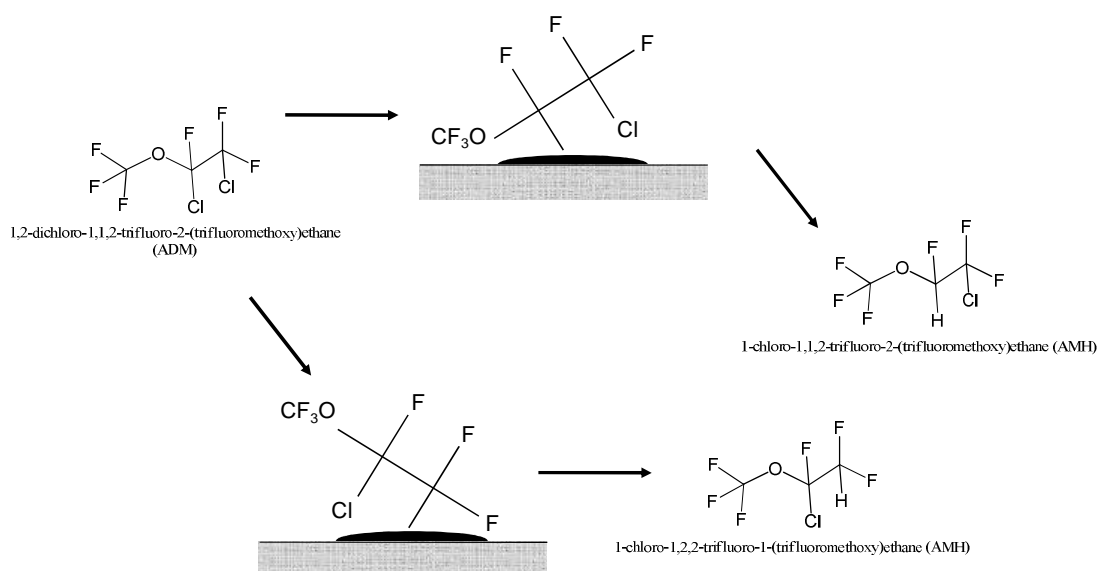


*Figure 4. Reaction products associated with mono-dentate intermediate.*

The previously mentioned mechanism for hydrodechlorination of vicinal halogen considers the multiple interaction of molecules with the active sites (or vicinal active sites), leading to the target product but also to $CF_3OCFHCF_2H$ ($AMH_2$) depending on the catalytic system used. Obviously, a single interaction with an isolated active site is already possible and promote a single dehalogenation reaction, producing a Cl/H substitution by-products like $CF_3OCFHCF_2Cl$ and $CF_3OCFClCF_2H$ (AMH). In the first case, $CF_3OCF=CF_2$ and $CF_3OCFH-CF_2H$ can be formed when vicinal active sites stabilized an intermediate comparable to $CF_3O*CF-CF_2*$. The activated hydrogen amount on catalyst surface determines how the intermediates $CF_3O*CF-CF_2*$ will be desorbed. On the other hand, the mono-hydrogenated molecules $CF_3OCFCl-CF_2H$ and $CF_3OCFH-CF_2Cl$, formed from $CF_3O*CF-CF_2Cl$ or $CF_3OCClF-CF_2*$ intermediates, are probably formed over isolated

30

active sites. Furthermore, a separate discussions should be done considering de-fluorinated by-products like $CF_3OCCl=CF_2$ (AMH*), and cracking molecules such as $CF_2=CFCl$ (CTFE) and $COF_2$ formed in different quantities depending on the catalytic systems used. In fact, the more are strong the interaction between active sites and species, the more are possible eliminations different from chlorine, such as $CF_3O*$ groups and F*.

Indeed, the selectivity trend observed, during the time on stream (Figure 2) may be explained by the hypothesis that the production of mono-hydrogenated species requires a single Ru active site and the formation of different intermediates, such as $CF_3O*CF-CF_2Cl$ or $CF_3OCClF-CF_2*$. Probably, the interaction between this single active site and the organic substrate could generate some kind of intermediate, such as the above reported, which are strongly hold-on the active sites. This condition could easily evolve to: i) blocking phenomena of the active sites involved; ii) side-reaction between the adsorbed intermediates leading to the formation of dimers and oligomers. Considering the hydrogen coverage of catalysts surface as a key factor for intermediates desorption, the more hydrogen availability decrease, the more this kind of active site could be deactivated.

Considering a second mechanism, proposed by d'Itri and co-workers, shown in Figure 5, is possible to adapt it for the reaction of dechlorination of ADM. This mechanism is particularly suitable to consider the different conditions of hydrogen coverage and the various distribution of the eventually different active sites of the catalyst [4].

In fact, the reagent, after suffering a dissociative adsorption of a chlorine atom, in section 1, may evolve into section 4, in case there is an abundance of hydrogen on the surface, or evolve to section 2 (or 2a) in presence of a vicinal site more active in coordinating halogens, or in the case of decreased hydrogen coverage of the catalyst surface.

The section 2a, 3 and 6 may evolve desorption of different reaction products. In the case of the section 2a is considered that the presence of hydrogen makes it more favorable bond rupture C-F, while in section 3, coordinating on a single site interaction with the intermediate of type x , it is possible to obtain the desired product or large excess of hydrogen , also the product $AMH_2$. The section 5, through the rotation of the bond, can evolve from coordination of four atoms with hydrogen, to a more stable coordination of six atoms with hydrogen and halogen, evolving rapidly to AMH. The presence of two possible isomers for the product AMH is explained by considering a different adsorption in section 4, coordinating, through the halogen, the secondary carbon.

.

## 4. Activated carbon supported catalysts
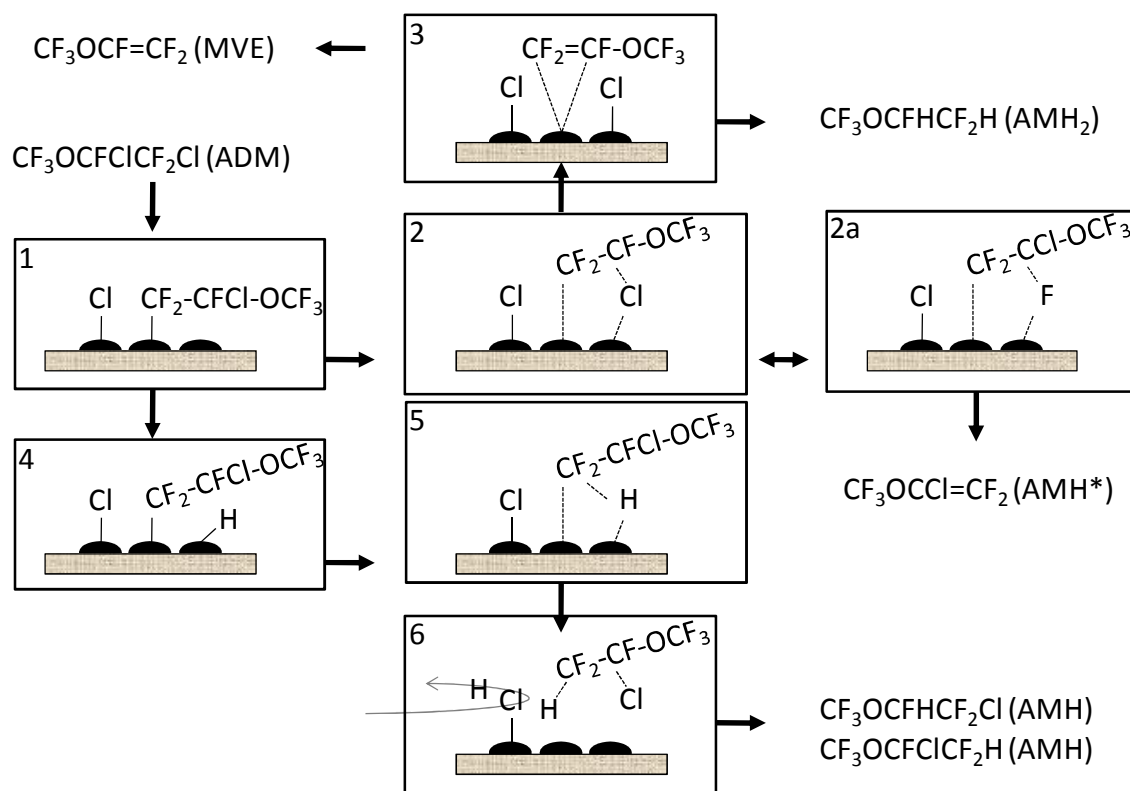


*Figure 5. Adapted and revised reaction scheme for the hydrodechlorination of ADM [3].*

Taking a look on AMH selectivity (Figure 2), which was slightly higher over 1.0-Ru/C, and the higher AMH$_2$ selectivity over 1.5-Ru/C, another hypothesis could be justified. At the beginning of reaction, the hydrogen coverage could be considered high on every catalysts, favoring hydrogenated products. When the catalysts with lower metal content were used on reaction, their high metal dispersion probably favors the formation of single-site interactions with halogenated species, leading to a high AMH formation. On the contrary, the catalyst with higher metal content, having a lower metal dispersion, promote the formation of multiple-site interactions and consequently a high AMH$_2$ formation. Thus, following this and the above mentioned observation, the optimal compromise between performance, metal dispersion and metal content was selected on 1%Ru/C.

### 4.2.1.2  Effect of operative conditions on catalytic activity

In order to observe the effects on product distributions, catalytic tests were conducted using different temperature, contact time (5 and 10 seconds) and various CF$_3$OCFClCF$_2$Cl feeding rate over the sample 1-Ru/C. The effect of temperature was studied in the range between 220°C and 280°C. Figure 6 and 7 shows the effect of temperature on the conversion and product selectivities using different reaction temperature for the

hydrodechlorination of $CF_3OCFClCF_2Cl$. The conversion of ADM increased around 35% with reaction temperature between 220°C and 280°C. It must be noted that this advantage was rapidly lost by different rates on deactivation phenomena, which lead to equal performance on ADM conversion after 9 hours of reaction. This evidence, supports the theorized deactivation mechanism that considers a strongly adsorption of a "mono-dentate" intermediate on active sites. Indeed, the turnover frequency was increased, generating a greater deactivation. Unexpectedly, operative temperature condition seems to have no effect on selectivity towards MVE, and thus extending this consideration, temperature condition seems to have no effect on reaction mechanism, obviously into the studied range of temperature.
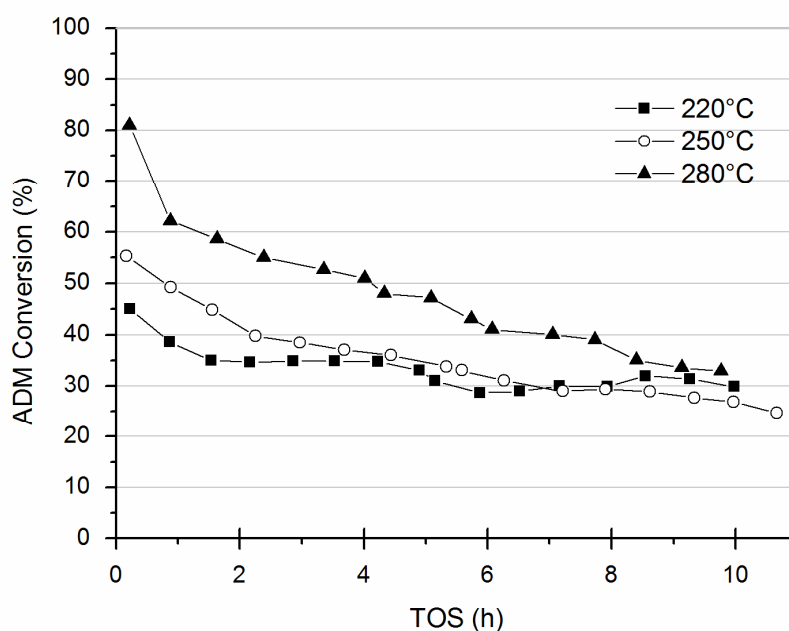


*Figure 6. 1.0% Ru-based catalysts performance in ADM conversion, at different reaction temperature. Reaction conditions: ADM = 16%v/v, contact time 10s, ADM/H₂ molar ratio = 1.*

## 4. Activated carbon supported catalysts
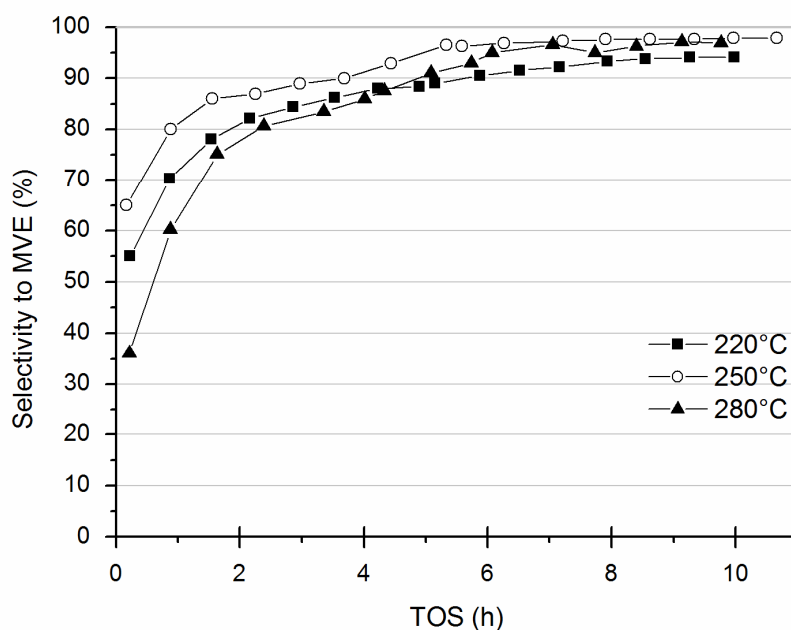


*Figure 7. Selectivity to MVE over 1.0% Ru-based catalysts, tested at different reaction temperature.*

When Ru-catalysts were used with different contact times or feeding rates, the catalytic performance on ADM conversion and product selectivity do not highlight significantly variations. The obtained results are summarized on Figures 8 and 9, where is also possible to observe the same trend of performance deactivation. With the best of our knowledge at this point of develop, a dramatic deactivation of Ru-catalysts was highlighted and no effect on this was related to the operative contact time and feeding rate of ADM. The only difference on deactivation trend could be related to the increase on reaction temperature, which makes the deactivation faster. This behavior is in agreement with an energetic consideration: the more the temperature is high, the more interactions will be effective for the formation of intermediates, and thus, if a fraction of intermediates can block the active sites, the more interactions will be effective on generate intermediates, the more intermediates will block the active sites, leading to a decrease on the catalytic conversion of ADM with time on stream. However, taking into account only this hypothesis, there's no way to explain how catalytic trials performed at different temperature lead to a similar steady-state value of ADM conversion in long-term run.
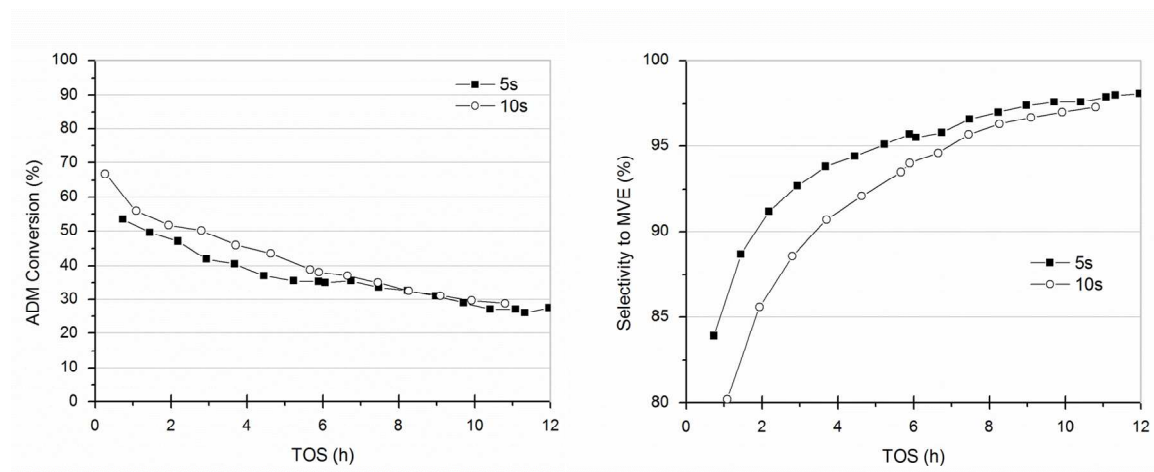
*Figure 8. 1.0% Ru-containing catalysts performance in ADM conversion (on the left side) and selectivity to MVE (on the right side), tested at different contact times. Reaction conditions: ADM = 16%v/v, temperature = 250°C, ADM/H₂ molar ratio = 1.*
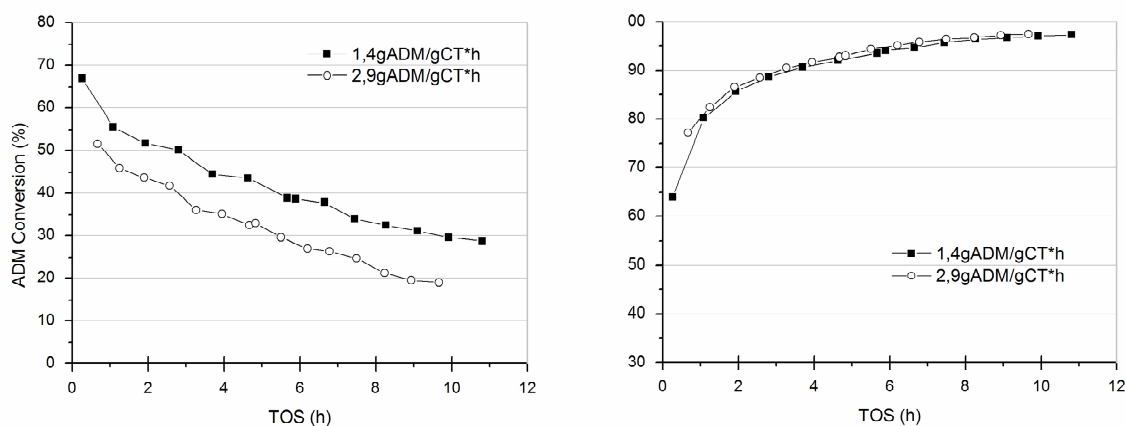


*Figure 9. 1.0% Ru-containing catalysts performance in ADM conversion (on the left side) and selectivity to MVE (on the right side), tested at different feeding ratios. Reaction conditions: ADM = 16%v/v and 33%v/v, temperature = 250°C, ADM/H₂ molar ratio = 1 and contact time = 10s.*

### 4.2.1.3  Effect of Ru content on catalysts chemical-physical properties

In order to investigate further the reason of deactivation and catalytic different activity of all the Ru-based materials a series of characterization analysis were carried out over fresh and spent catalysts. With the aim of obtaining a clear discussions, the results will be reported following an order based on the sought information. Firstly, the question to be answered was why the Ru-based catalysts activity on hydrodechlorination seems to be not proportional with respect to the metal content. In literature, dispersion of metal nanoparticle were reported to play an important role in several hydrodechlorinations, in fact, these reactions have been shown to be influenced by surface metal size and amount of spillover hydrogen [5-7]. Furthermore, hydrodechlorination reactions have been considered

as structure sensitive reaction, observing that the dechlorination rates seems to be enhanced at lower metal dispersion, probably depending on a greater exposition of atomic orbitals over smaller particles. [8, 9].

Temperature-programmed reduction analysis were carried out over these catalysts and allowed to observe the presence of different Ru-phase deposited over the carbon surface reporting a different $H_2$-consumption profile (Figure 10). The low ruthenium content catalysts (0.5-Ru and 1.0-Ru/C) showed a single reduction peak, in particular with a peak maximum on profile placed around 130°C that could be attributed to the reduction of amorphous or highly dispersed ruthenium oxide. Onto the low temperature sides of these reductions peaks, a small shoulder between 60 and 80°C, clearly observable over 0.5-Ru/C, could be assigned to the reduction of non-stoichiometric ruthenium oxide usually indicated as $RuO_x$. On the contrary, over the higher metal content Ru-catalyst (1.5-Ru/C) three reduction peaks on the $H_2$-consuption profile were showed, respectively at 135, 170 and 230°C.

The lower temperature peak, as above, were assigned to the reduction of ruthenium oxide, while the higher one (230°C) was due to a ruthenium species with lower dispersion or strongly interacting with the surface [10, 11]. Moreover, the peak at 170°C was attributed to the reduction of residual ruthenium oxychlorides formed during the preparation of the catalysts [12, 13].

In order to compare different analysis, the obtained results were normalized with the samples weight. For all the samples analyzed, there were a high temperature profile due to support degradation [14], while, on the lower range of temperature, the intensity of reduction profile was correlate with the metal content, highlighting the increase in ruthenium content.

Based on this consideration, was quite expected the high value of ADM conversion reported at the very beginning of catalytic test over 1.5-Ru/C. On the other hand, the exhibited higher selectivity to $CF_3OCFHCF_2H$ (AMH$_2$) was probably due to the presence of different active sites or a particularly high density of activated hydrogen on the surface of catalyst.

When the lower Ru-content catalysts (0.5-Ru and 1.0-Ru/C) were used on reaction, as previously explained, the achieved values of ADM conversion were the same despite the difference on ruthenium content. In fact, observing the reduction profiles, only the 1.5-Ru/C showed more phases, probably active on hydrodechlorination reaction, but also more affected by deactivation.
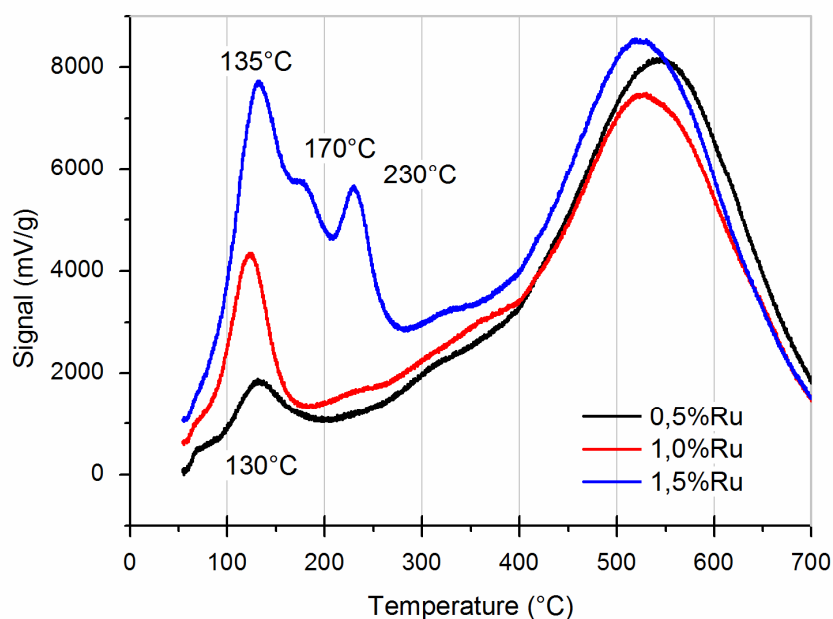
*Figure 10. Temperature programmed reduction profile of Ru-containing catalysts with different metal loading.*

With the goal of better observe the metal dispersion over the surface of catalysts, $N_2$-adsorption and HR-TEM analysis were carried out. Obviously, the best method to be performed should include the chemisorption of probe-molecule, but in the case of activated-carbon supports, this kind of analysis can be unreliable. $N_2$-adsorption and desorption analysis performed at -196°C reported all the ruthenium catalysts as not affected by pore occluding into the activated-carbon matrix during the preparation procedure (Table 2). In particular no evidence of surface areas decrease related to the metal content were found.

| Sample | Active Phase | Composition | Surface area ($m^2$/g) | |
|---|---|---|---|---|
| | | | Fresh | Spent |
| 0,5-Ru/C | Ru | 0,5 | 920 | () |
| 1,0-Ru/C | Ru | 1,0 | 1041 | 795 |
| 1,5-Ru/C | Ru | 1,5 | 990 | () |

*Table 2. Composition and surface areas of Ru-based catalysts studied.*

XRPD analysis were carried out over the Ru-based catalysts with the aim of observing different phases and eventually, calculate the crystallite size, but no reflects were highlighted together with the activated-carbon amorphous background (Figure 11). Taking into account this evidence, the ruthenium species could be considered in an amorphous

## 4. Activated carbon supported catalysts

state or smaller with respect to the XRPD limit of about 4 nm, also generally indicated as 1-2%wt. of crystalline species over an amorphous matrix.



| Metallic Ru - PDF 00-006-0663 | |
|---|---|
| **Angle** | **Intensity** |
| **2theta** | **%** |
| 38,388 | 40 |
| 42,153 | 35 |
| 44,007 | 100 |
| 58,325 | 25 |
| 69,407 | 25 |
| 78,39 | 25 |
| 82,224 | 6 |
| 84,705 | 25 |
| 85,96 | 20 |
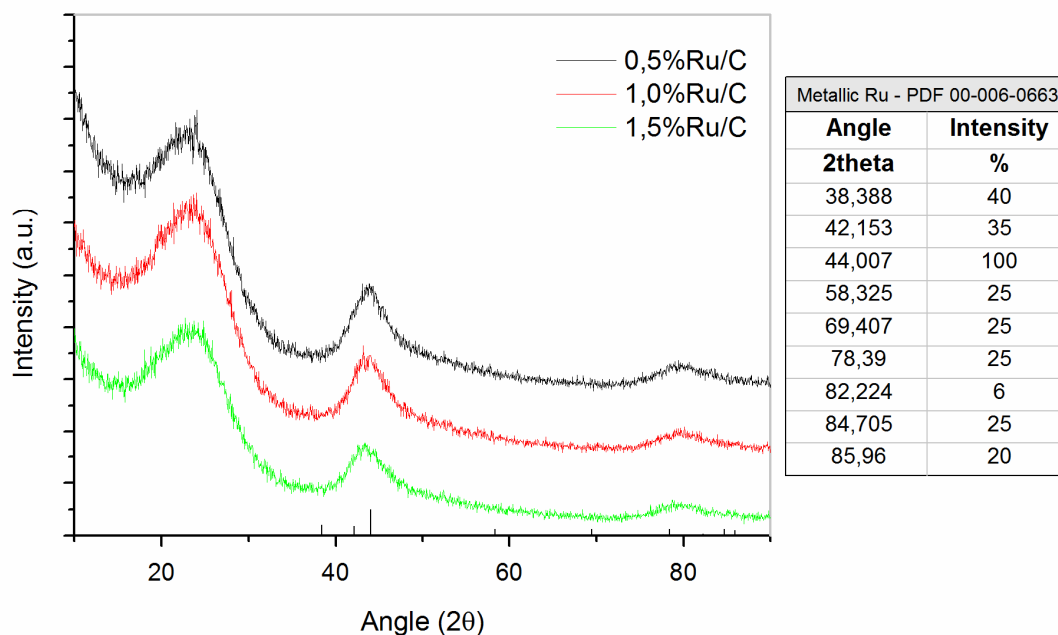
*Figure 11. X-ray diffraction analysis performed over Ru-based catalysts and standard Ru diffraction pattern (degrees and reflections relative intensity), PDF 00-006-0663.*

When Ru-based catalysts, with 1.0 and 1.5%wt. metal content, were analyzed by HR-TEM microanalysis the same results were showed, highlighting a homogeneous dispersion of Ru particle all over the catalysts surface. Regarding the 1.0-Ru/C histogram on Figure 12, Ru-particle have reported a size of 1.4±0.6 nm, in agreement with the absence of XRPD reflects (under the detection limit). Increasing the Ru content around 1.5%wt. a partial aggregation of particles could be noted resulting on the histogram showed on Figure 13.
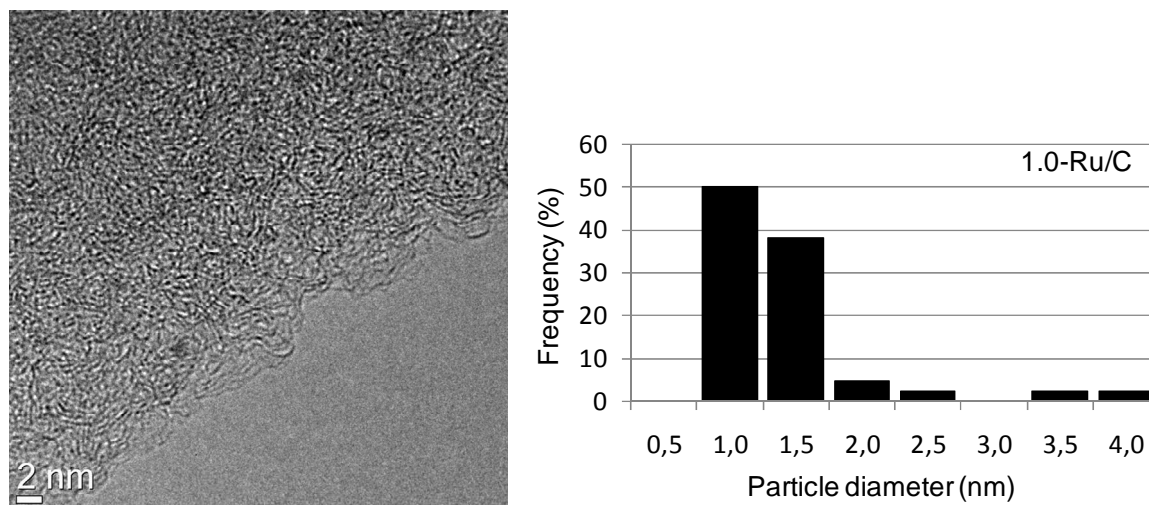


*Figure 12. HR-TEM image, reporting the well-disperse Ru-phase and Ru particle size distribution histogram associated with 1.0-Ru/C.*
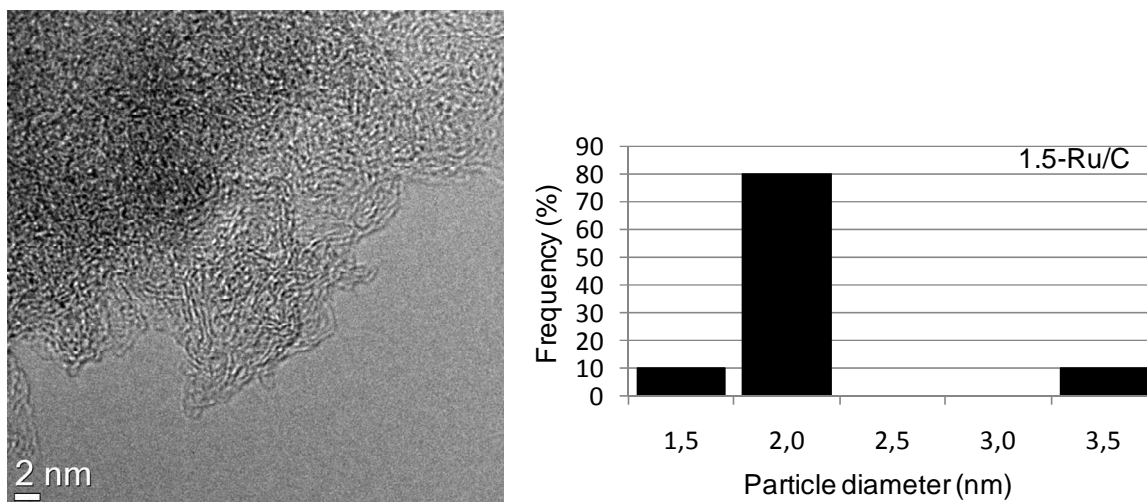
*Figure 13. HR-TEM image, reporting the Ru-phase dispersion and Ru particle size distribution histogram associated with 1.5-Ru/C.*

Taking into account that the ADM conversion over ruthenium containing samples significantly depends on the metal content, HR-TEM analysis indicated the presence of very dispersed ruthenium species over all active carbon supported catalysts. Furthermore, around 1.5% Ru of metal loading was noted a partial agglomeration of metal particles leading to moderate increase of dimension of crystallites. These evidence were consistent with the previously reported XRPD and TPR analysis allowing to theorized that the observed not-proportional catalytic performance in terms of ADM conversion could be assigned to the formation of a different Ru-phase around the 1.5%wt. metal content.

### 4.2.1.4  Study on catalysts deactivation

At this point of the investigation, the killing factor for these Ru-based catalysts must be certainly considered as the low stability showed during the time on stream, with respect to an evidenced remarkable high selectivity for the expected product MVE. In literature, the deactivation of catalysts used in hydrodechlorination processes is attributed to different phenomena such as [15-17]:

- metal sintering

- surface poisoning by HCl

- heavy halogenated carbon deposition and occlusion of the active sites.

Furthermore, the question to be answered was not just why the Ru-based catalysts activity on hydrodechlorination has showed a gradual deactivation with the time on stream, but also why these catalysts have reported a concomitant change into the products distribution. In order to investigate these behaviors revealed on Ru-based catalysts, XRPD, FE-SEM, TPR, $N_2$-adsorption, TPD-MS analysis and various reactivation procedures were tried.

## 4. Activated carbon supported catalysts

First of all, considering the possible deactivation caused by sintering of the active metal phase, XRPD analysis over Ru/C fresh and spent catalysts were carried out. The results for the 1.0%Ru catalysts, were reported on Figure 14 and clearly showed no evidence of increased reflections that could be ascribed to sintered ruthenium phases. Moreover, the obtained patterns of diffraction did not presents any reflections attributable to chlorinated species, excluding chloride or oxychloride formation as poisoned ruthenium phases.
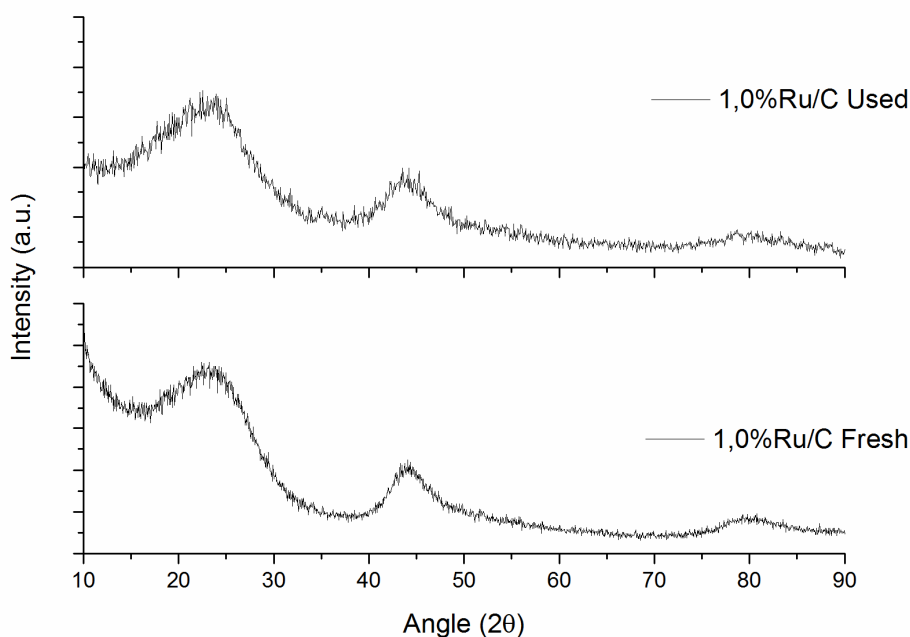


*Figure 14. X-ray diffraction analysis performed over fresh and spent 1.0-Ru/C catalysts.*

As above mentioned, the detection limit of XRPD analysis, did not allow to reveal variations on active phases under 4 nm. FE-SEM were carried out over fresh and spent catalysts with the aim of further investigating a possible sintering phenomena. Figure 15 shows the microscope imaging of 1.0-Ru/C catalyst, both in the fresh state (A) than on the spent state (B). Regarding the fresh catalyst, a well disperse phase of ruthenium particles were observed. On the contrary, over the spent catalyst the ruthenium phase reported a good dispersion but also some greater particles, revealing a slight sintering. These data have suggested the presence of a slight sintering phenomena, but it was not clear if the deactivation observed in catalytic performance could be assigned to.

40
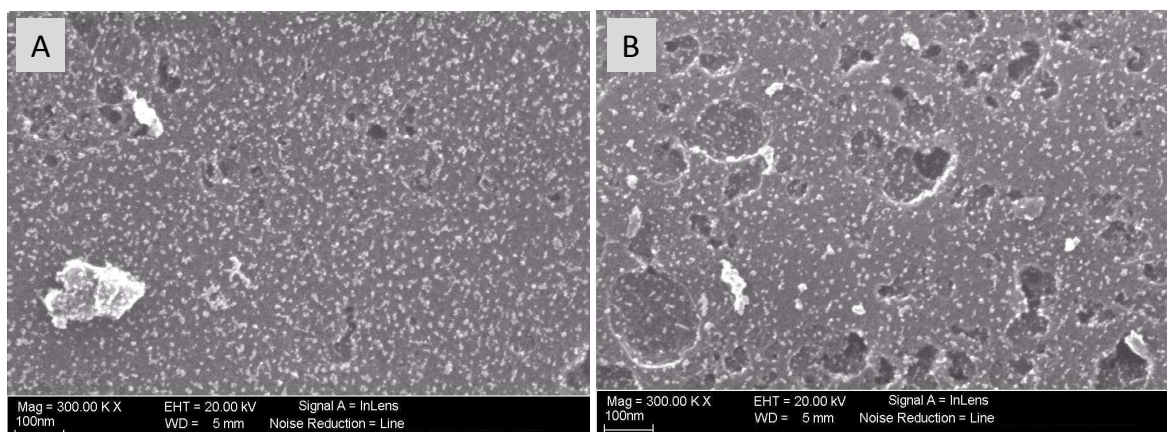
*Figure 15. FE-SEM imaging of fresh 1.0-Ru/C (A) and spent 1.0-Ru/C (B).*

Temperature-programmed reduction analysis, were previously considered in order to obtain information about the different phases over Ru containing catalysts.

Taking into account the observed different ruthenium phases as showed on Figure 10, it can be assumed how the faster deactivation rate (observed over 1.5-Ru/C) could be due to stronger interaction between halogenated species and the different active sites evidenced by this sample, leading to a halogenated species coverage greater with respect to the lower ruthenium content catalysts.

In terms of surface coverage, the performed analysis by $N_2$-adsorption over spent catalysts have showed a loss of surface area from 1041 to 765 $m^2$/g (Table 2). In fact, a significant decrease on surface area were evidenced over all the spent catalyst, which could indicate some kind of organic deposition. Nevertheless, the relationship of this surface area decrease with observed catalyst deactivation is unclear, because also palladium containing samples suffered from similar decrease, but did not evidenced any deactivation phenomena related to the formation of carbonaceous.

In order to obtain information about the reason of deactivation, several regeneration step of Ru-supported catalysts was studied by means of $H_2$ or He thermal treatments during a performed trial (Figure 16).

# 4. Activated carbon supported catalysts
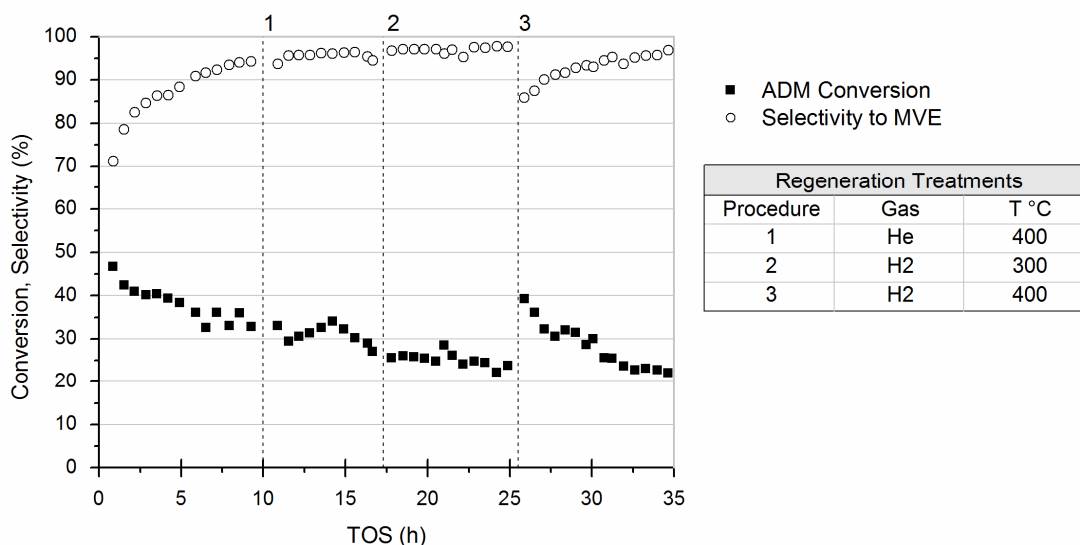


*Figure 16. Effect of different regeneration procedures on ADM conversion (full squares) and selectivity to MVE (empty circles) over 1.0-Ru/C. Reaction conditions: ADM = 16% v/v, contact time = 10s, ADM/$H_2$ molar ratio = 1 and temperature = 250°C.*

Regeneration steps were carried out approximately after 10 hours of reaction at 250°C switching the reactor feed to flowing He or $H_2$ and the catalyst was heated for 2 h at different temperatures (300°C and 400°C). Thus, the system was switched back again to the reaction feed.

Figure 16 reported the obtained results over the 1.0-Ru/C catalyst, showing ADM conversion and selectivity to MVE before and after several treatments. Regeneration steps were revealed to be un-effective when He or $H_2$ were used at low temperature (<400°C), instead of the significant performances recovering after a reductive treatment with $H_2$ at 400°C. However, the regeneration treatment has generated a partial recovery on ADM conversion but also a concomitant decrease on selectivity to MVE due to an increased formation of Cl/H mono-hydrogenated products. These behaviors could suggest a partial recovery of the hydrogenation activity caused by an increase on hydrogen coverage, bringing the surface to similar condition with respect to the beginning of the reaction. The causes of this behavior could be also consider as a temporary unblocking of surface, as above mentioned, occluded by some kind of intermediates strongly interacting with active sites. Nevertheless, the recovered activity on hydrodechlorination was rapidly lost and the trend in ADM conversion has resumed the same rate of deactivation reported before the regenerative treatment, indicating that the treatment with hydrogen temporary improve the cleavage of strong interactions between active sites and halogenated adsorbed species.

With the goal of investigate the nature of the hold-on species over the Ru containing catalysts, several TPR/TPD analysis were performed on spent catalysts, trying to reproduce the above mentioned treatments condition and following the off-gas with a process mass spectrometer able to detect up to 100 AMU. These data evidence the presence of two main adsorbed species over the catalyst surface, at low-temperature ($T_{max} \approx 260°C$), where the desorption was probably due to species physisorbed on active carbon porosity, and at high-temperature ($T_{max} \approx 420°C$), where the desorption was probably due to species strongly bonded to the catalyst surface. The first investigation to deeper the knowledge about these observations was performed with a TPD analysis over spent activated-carbon (without metal active phase) where, only the low-temperature desorbed species were evolved, and thus, were ascribed to physisorbed species into the microporous structure of activated-carbon. Moreover, another investigation with the aim of shedding light over these evidences, was showed on Figure 17. The fragments assignable to carbon support degradation were reported (oxidized evolved gas CO and $CO_2$), even if performed in He flow, at high temperature ($<400°C$).
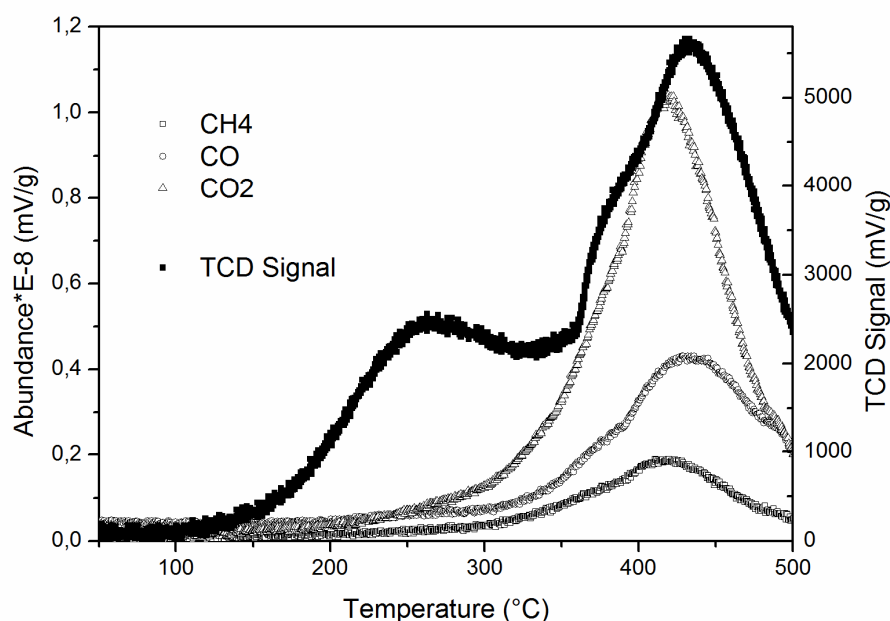


*Figure 17. MS-monitored He-TPD analysis over spent activated-carbon.*

Excluding the mentioned species produced by degradation of carbonaceous support, on Figure 18 were reported the obtained distribution of fragments due to halogenated adsorbed species, performing a desorption analysis in He flow. Various peaks assigned to *CF3, *CF2Cl, *CF2, *COF, and *CFH2 were observed in the temperature range 150-

## 4. Activated carbon supported catalysts

500°C and were formed following the reaction showed on Figure 19. The $*CF_3$ fragment was present from 170°C to 400°C, and may be attributed to trifluorometoxy substituent cleavage, common to reagents ($CF_3OCFClCF_2Cl$) and main products such as $CF_3OCF=CF_2$ and $CF_3OCFClCF_2H$. On the contrary the $CF_2Cl*$ fragment was present only after 350°C, thus were probably due to the thermal decomposition of chemisorbed compounds mainly present in the form of saturated molecules. Moreover, the presence at high temperatures of $*CFH_2$ and $*CF_2$ fragments may be ascribed to the degradation of hydrogenated compounds, which are strongly adsorbed on catalyst surface.
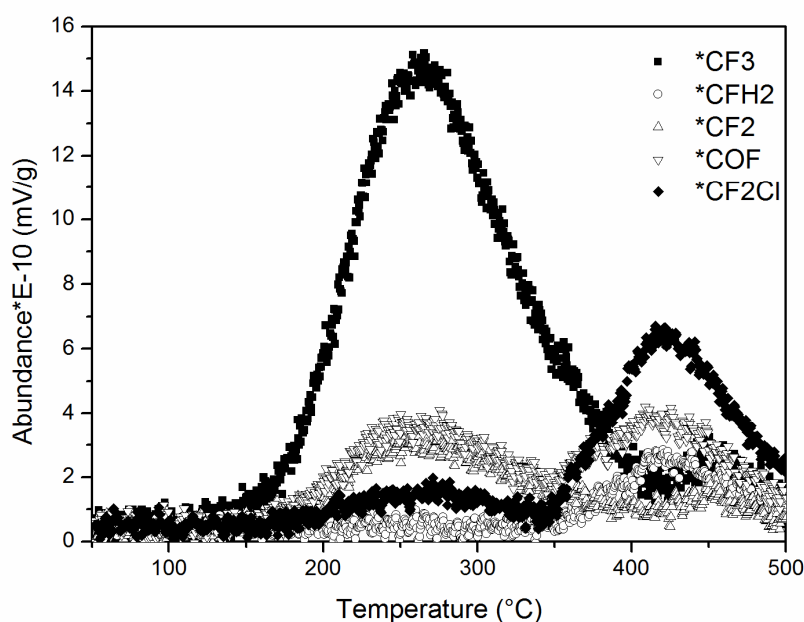


*Figure 18. MS-monitored He-TPD analysis over spent Ru-based catalyst.*
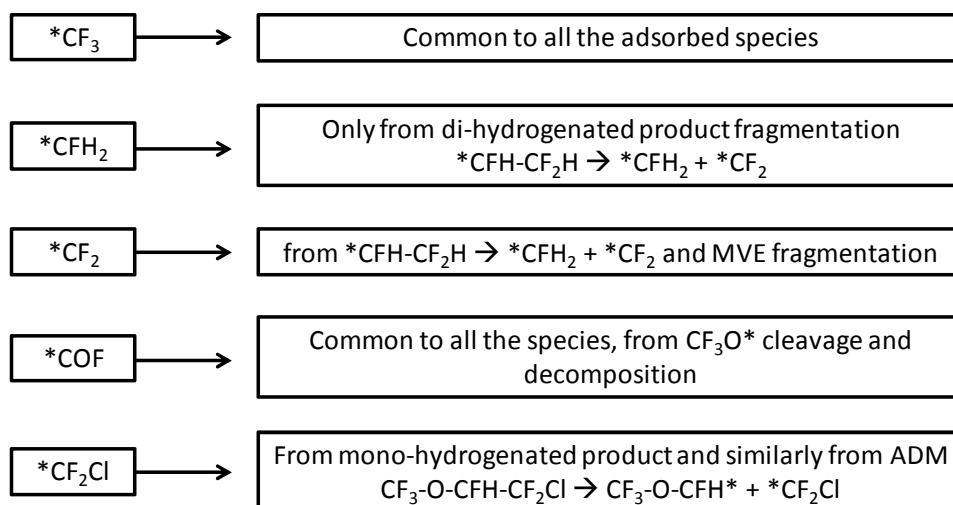


*Figure 19. MS-monitored He-TPD analysis; Identification and assignment of observed fragments.*

When the Ru spent catalyst was analyzed by temperature-programmed method with reducing mixture (5%$H_2$/95%Ar), the adsorbed species were destroyed by thermal degradation and hydrogenolysis at a lower temperature with respect to the treatment of flowing He. The regeneration treatment in He flow probably requires higher temperatures than 400°C to degrade the heavy halogenated compounds that are deposited on catalysts.

Taking into account all the explained evidence, the deactivation of Ru-based catalysts can be ascribed to halogen-containing carbonaceous species accumulated on the Ru surface during the reaction. These species can be partially removed from the surface of the catalyst by hydrogen treatment at high temperature.

In order to conclude this survey on Ru-based catalysts, an overall interpretation of catalytic performance can be proposed.

Hypothesis that:

- ruthenium activity is insufficient on the activation of hydrogen
- [AMH] and [AMH$_2$] are proportional to the amount of activated hydrogen on the surface
- regeneration treatments unblock ruthenium active sites

Introducing:

$$r_{deact.} \propto \frac{[INT]^a}{[H_{ads}]^b} \quad and \quad r_{desorb} \propto [H_{ads}]$$

where:

$r_{deact}$ is used to indicate the deactivation rate observed

a and b are the reaction order, and a > b

INT is used to indicate some strongly interactive species (not the total) formed on the surface

$H_{ads}$ is used to indicate the <u>residual</u> activate hydrogen on the surface

$r_{desorb}$ is used to indicate the desorption velocity from the surface

The hydrodechlorination performed over a high metal content Ru-catalyst, take place on a greater number of active sites and generates a high amount of intermediates adsorbed on the surface of catalyst (high [INT]). As suggested on the hypothesis, an insufficient ability on hydrogen activation, joint to a high $H_{ads}$ consumption (low [$H_{ads}$]), lead to a higher deactivation rate. During the catalytic trial, the insufficient ability in hydrogen activation

45

caused a gradual decrease in desorption rates for the intermediates due to lower availability of hydrogen on the catalyst surface. At the same time, decreasing the free active sites, a gradual decrease in generated intermediates and adsorbed hydrogen make slow the rate of deactivation more than the decreased hydrogen on surface could make the deactivation faster because the [INT] exponent a is greater than the [$H_{ads}$] exponent b.

Based on the same consideration (a > b), catalytic trials performed at higher temperature have reported a higher deactivation rate, in fact, with respect to an thermodynamic increase (even if equal) in formation of [INT] and [$H_{ads}$] the different exponent make the deactivation faster at higher temperature and generally in the case of higher amount of effective interactions.

Regarding the regeneration treatments, obviously, when hydrogen is used as flowing gas increases the amount of activated hydrogen on the surface (there are not competitive chlorinated species in the gas flow) making faster the desorption of blocked intermediates. When the reaction feed was switched back to the reactor, the catalyst presents a larger amount of activated hydrogen (with respect to the equilibrium regulated by competitive interactions during reaction) leading to an improved selectivity to hydrogenated species such as AMH and $AMH_2$. In this case, the deactivation rate after the treatment seems to be higher with respect to the previous observation probably because the cleaned up sites are sterically more favorable to form intermediates strongly adsorbed and responsible for the deactivation.

### 4.2.2 Catalytic performance of Pd-based catalyst

A several number of papers [2,18] identified the Pd-based active phase as an active noble metal in the hydrodehalogenation of $CCl_2F$-$CClF_2$ (CFC-113). Pd-base catalyst, reported on Table 3 is compared on catalytic performance with the same metal content of Ru-catalyst.

| Sample | Description | Metal Content [%wt] | Precursors |
|--------|-------------|---------------------|------------|
| 1,0 Pd | IWI[a] on Activated Carbon (AC2) | 1,0 | $PdCl_2$ |
| 1,0 Ru | IWI[a] on Activated Carbon (AC2) | 1,0 | $RuCl_3$ |

[a] Incipient Wetness Impregnation

*Table 3. Materials and composition of the catalysts involved in the hydrodechlorination study.*

When Pd-based sample was employed for the hydrodechlorination of $CF_3OCFClCF_2Cl$, the initial conversion was greater than Ru-catalysts (Figure 20) and there was no evidence of deactivation during all the trial's time on stream.
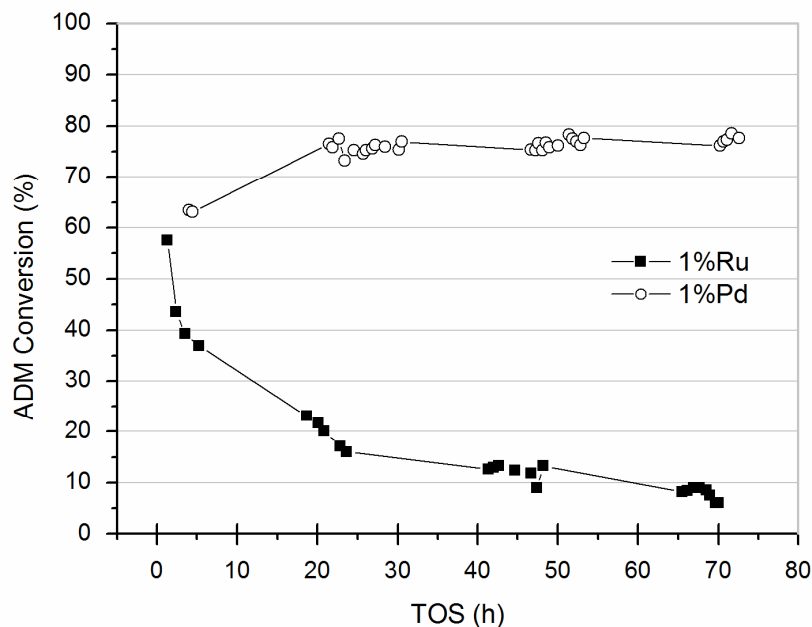


*Figure 20. Catalytic performance in ADM conversion over 1.0-Ru/C and 1.0-Pd/C catalysts. Reaction conditions: ADM = 19%v/v, temperature = 250°C, ADM/$H_2$ molar ratio = 1 and contact time = 10s.*

Observing the high stability of catalytic performance over Pd-catalyst, on the first catalytic trials (not reported), the laboratory equipments were upgraded to be suitable for long run trials. This upgraded lab-scale plant has a larger catalytic bed, lengthening the stabilization time, but allowing the study of longer-term deactivation.

## 4.3 Bi-metallic catalysts

In the last years, a relevant number of catalysts based on noble metals such as rhodium, ruthenium, palladium and platinum have been studied on the hydrodechlorination of different chlorofluorocarbons [19, 20]. One of the key factor to understand the different reactivity of the metals, could be considered as a competitive interaction onto active sites with both hydrogen or halogenated species, that could generated an excess of activated hydrogen on surface of catalysts. The different affinity of metals with hydrogen or halogenated species was explained in terms of their different electronic structure and the physicochemical properties. Another factor which was considered is the halogen exchange activity. Indeed, the hydrodehalogenation reaction could produce a relevant coverage of

halogen on catalyst surface, avoiding a correct exchange between the adsorbed halogen and the adsorbed species (reagents, products or intermediates) leading to side-reactions, destructive cracking and fragmentation, which can decrease the expected product selectivity.

Palladium and platinum based catalysts are very well considered for the hydrodechlorination of different chlorocarbons and chlorofluorocarbons. Indeed, these catalytic systems shows high activity and selectivity to non-chlorinated products [21]. However, in the case of platinum catalysts a not negligible metal leaching, caused by volatility behavior of tetra-chloro coordinated platinum, must be considered. However, both of them, mainly produce a fully hydrogenated compounds, for a rapid hydrogenation of the produced olefin, due to their high capacity to activated $H_2$ [22]. On the contrary, the high energy of absorption of intermediates on Ru-based catalysts leads to problems of deactivation probably due to a lower capacity to activate hydrogen and thus to promote a dissociative desorption of intermediates from catalyst surface.

In order to modify the competitive interaction onto active metal sites with both hydrogen or halogenated species, is possible to formulate a bi-metallic active phases, trying to obtain both the ability to activate hydrogen than the ability to interact with halogenated species [23].

This development was generally accepted as a way to induce a modification on the metal electronic state by the introduction of a second metal. In fact, palladium based catalysts were reported as strongly affected on catalytic performance by the presence of a second component [24]. Nevertheless, it must be noted that the most part of literature deals about CFC's destruction through complete dehalogenation and it is not predictable if this modification is important for the selectivity toward olefin sought on ADM hydrodechlorination reaction [22].

Taking into account these considerations, a series of bi-metallic catalysts was prepared such as Pd/Au, Pd/Ag and Pd/Cu based catalysts.

### 4.3.1 Catalytic performance over Ru/Pd catalysts

Prior to that, a series of catalysts that comes from a different idea was prepared, trying to combine the selectivity to target product, observed on Ru-based catalysts, to the ability of activate and release hydrogen (spillover properties) observed on Pd-based catalysts.

On the basis of this consideration, in order to improve the selectivity to the desired product, Ru/Pd bimetallic catalysts at different metal ratio were prepared and employed in the reaction (Table 4).

| Sample | Description | Metal Content [%wt] | Precursors |
|---|---|---|---|
| $Ru_4Pd_1$ | IWI[a] on AC2, molar ratio 4:1 | 3,2 Ru - 0,8 Pd | $RuCl_3$ - $PdCl_2$ |
| $Ru_8Pd_1$ | IWI[a] on AC2, molar ratio 8:1 | 3,2 Ru - 0,4 Pd | $RuCl_3$ - $PdCl_2$ |

[a] Incipient Wetness Impregnation

*Table 4. Materials and composition of the catalysts involved in the hydrodechlorination study.*

Figure 21 and 22 show the data obtained over the catalyst $Ru_4Pd_1$/C and $Ru_8Pd_1$/C (4/1 and 8/1 Ru/Pd molar ratio). Over this catalysts, Cl/H substitution and hydrogenated by-products were produced in very low amounts, while $CF_3OCF=CF_2$ was formed with very high selectivity. However, as also observed for all ruthenium-based catalysts, the $CF_3OCFClCF_2Cl$ conversion gradually decreased with time on stream, suggesting an active sites covering during reaction. The deactivation phenomena was proportional to the Ru content, indeed, an increase on the Pd molar ratio, can be generally related to the capability of activate hydrogen, favoring the intermediates desorption, as mentioned in the case of mono-metallic Ru-based catalysts.
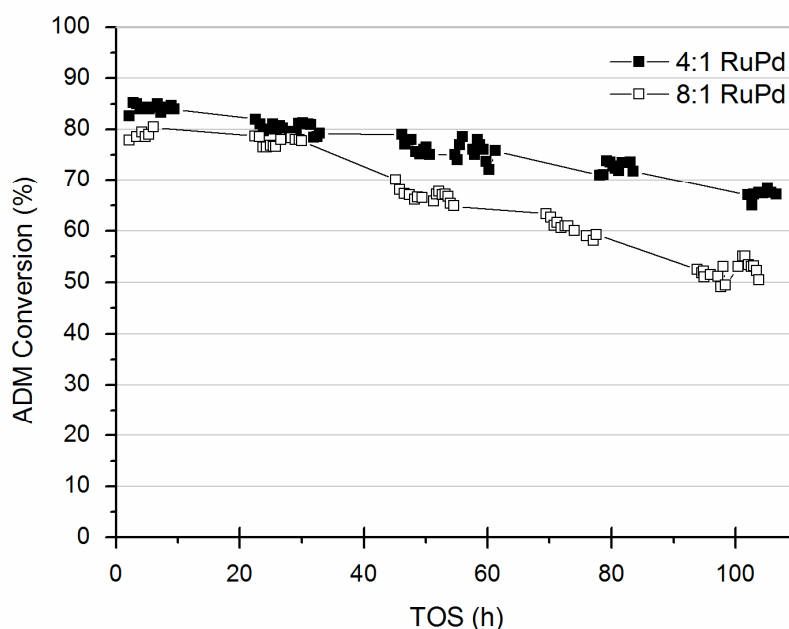


*Figure 21. Catalytic performance in terms of ADM conversion over 4/1 and 8/1 Ru/Pd molar ratio catalysts. Reaction conditions: ADM = 19%v/v, temperature = 250°C, ADM/H₂ molar ratio = 1 and contact time = 10s.*

4. Activated carbon supported catalysts
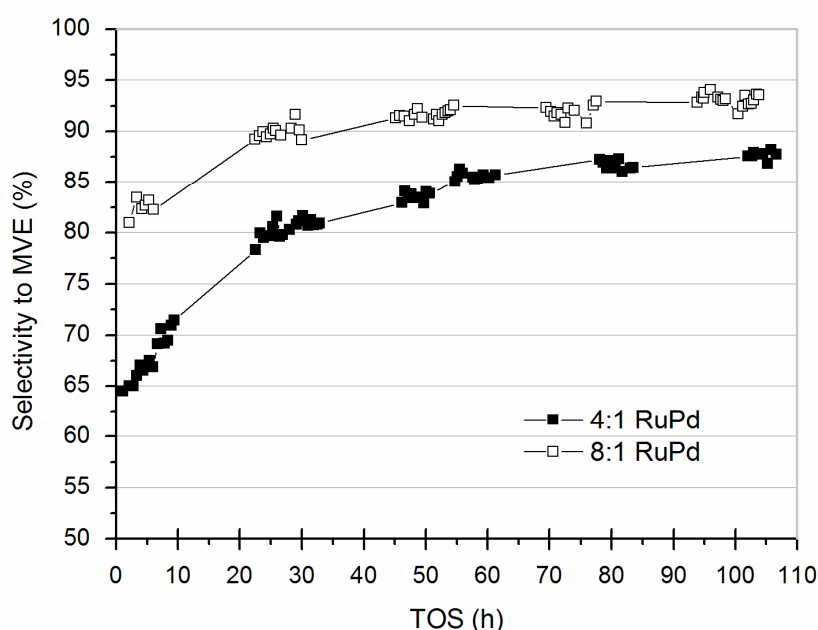


*Figure 22. Catalytic performance in terms of selectivity to MVE, over 4/1 and 8/1 Ru/Pd molar ratio catalysts. Reaction conditions: ADM = 19%v/v, temperature = 250°C, ADM/H$_2$ molar ratio = 1 and contact time = 10s.*

### 4.3.2 Catalytic performance over Pd/Au catalysts

In order to confirm the role of a second metal over the palladium properties in the hydrodechlorination of CF$_3$OCFClCF$_2$Cl, different elements were used in combination with Pd in the active phase. Following the idea of introduce an elements much more interactive with halogenated compounds, various Pd/Au-based catalysts were prepared, which are reported on Table 5.

| Sample | Description | Metal Content [%wt] | Precursors |
|--------|-------------|---------------------|------------|
| 1:1 PdAu | IWI[a] on AC2, molar ratio 1:1 | 1,0 Pd - 1,85 Au | PdCl$_2$ - HAuCl$_4$ |
| 1:2 PdAu | IWI[a] on AC2, molar ratio 1:2 | 1,0 Pd - 3,7 Au | PdCl$_2$ - HAuCl$_4$ |
| 1:4 PdAu | IWI[a] on AC2, molar ratio 1:4 | 1,0 Pd - 7,4 Au | PdCl$_2$ - HAuCl$_4$ |

[a] Incipient Wetness Impregnation

*Table 5. Materials and composition of the catalysts involved in the hydrodechlorination study.*

When molar ratio 1:1 and 1:2 Pd/Au-based catalysts were used on the hydrodechlorination of CF$_3$OCFClCF$_2$Cl, the conversion of ADM ranged between 60 and 80%). The reported conversion for these catalysts increase proportionally with the increase in Au content (Figure 23).
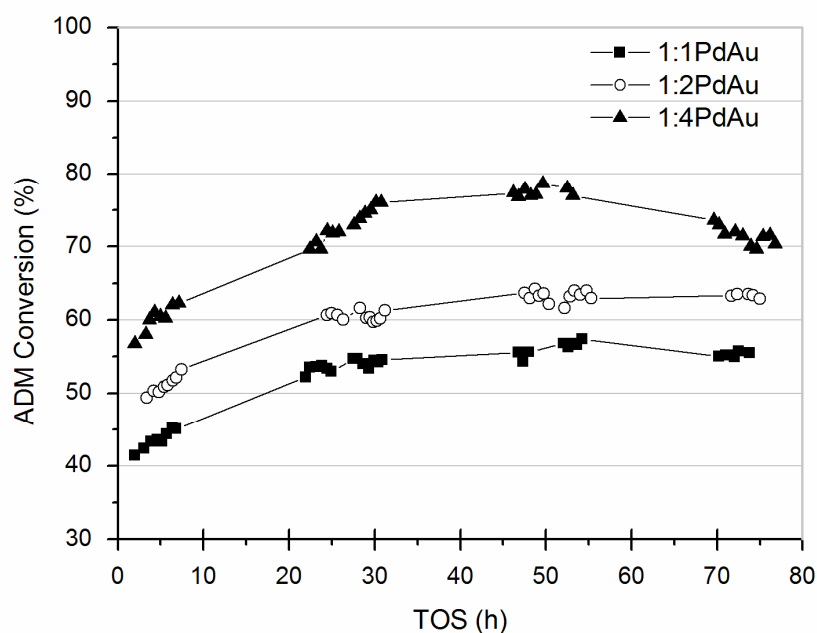
*Figure 23. Catalytic performance in terms of ADM conversion over 1:1, 1:2 and 1:4 Pd/Au molar ratio catalysts. Reaction conditions: ADM = 19%v/v, temperature = 250°C, ADM/H$_2$ molar ratio = 1 and contact time = 10s.*

On the contrary, the observed selectivities to the target product were not proportional to the Au content. Over these catalysts, the Cl/H mono-hydrogenated species were produced without any decrease with the time on stream. Differently with respect to the pure Pd catalyst, the target product selectivity has been decreased by light cracking fragment and a hydrofluoroether identified as CF$_3$OCH=CF$_2$.

The observed different performances in the hydrodechlorination of ADM could be explain considering the structure-sensitive behavior of reaction, mentioned by Mori and coworkers, and considering the effect of hydrochloric acid on Au-containing catalysts [3]. In fact, hydrochloric acid is a well-known sintering agent for gold particles, and this phenomena cannot be excluded during reaction [25]. Figure 24 shows the XRPD characterization analysis carried out over fresh and spent Pd/Au -based catalysts, where several number of diffraction's lines could be attributed to cubic gold phase (PDF 01-089-3697) and palladium hydride (PDF 03-065-0557). Moreover, an increase in the intensity of reflections was clearly observable, and could be related to a sintering phenomena, but the presence of vicinal reflections between the Pd hydride and the Au diffraction patterns didn't allow to apply the Debye-Scherrer Law and calculate the crystallite size.

4. Activated carbon supported catalysts
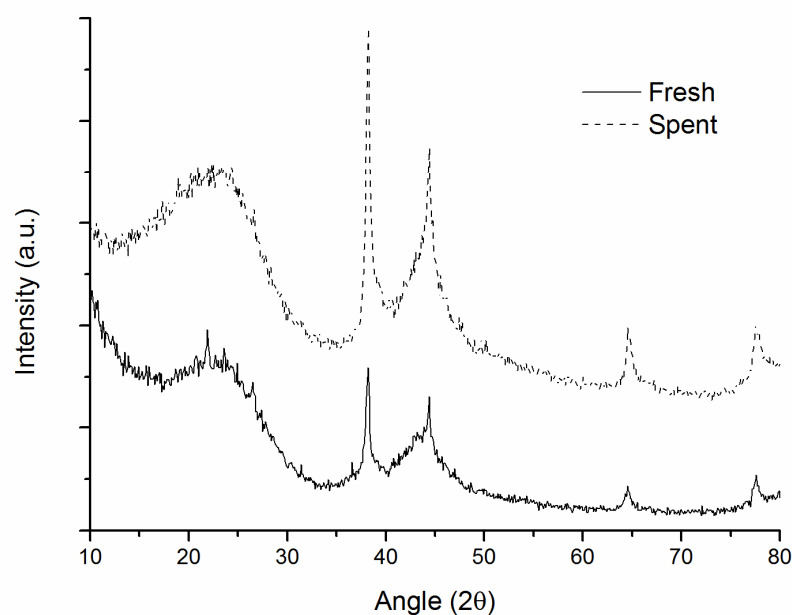


*Figure 24. X-ray diffraction analysis performed over fresh and spent 1:1 Pd/Au molar ratio catalysts.*

### 4.3.3 Catalytic performance over Pd/Ag catalysts

With the aim of investigating the effect of the second component on Pd catalytic performance, a series of Pd/Ag catalysts were prepared by incipient wetness impregnation. In order to avoid precipitation of silver chloride , differently from the others catalysts, Pd were impregnated as nitrate. The Pd/Ag catalysts tested on hydrodechlorination are shown on Table 6.

| Sample | Description | Metal Content [%wt] | Precursors |
|--------|-------------|---------------------|------------|
| 1:1 PdAg | IWI[a] on AC2, molar ratio 1:1 | 1,0 Pd - 1,0 Ag | $Pd(NO_3)_2$ - $AgNO_3$ |
| 1:2 PdAg | IWI[a] on AC2, molar ratio 1:2 | 1,0 Pd - 2,0 Ag | $Pd(NO_3)_2$ - $AgNO_3$ |

[a] Incipient Wetness Impregnation

*Table 6. Materials and composition of the catalysts involved in the hydrodechlorination study.*

The hydrodechlorination of ADM, conducted over Pd/Ag-based catalysts, has reported different results, especially compared to Pd/Au-based catalysts (Figure 25). In fact, respect to the Pd/Au catalysts, increasing the content of the second component, the $CF_3OCFClCF_2Cl$ conversion decreases. Probably, on the hydrodechlorination reactions, Ag has an own activity lower than Au, so introducing Ag to Pd can lead to the expected electronic modification of palladium atoms but gave rise to a conversion decrease.
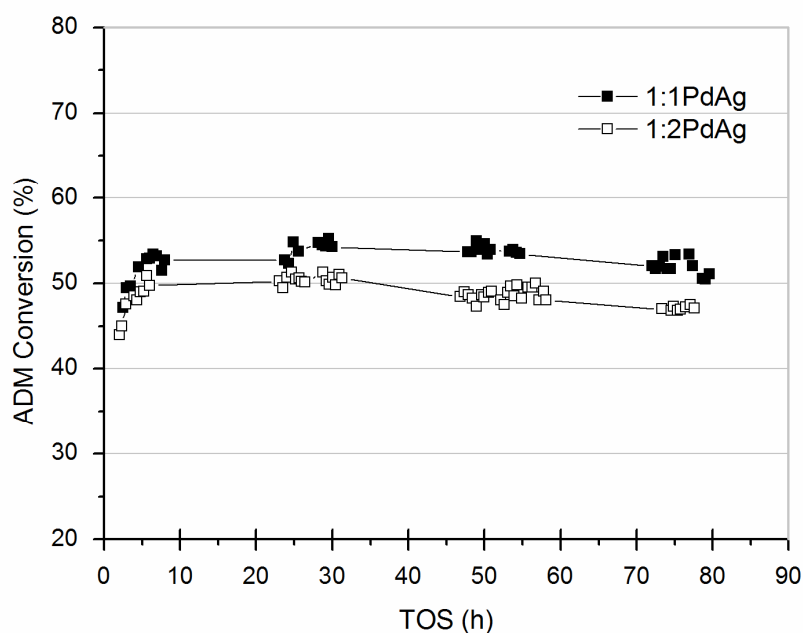
*Figure 25. Catalytic performance in terms of ADM conversion over 1:1 and 1:2 Pd/Ag molar ratio catalysts. Reaction conditions: ADM = 19%v/v, temperature = 250°C, ADM/H$_2$ molar ratio = 1 and contact time = 10s.*

Figure 26 shows the catalytic performance in terms of selectivity to the expected product for the Pd/Ag -based catalysts. First of all, differently with respect to the previously reported catalysts, this materials have reported a transient time to achieve the steady-state in terms of selectivity that has exceed the entire trial time on stream. During all the test, the selectivity to the expected product increased with time on stream, from an initial value around 50% to 80%. 1:1 Pd/Ag and 1:2 Pd/Ag have reported similar performances, with a slight difference from the fiftieth hours, reporting a final higher selectivity for the high Ag-contend catalyst, 1:2 Pd/Ag. Taking into account the previously reported performance for the Pd-based catalyst, the introduction of Ag to the Pd-containing active phase produce a general decrease of by-product formation (Figure 27), more preeminent for the de-fluorinated product CF$_3$OCCl=CF$_2$ (AMH*).
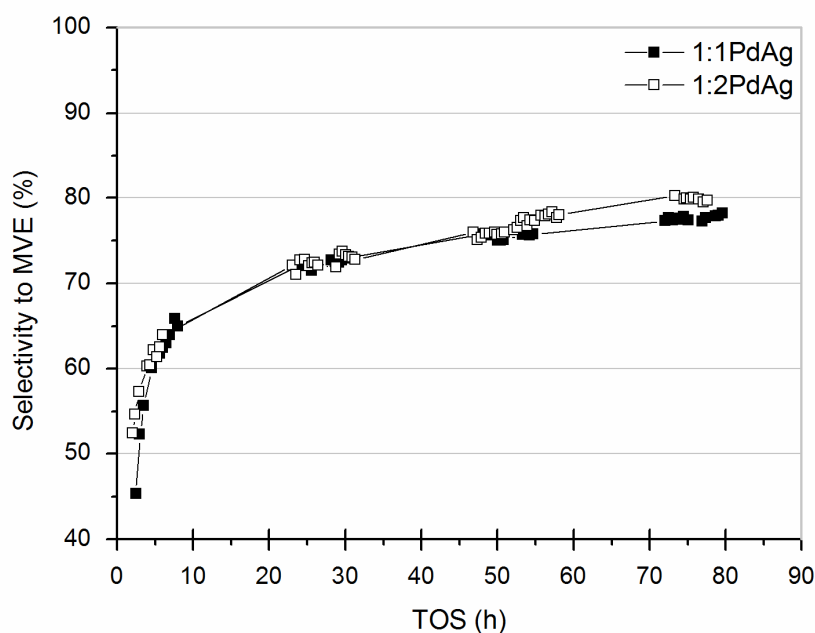
*Figure 26. Selectivity to MVE over 1:1 and 1:2 Pd/Ag molar ratio catalysts. Reaction conditions: ADM = 19%v/v, temperature = 250°C, ADM/H₂ molar ratio = 1 and contact time = 10s.*

The observed properties of Pd/Ag active phases on catalyzing hydrodechlorination reaction could be explained considering the key factor of activity: the ability in hydrogen activation. In fact, differently with respect to the others bimetallic Pd containing active phases, the introduction of silver make greater the hydride formation enthalpy. Figure 28 shows relationships between the heat of hydride formation and the alloying effect with the content of second metal. This figure shows an approximately linear trend where the heat of formation decreases introducing Cr, Co, Ni, Cu, Rh, Pt and Au. When the fraction of Ag increase, on the other hand, the heat of formation increase leading to a more stable hydride. Taking into account this evidence, reported in literature by Hara and co-workers, the formed hydride species over Pd/Ag - based catalysts could be considered more stable. With regard to the catalyst performance in terms of selectivity to perfluoromethylvinylether, it seems to be clear that this active phase containing Pd and Ag, stabilizing a strong interaction with hydrogen, gives rises to less hydrogenated products [26]. Considering this, the greater enhancement on the expected product selectivity, could be considered related to hydrogenated products, but is not the whole truth. The largest contribution in increase the target product selectivity depends on a great decrease in the formation of de-fluorinated product $CF_3OCCl=CF_2$ (AMH*), probably due to a decrease in the strength of the interactions with the halogenated species (Figure 27). In fact, a C-F cleavage results more

difficult to be achieve when the interactions between active sites and species are less strong.
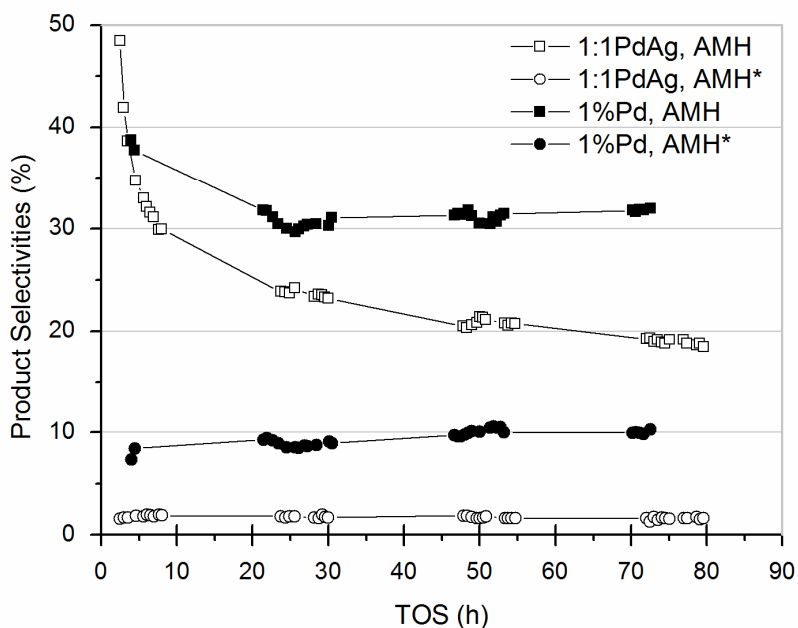


Figure 27. Comparison in hydrogenated and defluorinated products between 1.0-Pd/C and 1:1 Pd/Ag molar ratio catalysts. AMH (CF₃OCFHCF₂Cl or CF₃OCFClCF₂H) and CF₃OCCl=CF₂ (AMH*) are shown.
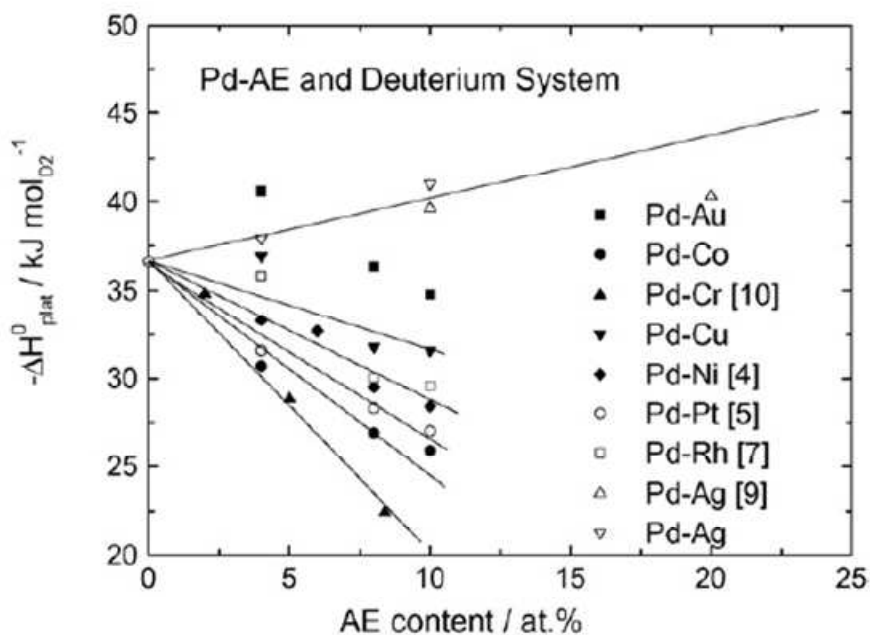


Figure 28. Change in the heat of hydride formation by Pd-AE alloys against AE contents [26].

### 4.3.4 Catalytic performance over Pd/Cu catalysts

A previously mentioned paper, by d'Itri and co-workers, consider the role of each metals into a bimetallic Pt/Cu based catalysts for the hydrodechlorination of 1,2-dichloroethane. The interactions with hydrogen and halogenated species could be respectively attributed to the noble metal and copper.

#### 4.3.4.1 Effect of active phase composition on catalytic activity

In order to complete the survey of possible electronic state modification on Pd-based catalysts, the introduction of copper has been considered, also for the well-known activity on oxychlorination reaction. Table 7 reports the Pd/Cu -based catalysts prepared and used on reaction.

| Sample | Description | Metal Content [%wt] | Precursors |
|--------|-------------|---------------------|------------|
| 1:1 PdCu | IWI[a] on AC2, molar ratio 1:1 | 1,0 Pd - 0,6 Cu | $PdCl_2$ - $CuCl_2$ |
| 1:2 PdCu | IWI[a] on AC2, molar ratio 1:2 | 1,0 Pd - 1,2 Cu | $PdCl_2$ - $CuCl_2$ |
| 1:4 PdCu | IWI[a] on AC2, molar ratio 1:4 | 1,0 Pd - 2,4 Cu | $PdCl_2$ - $CuCl_2$ |

[a] Incipient Wetness Impregnation

*Table 7. Materials and composition of the catalysts involved in the hydrodechlorination study.*

The hydrodechlorination reaction performed over Pd/Cu -based catalysts have reported very high value of ADM conversion for all the molar ratio, between metals, investigated (Figure 29). The introduction of copper to the active phase seems to enhance not only the selectivity (as explained below) but also the equilibration rate on the transient time to achieve the steady-state. Indeed, to an higher amount of copper, correspond a faster equilibration, especially in the case of 1:4 Pd/Cu catalyst which is shown stable after just 5 hours with respect to the 25-30 hours of the catalysts with low Cu-content. On the other hand, as in the case of ruthenium catalysts, it's worth noting an initial evidence of deactivation for the higher Cu-content catalysts. Regarding the absolute values in terms of ADM conversion, and considering the intention to decrease the hydrogenation ability of palladium active sites, it seems surprising that all the Pd/Cu -based catalysts have shown higher values in ADM conversion with respect to the pure Pd-containing catalyst.
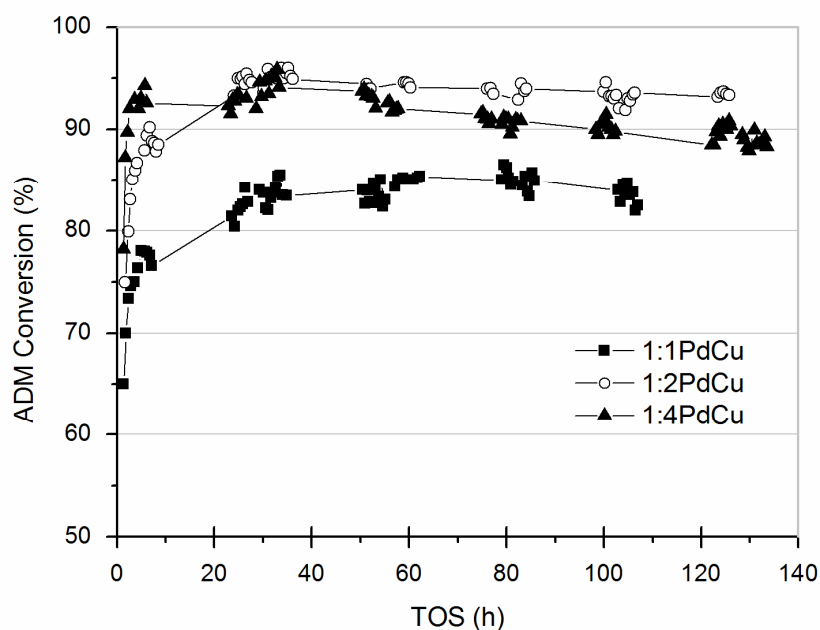
*Figure 29. Catalytic performance in terms of ADM conversion over 1:1, 1:2 and 1:4 Pd/Cu molar ratio catalysts. Reaction conditions: ADM = 19%v/v, temperature = 250°C, ADM/H$_2$ molar ratio = 1 and contact time = 10s.*

When the hydrodechlorination were performed over Pd/Cu -based catalysts the expected product was produced as main species with trace amounts of Cl/H mono-hydrogenated and de-fluorinated products (Figure 30). In the case of 1:2 Pd/Cu and 1:4 Pd/Cu catalysts, the selectivity to the expected product were closed to 90%. As previously mentioned and explain in details, in the case of Ru-containing catalysts, the hydrogen coverage seems to have a great influence in desorption of intermediates, reacting with adsorbed species leading to hydrogenated molecules, but also favoring the desorption rate and indirectly some deactivation phenomena. The increase of Cu-content on the active phases, probably introduce an electronic modification in palladium atoms, which have been revealed to be poorly active in hydrogen activation and probably in the well-known palladium behavior of spillover [27].
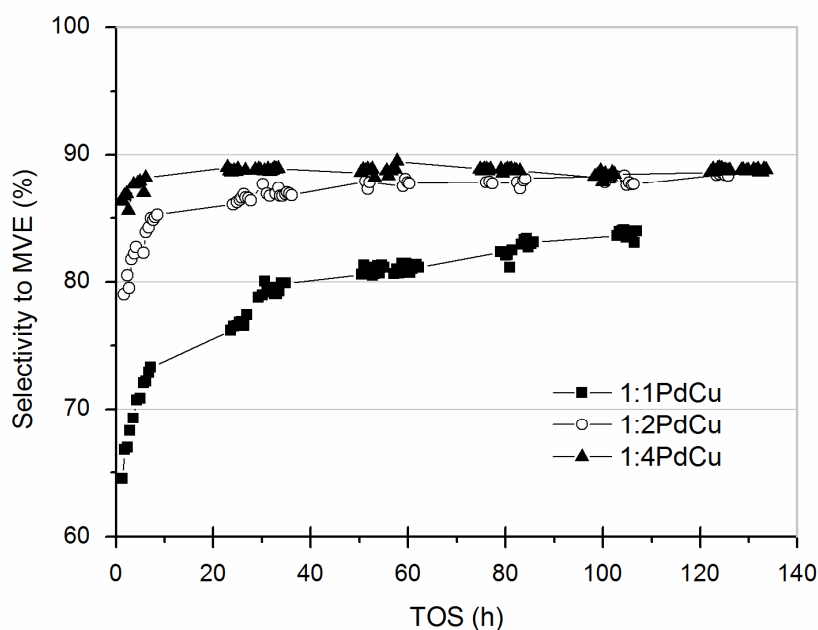
*Figure 30. Selectivity to MVE over 1:1, 1:2 and 1:4 Pd/Cu molar ratio catalysts. Reaction conditions: ADM = 19%v/v, temperature = 250°C, ADM/H$_2$ molar ratio = 1 and contact time = 10s.*

### 4.3.4.2 Effect of metal precursors on catalytic activity

In order to optimize the catalyst preparation procedures, some different kind of metal precursors were involved in catalyst synthesis and in the reactivity survey, summarized on Table 8.

| Sample | Description | Metal Content [%wt] | Precursors |
|--------|-------------|---------------------|------------|
| Chlorides | IWI[a] on AC2, molar ratio 1:2 | 1,0 Pd - 1,2 Cu | PdCl$_2$ - CuCl$_2$ |
| Nitrates | IWI[a] on AC2, molar ratio 1:2 | 1,0 Pd - 1,2 Cu | Pd(NO$_3$)$_2$ - Cu(NO$_3$)$_2$ |
| AcAc | IWI[a] on AC2, molar ratio 1:2 | 1,0 Pd - 1,2 Cu | AcetylAcetonates |

[a] Incipient Wetness Impregnation

*Table 8. Materials and composition of the catalysts involved in the hydrodechlorination study.*

For all the studied precursors, a target molar ratio between metals were decided, as 1:2 Pd/Cu. Regarding the metallorganic acetyl acetonates complex, differently with respect to the other, the impregnation procedures were carried out using a toluene/ acetic acid solution of precursors. When this catalysts were used in reaction, the obtained value of ADM conversion were similar to the chloride-prepared catalyst. On the contrary, in terms of selectivity to MVE, the chloride-prepared catalyst have reported values slightly higher with respect to the acetyl acetonate-prepared catalyst.

For graphical reason, this last one catalyst, was omitted because the trial time on stream was too short (just 30 hours) and the performance obtained mainly coincident with the chloride-prepared catalyst. Moreover, materials and procedures involved in the preparation of acetyl acetonates-containing catalysts were respectively much more expensive and difficult to be performed, nullify the interest in industrial optics.

On the basis of these considerations, on Figure 31 are reported the results obtained for chloride-prepared and nitrate-prepared catalysts. In terms of ADM conversion, these catalysts revealed differences, not only in the absolute value, but also on the transient time to reach the steady-state, which seems to be achieved after fifty hours differently with respect to the chloride-prepared catalysts (stable after 25 hours).
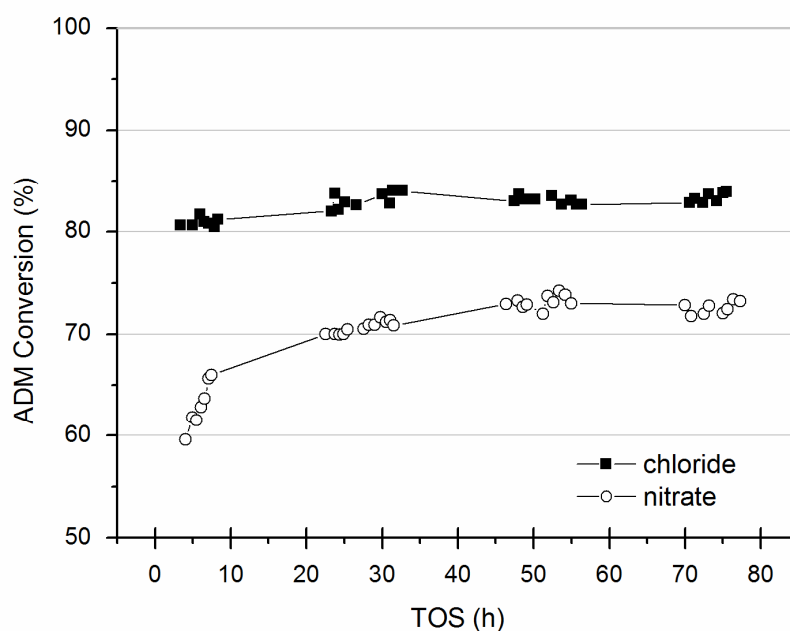


*Figure 31. Catalytic performance in terms of ADM conversion over 1:2 Pd/Cu molar ratio catalysts, prepared using different precursors. Reaction conditions: ADM = 19%v/v, temperature = 250°C, ADM/$H_2$ molar ratio = 1 and contact time = 10s.*

Observing the obtain results in terms of selectivity to the expected product, shown on Figure 32, some consideration about catalyst's performance could be expressed. First of all, it's worth note that the Y-axis scale is more enlarged, because the difference between this materials could be considered thin but significant. Differently with respect to the others discussed comparisons, in this case, after the reductive treatment, from the metal content point of view these catalyst ere equal. The nitrate-prepared catalysts have reported a slightly lower selectivity to MVE, increasing during all the test time with time on stream much more than the chloride-prepared catalyst, suggesting a continuative modification of

59

## 4. Activated carbon supported catalysts

the active sites. In order to understand the reasons behind these differences, on Figure 33 are reported the main by-product selectivities, where is possible to observe how the Cl/H mono-substituted product (labeled AMH) is responsible for the lower selectivity at the beginning of the catalytic trial.
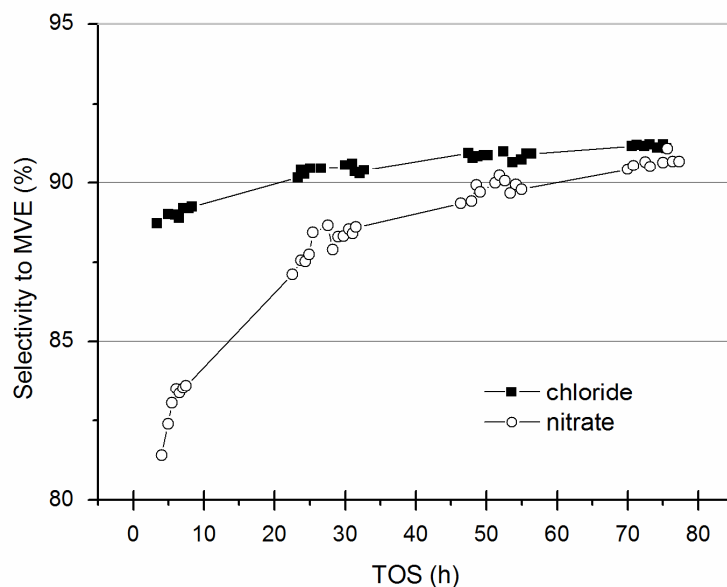


Figure 32. Selectivity to MVE over 1:2 Pd/Cu molar ratio catalysts, prepared using different precursors. Reaction conditions: ADM = 19%v/v, temperature = 250°C, ADM/H$_2$ molar ratio = 1 and contact time = 10s.
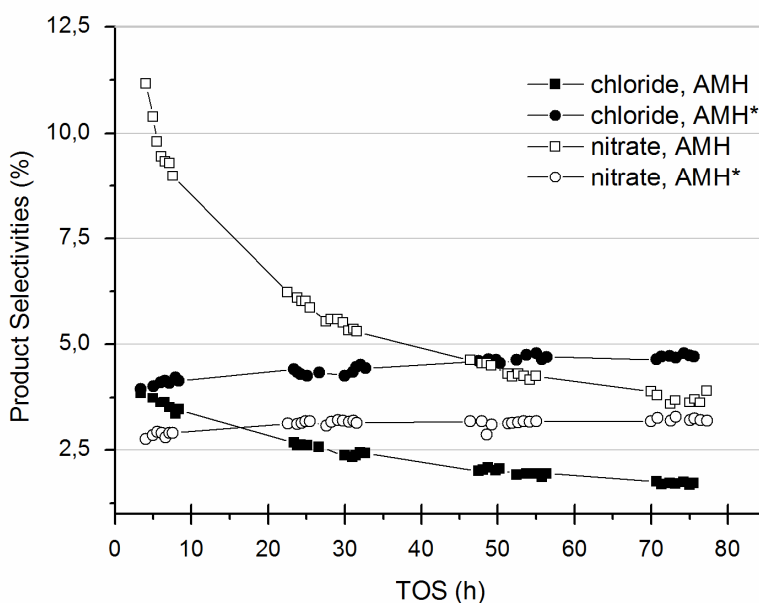


Figure 33. Comparison in hydrogenated and defluorinated products over 1:2 Pd/Cu molar ratio catalysts, prepared using different precursors. AMH (CF$_3$OCFHCF$_2$Cl or CF$_3$OCFClCF$_2$H) and CF$_3$OCCl=CF$_2$ (AMH*) are shown.

Taking into account all the previous considerations and the observed results, an overall hypothesis can be proposed, which provides a possible explanation for this effect of precursor. Several times in the course of this study were highlighted the importance about the hydrogen coverage, the competitive absorption of halogenated species on the active sites. Substantially, the structure sensitive behavior starts with the effective distribution of halogenated species and hydrogen over the surface of catalysts. When different metal precursors were used to prepare catalysts, different crystallite (dimension, orientation and interaction with the surface) were formed. Indeed, the nitrate-prepared catalyst reported a lower ability to interact with halogenated species (on the other hand, a higher interaction with hydrogen) and consequently a lower ADM conversion, a lower interaction with ADM and thus a lower C-F bond cleavage (lower selectivity to AMH*, because C-F bond is more strong than C-Cl bond) and a higher formation of Cl/H mono-substituted product caused by a greater hydrogen coverage of the catalyst surface.

Concluding, the nitrate-prepared catalysts have reported an increase of selectivity to MVE, during all the test time with time on stream caused by an initial greater distribution in hydrogen with respect to the chloride-prepared catalyst.

XRPD analysis were performed over the Pd/Cu-based catalysts in order to observe different phases and eventually, calculate the crystallite size, but no reflects were evidenced together with the activated-carbon amorphous background (Figure 34).
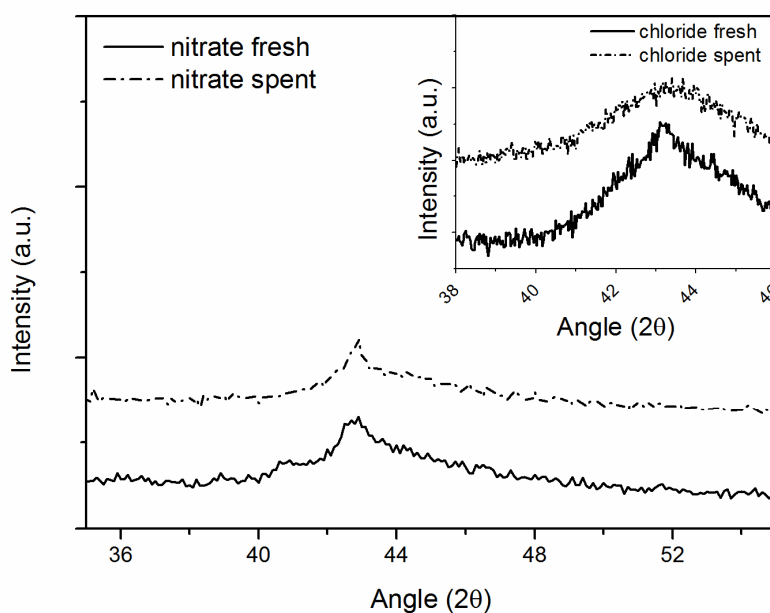


*Figure 34. XRPD analysis performed over the Pd/Cu-based catalyst prepared using nitrate-precursors and Pd/Cu catalyst prepared using chloride-precursors (inlay figure).*

### 4.3.4.3 Effect of contact time on catalytic activity

In order to better understand the nature of the observed byproducts and the pathway of reactions, some catalytic trials were conducted with different contact time, such as 2.5, 5 and 10 seconds.

As above explained, a target molar ratio between metals were decided, as 1:2 Pd/Cu.

Thus, when the obtained results were analyzed, it was immediately clear how the contact time could influence the absolute value of ADM conversion, limiting the time allowed to the course of the reaction. Obviously as expected, the more was high the contact time, the more were high the values of conversion reported. Observing the performance trends over this catalyst, on Figure 35, it must be noted how this catalytic system have been stable and performant since the first hours of reaction, on each contact time conditions.
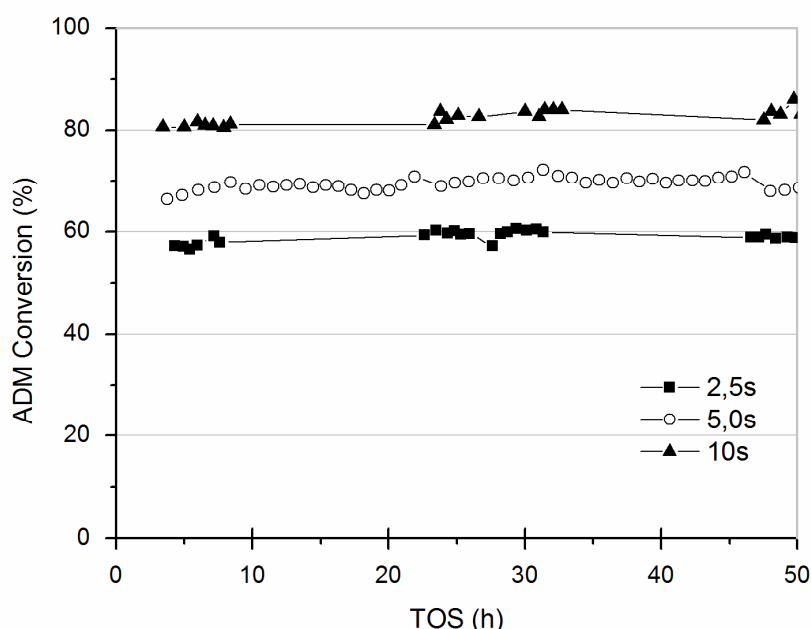


*Figure 35. Catalytic performance in terms of ADM conversion over 1:2 Pd/Cu molar ratio catalyst, tested with different contact times. Reaction conditions: ADM = 19%v/v, temperature = 250°C, ADM/H₂ molar ratio = 1 and contact time = 10, 5 and 2.5 s.*

Observing the results in terms of selectivity to MVE (Figure 36), is interesting to highlight that the best performance has been reported in the trial conducted at lower contact time. Trials conducted at 5 and 10 seconds have reported the same performance, except a small difference at high time on stream, where the trial carried out at 10 seconds had slightly better values. Figure 37 shows the obtained values in terms of selectivity to AMH, the main by-product evidenced, completely in agreement with the trends observed for the selectivity to MVE. On the bases of these considerations and which is reported on Figure

37, is possible to hypothesis that the expected product (MVE) and the Cl/H mono-substituted product (AMH) were formed over different active sites, characterized by different interactions with halogenated species and able to stabilize different intermediates, and obviously different turn over frequency. In fact, according to the previous explained reaction mechanisms, the production of MVE is consequent to the formation of an intermediate like $CF_3O^*CF\text{-}CF_2^*$, bound in a bi-dentate structure, and probably easily desorbed as MVE. On the other hand, the evolution to the main by-product AMH is consequent to the formation of an intermediate like $CF_3O^*CF\text{-}CF_2Cl$ or $CF_3OCClF\text{-}CF_2^*$ which evolves into a cyclic structure with six atoms, probably hardly desorbable from the catalyst surface.
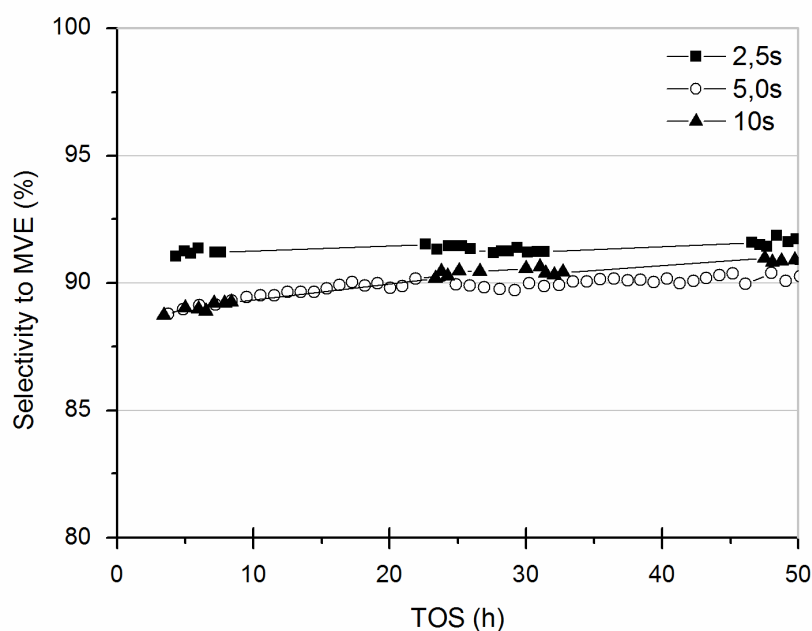


Figure 36. Selectivity to MVE over 1:2 Pd/Cu molar ratio catalyst, tested with different contact times. Reaction conditions: ADM = 19%v/v, temperature = 250°C, ADM/H₂ molar ratio = 1 and contact time = 10, 5 and 2.5 s.
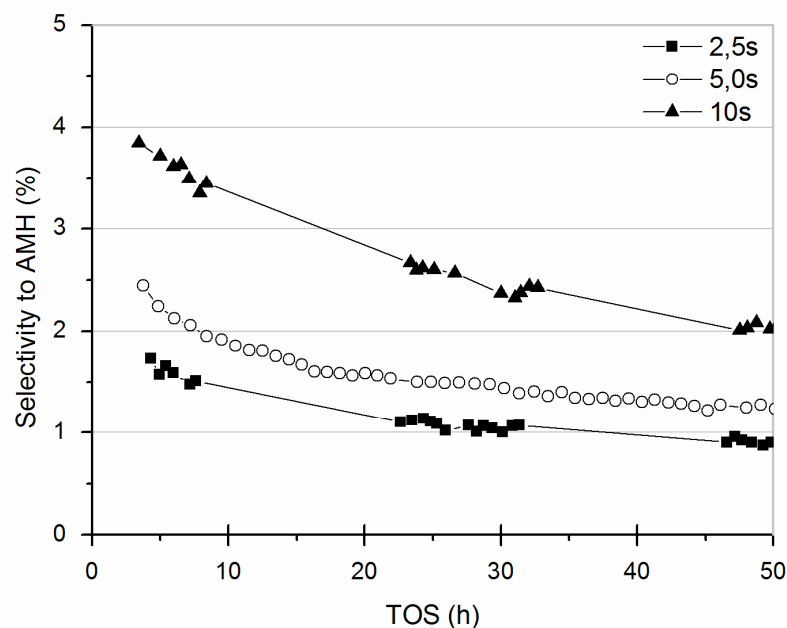
*Figure 37. Effect of contact time in the selectivity to AMH over 1:2 Pd/Cu molar ratio catalyst.*

## 4.4 Conclusions

Activated carbon supported metal catalysts were widely studied on the dechlorination of $CF_3OCFClCF_2Cl$ to $CF_3OCF=CF_2$ in the presence of hydrogen. This part of the research, was mainly focused on evaluating the different catalytic performance of various active phases, mono- and bi- metallic, and allowed to evidence the key factors that the catalyst must possess. All studies catalysts yielded the target product, and the best performing in terms of selectivity to perfluoromethylvinylether, resulted Ru-based catalysts; however, factors including hydrogen coverage of the catalyst surface, stability and deactivation of the catalyst are to be considered in the catalyst's choice.

Pd-based catalysts showed high stability in terms of ADM conversion, and seem not to be affected by desorption problems, and as a consequence, by active sites blocking.

Taking into account all the evidenced performances it seems to be clear that the best collection of properties could be possessed by a bimetallic catalysts, such as the first explored Pd/Ru -based one. Carrying out a series of catalytic trials over Pd/Ru and Pd/IB elements, the long-term selectivity and stability of Pd/Ru and Pd/Cu bimetallic catalysts were observed.

In conclusion, Pd/Ru and Pd/Cu bimetallic catalysts could be employed in the gas-phase hydrodechlorination of ADM, with high selectivity and high conversion.

**References**

[1] M. Gregori, G. Fornasari, G. Marchionni, V. Tortelli, S. Millefanti, S. Albonetti, *Appl. Catal. A: General* **470** (2014) 123-131.

[2] S. Millefanti, V. Tortelli, G. Marchionni, **WO Patent 150091** (2009) assigned to Solvay Solexis S.p.A. [IT/IT].

[3] T. Mori, T. Yasouka, Y. Morikawa, *Catal. Today* **88** (2004) 111-120.

[4] V. I. Avdeev, V. I. Kovalchuk, G. M. Zhidomirov, J. L. d'Itri, *J. Struct. Chem.* **48** (2007) S171-S180.

[5] E.J. Shin, A. Spiller, G. Tavolaris, M. A. Keane, *Phys. Chem. Chem. Phys* **1** (1999) 3173-3181.

[6] C. Amorim, M.A. Keane, *J. Colloid Interf. Sci.* **322** (2008) 196-208.

[7] C. Amorim, M.A. Keane, *J. Hazard. Mater.* **211-212** (2012) 208-217.

[8] K.V.R. Chary, C.S. Srikanth, V. V. Rao, *Catal. Comm.* **10** (2009) 459-463.

[9] W. Juszczyk, A. Malinowski, Z. Karpinski, *Appl. Catal. A General* **166** (1998) 311-310.

[10] L. Li, L. Qu, J. Cheng, J. Li, Z. Hao, *Appl. Catal. B: Environmental* **88** (2009) 224-231.

[11] S.Y. Huang, S.M. Chang, C.T. Yeh, *J. Phys. Chem. B* **110** (2006) 234-239.

[12] P. Betancourt, A. River, R. Hubaut, C.E. Scott, J. Goldwasser, *Appl. Catal. A: General* **170** (1998) 307-314.

[13] P.G.J. Koopman, A.P.G. Kieboom, H. van Bekkum, *J. Catal.* **69** (1981) 172-179.

[14] C. Zhou, Y. Zhu, H. Liu, *J. Rare Earth* **28** (2010) 552-555.

[15] T. Janiak, J. Okal, *Appl. Catal. B: Environmental* **92** (2009) 384–392.

[16] B. Heinrichs, F. Noville, J.P. Schoebrechts, J.P. Pirard, *J. Catal.* **220** (2003) 215–225.

[17] T. Lopez, A. Lopez-Gaona, and R. Gomez, *Langmuir* **6** (1990) 1343-1346.

[18] R. Ohnishi, W. Wang, M. Ichikawa, *Appl. Catal. A: General* **113** (1994) 29-41.

[19] M.A. Alvarez-Montero, L.M. Gomez-Sainero, J. Juan-Juan, A. Linares-Solano, J.J. Rodriguez, *Chem. Eng. J.* **162** (2010) 599–608.

4. Activated carbon supported catalysts

[20] M. Legawiec-Jarzyna, A. Srebowata, W. Juszczyk, Z. Karpinski, *React. Kinet. Catal. L.* **87** (2006) 291–296.

[21] M. Martin-Martinez, L.M. Gómez-Sainero, M.A. Alvarez-Montero, J. Bedia, J.J. Rodriguez, *Appl. Catal. B: Environmental* **132-133** (2013) 256-265.

[22] V. I. Kovalchuk, J. L. d'Itri, *Appl.Catal. A: General* **271** (2004) 13–25.

[23] L.S. Vadlamannati, V.I. Kovalchuk, J.I. d'Itri, *Catal. Lett.* **58** (1999) 173-178.

[24] B. Coq, F. Figueras, *J. Mol. Catal. A: Chemical* **173** (2001) 117-134.

[25] M. Conte, C.J. Davies, D.J. Morgan, A.F. Carley, P. Johnson, G.J. Hutchings, *Catal.Lett.* **144** (2013) 1-8.

[26] M. Hara, L. Wan, M. Matsuyama, K. Watanabe, *J. Alloys Compd* **428** (2007) 252-255.

[27] A.D. Lueking, R.T. Yang, *Appl.Catal. A: General* **265** (2004) 259-268.

# Chapter 5

## 5   Mesoporous silicate supported catalysts

### 5.1   Introduction

We demonstrated in the previous chapter that Pd/Cu on carbon are eligible catalysts for the hydrogen assisted gas-phase dechlorination of $CF_3OCFClCF_2Cl$ to produce $CF_3OCF=CF_2$. Nevertheless, the microporous texture of the activated carbon support can significantly limit possible applications of this catalytic system, because of reduced mass transfer. Supports with larger pores will overcome the drawbacks and, in particular, MCM-41 silicate mesoporous materials can be used as alternative. $SiO_2$ has been used as support for hydrodechlorination processes since it seems to be suitable in terms of inertness against HCl. MCM-41 materials, constituted by an hexagonal arrangement of silica mesopores, display higher surface area than conventional $SiO_2$ and appreciable resistance to strong acids, hence, they could be an interesting alternative to conventional supports. The inclusion of monometallic Pd or Cu active species on MCM-41 structure can be performed by impregnation, ion-exchange, anchoring or direct introduction of the ions of the metal into the MCM-41 framework.

In this part of the work several heterogeneous metal catalysts supported on mesoporous silicate MCM-41 were prepared by impregnation or incorporation of the Pd and Cu active species during the MCM-41 synthesis, and studied on the hydrodechlorination of $CF_3OCFClCF_2Cl$ (ADM) in the presence of hydrogen. The hydrodechlorination activities of catalysts containing Pd and Cu were investigated at different metal content, different introduction method for metal precursors and also utilizing different silica source (sodium silicate or TEOS). The main purpose of the first part of the investigation is to provide a relationship between the various procedures used during the synthesis and the properties of the final material, while in the second part the catalytic performances of the catalysts prepared are examined.

### 5.2   Synthesis of MCM-41 supports

Since their development in 1991, several methods and silica sources suitable to prepare the mesophase called MCM-41 were proposed. Sodium silicate and tetraethyl orthosilicate were used as precursors and cetyltrimethylammonium bromide as surfactant, modifying

 the previously reported synthesis, by Beck for the sodium silicate based materials and by Cassiers for tetraethyl orthosilicate based materials [1, 2].

The synthetic methodology used for preparing an ordered mesoporous silicate is composed by different steps, such as the preparation of the gel, a hydrothermal treatment and finally the removal of the organic template, which also favors a structural stabilization of the obtained materials [3]. Various procedures within these steps have been proposed over the years, enriching the range of procedures useful for the preparation of the MCM-41 [4]. Scheme 1 reports the typical steps utilized in the synthesis of MCM-41 structure.
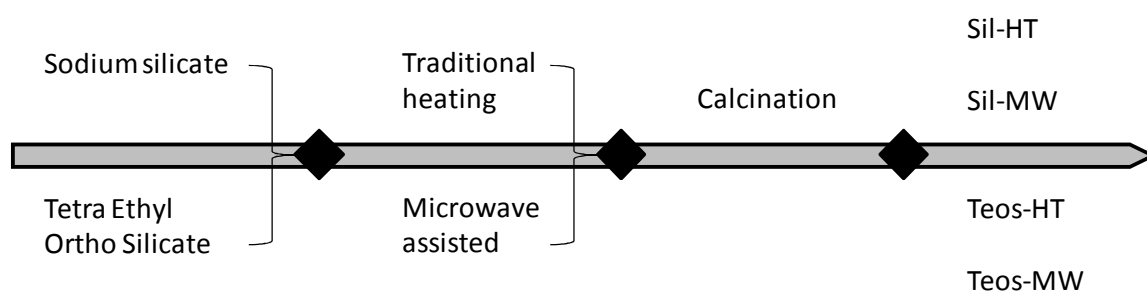


*Scheme 1. Synthetic methodology for preparing an ordered mesoporous silicate.*

From an analytical point of view, each procedure and each possibility therein, can lead to morphological variation in the obtained materials, which can be evaluated observing the formed mesoporous phase, or something like, during the different stages of the preparation.

### 5.2.1  Effect of the silica source

The hexagonal arrangement of the primary mesopores formed in the material, is developed during the hydrothermal treatment, due to the presence of an organic template (cetyltrimethylammonium bromide) which is organized in parallel rod-micelle. Indeed, prior to the hydrothermal treatment, often there are no evidence of small angle diffraction reflections related to the presence of the mesophase precursors. At the end of the synthesis, the organic template is removed from the material, leading to pores formation and causing a variation in the structural equilibria with a consequent decrease in the size of the porosity. Following the displacement of the fundamental MCM-41 reflections, through XRPD analysis, this contraction can be measured. Indeed, the most part of the morphological parameter are ordinarily expressed in terms of cell parameter, recalling some crystallographic concepts [5].

On Figures 1 and 2 are reported the small angle diffraction patterns of MCM-41 supports prepared by using different silica sources (sodium silicate and TEOS) both dried and calcined (unless otherwise specification, the XRPD analysis were carried out on calcined samples). The silicate-based material (Sil-HT) showed the presence of intense well defined (100), (110), (200) and (210) reflections before the template removal, indicating a long-range order, but unfortunately a large part of this was lost during the procedure of template removal by calcinations.

After the hydrothermal treatment, the TEOS-based materials are poorly crystallized and the template removal treatment, did not modify the long range order (Figure 2).

Moreover, within the inlay tables on figures, are shown and calculated the decreases in the pore size, through the cell parameter $a_0$, which represent geometrically a measure of the distance between the center of adjacent pores, calculated from the planes spacing ($d_{spacing}$, calculated as $a_0 = 2d_{(100)}\sqrt{3}$). Observing the calculated shrinkage, the silicate-based material and the TEOS-based material have evidenced basically different variation, where the structural equilibria of the silicate-based ones (Sil-HT) appeared less strong (shrinkage of about 16% of the initial pore size). Furthermore, it must be evidenced that, despite of the use of the same surfactant, the rod-micelles formed had different sizes as well as the resulting mesoporous channels, because of the different conditions (T and pH) of the mentioned synthesis [6].

| Sample | FWHM | d spacing | a0 | delta |
|--------|------|-----------|------|-------|
| Sil-HT-nc | 0,29 | 43,77 | 50,54 | -- |
| Sil-HT | 0,5 | 36,75 | 42,44 | 8,1 |
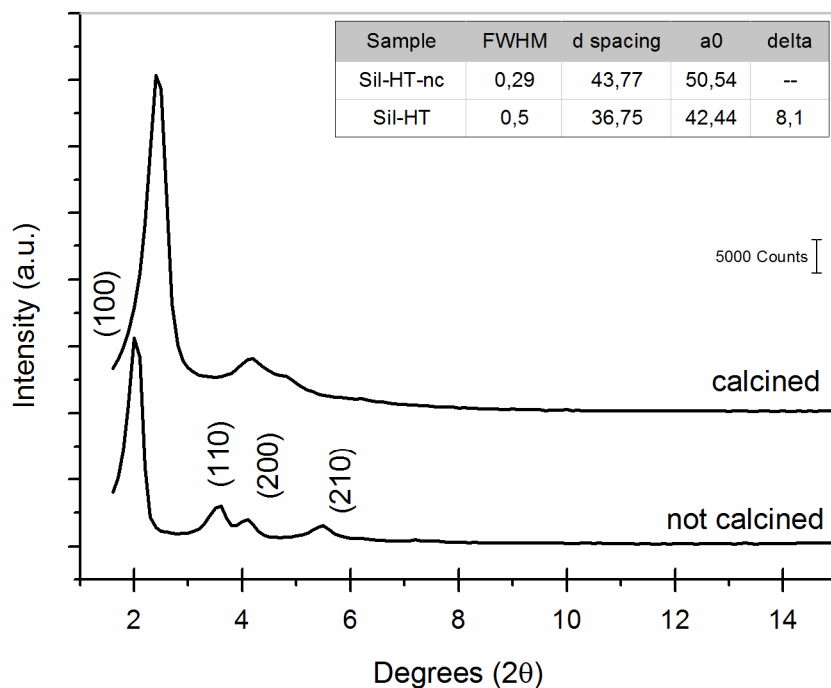
*Figure 1. XRPD analysis for the sodium silicate-based MCM-41, highlighting the shrinkage due to the thermal removal of the organic template.*

| Sample | FWHM | d spacing | a0 | delta |
|--------|------|-----------|------|-------|
| TEOS-HT-nc | 0,72 | 45,18 | 52,17 | -- |
| TEOS-HT | 0,73 | 42,14 | 48,66 | 3,51 |
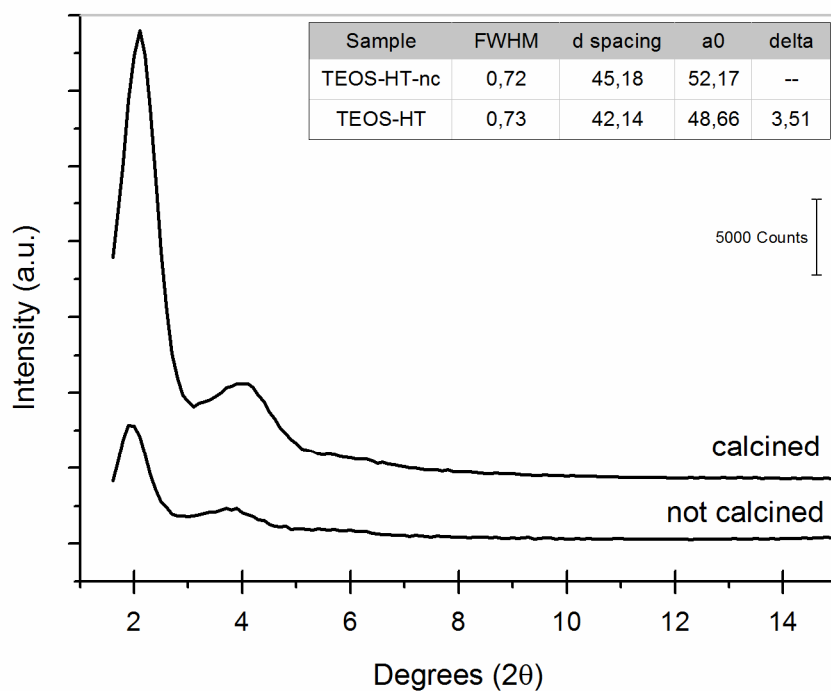
*Figure 2. XRPD analysis for the tetraethyl orthosilicate-based MCM-41, highlighting the shrinkage due to the thermal removal of the organic template.*

70

Taking into account all the previous considerations, it must be highlighted the possibility that the large amount of organic charged on the samples before removal of the template may affect the response in diffraction, decreasing the electron density contrast between the pore walls and the pore [7]. On Figure 3 are reported the thermogravimetric analysis for silicate-based and TEOS-based materials (TEOS-HT) replicating the calcination procedure that will shortly considered. The profiles of weight loss can be divided into three sections, attributable to various degradative phenomena. The first inflection of the curve, at about 100°C, is related to the evolution of water, present in the samples. In the area between 100 and 350°C, the removal of the template through the Hoffmann's degradation takes place, decomposing the trimethylamine group, while in the final stretch of the profile the degradation of nitrogeneous and carbonaceous deposits were observed [5]. The weight loss related to the removal of the template was about the 50%, and thus, is clearly understandable how this great degradation into the channels can cause wide structural variations in the final material.
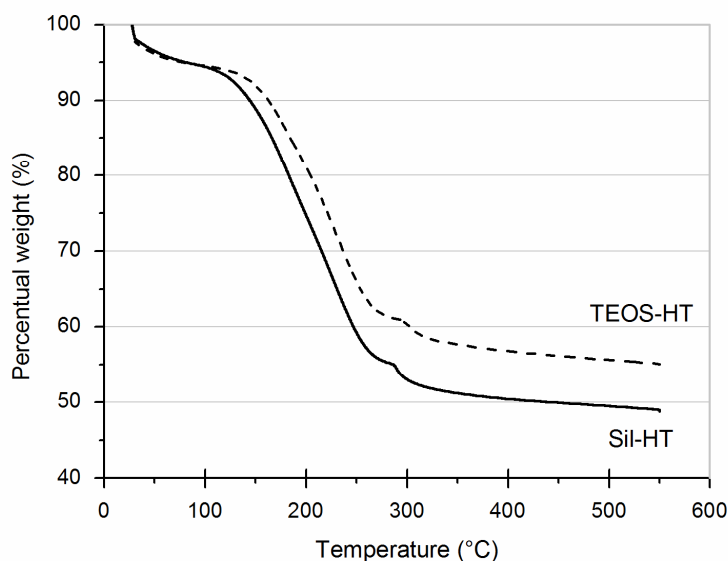


*Figure 3. Thermo-gravimetric analysis, organic template degradation.*

Considering into detail the differences between the used silica sources, nevertheless the loss into the reflections resolution explained on Figure 1, the silicate-based materials have evidenced superior morphological characteristics. Figure 4 shows a comparison between Sil-HT and TEOS-HT where is possible to observe the higher intensity and definition of the small angle reflections of Sil-HT mesophase. In particular, the smaller (110) and (200) reflections were still partially solved, while in TEOS-HT samples these reflections have never been solved, indicating a lower long-range order.

## 5. Mesoporous silicate supported catalysts

Furthermore, another useful parameter to verify the morphological characteristics of the obtained material is the enlargement of the (100) reflection, labelled FWHM (full width at half maximum) and referred in degrees. Indeed, the lower FWHM of the silicate-based sample is caused by a greater homogeneity in the size of the mesoporous channels. Obviously, it must be highlighted that a width of the (100) reflection of about 0.5-1 degrees is considered as an index of excellent homogeneity [8].

| Sample | FWHM | d spacing | a0 |
|--------|------|-----------|------|
| Sil-HT | 0,5 | 36,75 | 42,44 |
| TEOS-HT | 0,73 | 42,14 | 48,66 |
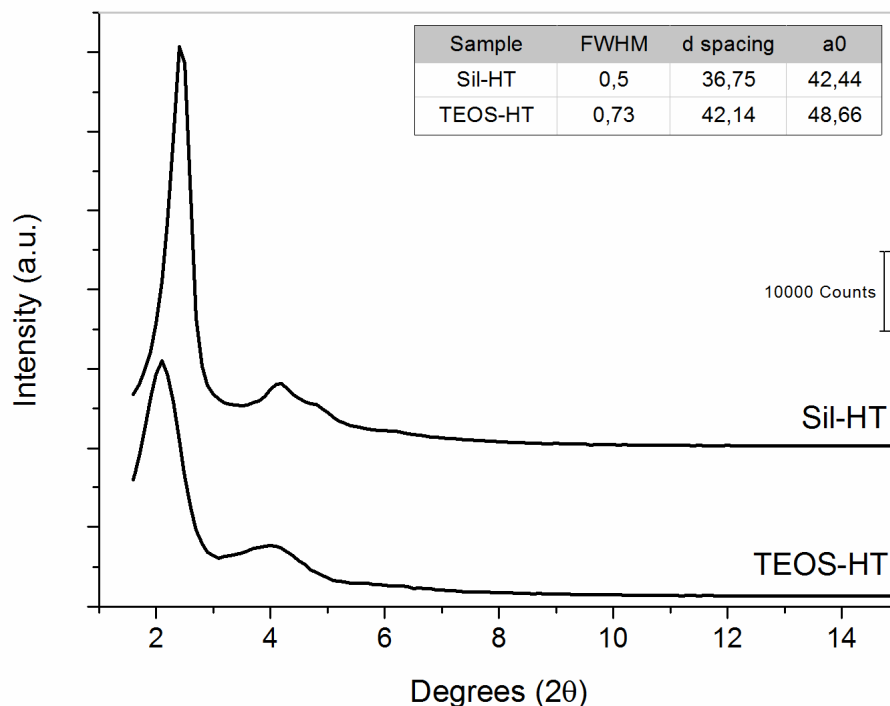
*Figure 4. X-ray diffraction pattern comparison between sodium silicate and TEOS-based MCM-41.*

Certainly, the more suitable analytical method for evaluating the quality of the obtained materials is the porosimetric analysis by $N_2$-adsorption. On Figure 5 are reported the $N_2$-adsorption/desorption isotherms for Sil-HT and TEOS-HT samples, jointly to a graphical representation of the NLDFT-calculated distribution for the pore size. Moreover, specific surface area values and others interesting parameters of the supports are shown in Table 1. In agreement with the values reported in the literature, all these reported supports have high specific surface areas (BET method) nevertheless, the TEOS-HT sample has reported lower surface area values (861 sqm/g). The obtained isotherms, on Figure 5, belong to the reversible type IV of the IUPAC classification. On the first section of isotherm, up to $0.05 p/p^0$ a large number of equilibrium point were used to calculated the microporous part

of the material porosity, while between 0.25 and 0.40 $p/p^0$ is shown the characteristic rapid increase of the $N_2$ adsorbed volume due to capillary condensation within uniform mesopore channels. Generally, the more is high the slope in the capillary condensation, the more is narrow the pore size distribution of the mesopores. On the other hand, the more are high the slope in the section before and after the capillary condensation, the more are present pores of a specific size other than the majority. In order to simplify the consideration, could be useful to consider the x-axis like an incremental axis of the pore size, where the case of increased adsorption corresponds to the presence of a defined pore size. The position of the capillary condensation and the slope of the curve, depend on the silica source and the hydrothermal treatment, evidencing differences in the mesopores distribution. Indeed, all the materials show a narrow mesopores size distribution, but Sil-HT has a distribution centred at 36Å while the TEOS-HT sample showed a maximum at 41Å. Finally, it must be remarked that in the last part of the isotherms, the adsorption between 0.9-1.0 $p/p^0$ indicates the presence of larger mesopore and macropores, probably attributable to different particle agglomeration.
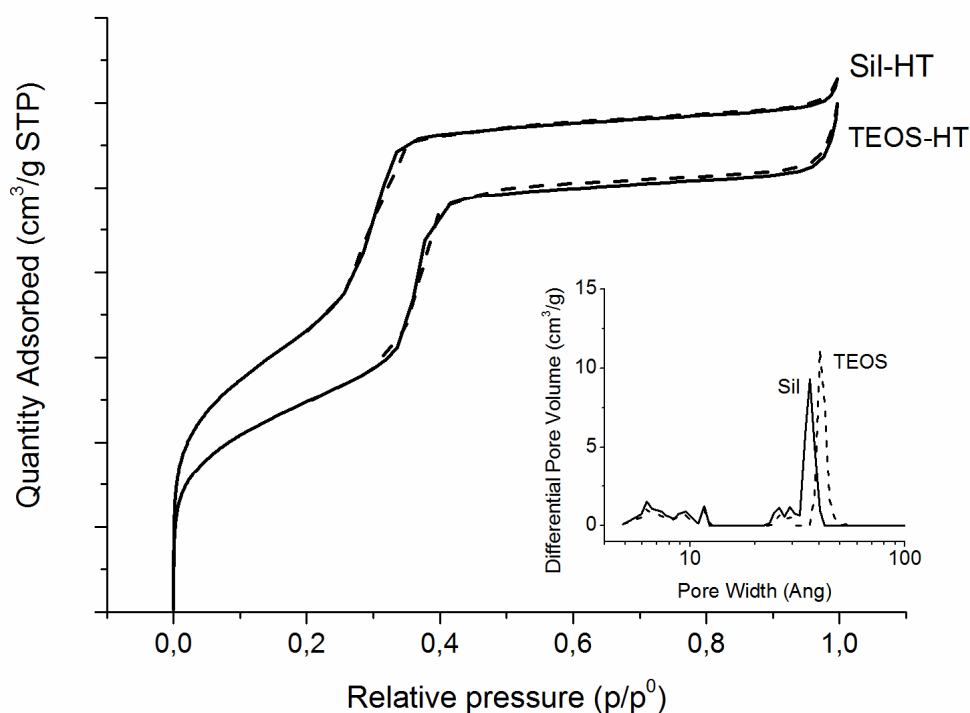


*Figure 5. $N_2$ adsorption/desorption isotherms and pore size distribution curves calculated through the NLDFT method of pure MCM-41 prepared using different silica source.*

## 5. Mesoporous silicate supported catalysts

Taking into account the previous consideration, in Table 1, are summarized the most important parameters (for our purposes), obtained applying to the $N_2$-adsorption/desorption isotherms some calculation models, like the BET equation, the t-Plot equation, the NLDFT and so on.

| Sample | SSA BET [sqm/g] | t-Plot mesopore area [sqm/g] | t-Plot mesopore volume [mL/g] | Total Vp [mL/g] | NLDFT diameter [Å] |
|---|---|---|---|---|---|
| Sil-HT | 1131 | 690 | 0,802 | 0,956 | 36 |
| TEOS-HT | 861 | 504 | 0,807 | 0,899 | 41 |

*Table 1. $N_2$ adsorption/desorption isotherms elaboration through BET, t-Plot and NLDFT methods.*

In order to complete our discussion, the last parameter, the pore-wall thickness, (Table 2) was calculated subtracting the pore size to the unit cell parameter, obtained from the XRPD d spacing ($d_{100}$) to better evaluate the differences in the mesoporous hexagonal framework [9-11]. In the case of traditional hydrothermal treatment for ageing the formed gel, no evidence of direct relation between pore-wall thickness and silica source, has been found.

| Sample | XPRD cell parameter $a_0$ [Å] | NLDFT diameter [Å] | Silica wall [Å] |
|---|---|---|---|
| Sil-HT | 42,4 | 36 | 6,4 |
| TEOS-HT | 48,7 | 41 | 7,7 |

*Table 2. Pore wall thickness calculation.*

Finally, because of their difference in the last part of the adsorption isotherms, several SEM analysis were performed over Sil-HT and TEOS-HT samples, in order to investigate possible differences in the agglomeration of particles (Figure 6).

Observing the obtained images, an objective assessment can only detect how the TEOS-HT sample appears to be constituted of spherical particles, while the Sil-HT sample appears to be more fragmented and presents some smooth areas.
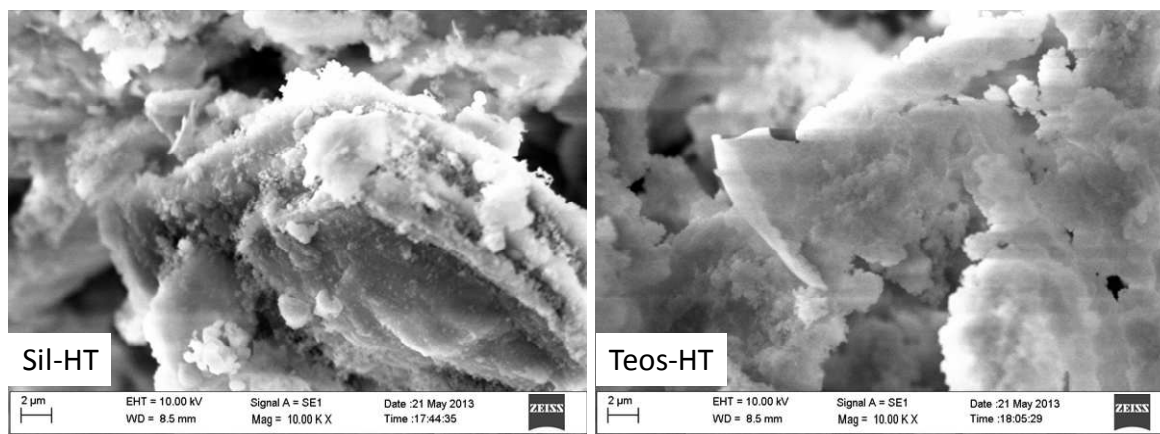
*Figure 6. SEM imaging of MCM-41 prepared using different silica source.*

## 5.2.2 Effect of the hydrothermal treatment

With the aim of investigating the performed ageing treatment (traditional and microwave-assisted) and the effect of these procedures on the final material, the kind of heating will be prior considered. Over the years, a large number of papers have reported studies focused on optimize and substitute the traditional hydrothermal treatment, conducted at 120°C, in a PTFE/PFA-filled autoclaves under autogenous pressure for 144 hours [12]. From all these studies, has appeared of fundamental relevance the hydrothermal treatment, because during it, the silica-framework was formed, and some of the final material behaviors depend on the hydrothermal treatment conditions, actually many times, the presence of the MCM-41 phase depends on the right treatment conditions [8].

On the following figure, are reported the small angle diffraction patterns of MCM-41 supports, obtained at 125°C and different microwave treatment time (Figure 7), as the subject of a preliminary study.

Whereas the foregoing, the largest order of the structure was reached after the removal treatment of the organic template, with the highest intensity values on the (100) reflection. Because of it, no major difference were observed on the diffraction patterns of the samples analyzed before the template removal. Another factor that negatively contributes to the interpretability of these results, was the procedure involved in carrying out these evaluation. Indeed, the repeated interruptions of the microwave treatment, to isolate the individual samples, probably interact with the success of the treatment, revealing an enormous difference between the sample treated with microwave heating for seven hours continuously or with breaks. Moreover, the sample treated continuously for seven hours has shown higher reflections resolution and intensity, jointly to a narrower distribution of

the pore size. At the same time, the repeated interruptions on microwave heating seems to have a relevant effect in the micelle dimension, and thus, in the absolute pore size of the final material.



| Sample | FWHM | d spacing | a0 |
|--------|------|-----------|-----|
| NT | 0,63 | 38,39 | 44,33 |
| 1h | 0,62 | 38,41 | 44,35 |
| 3h | 0,54 | 39,18 | 45,24 |
| 5h | 0,57 | 38,37 | 44,31 |
| 7h | 0,64 | 38,01 | 43,89 |
| 7h - cont. | 0,5 | 36,75 | 42,44 |
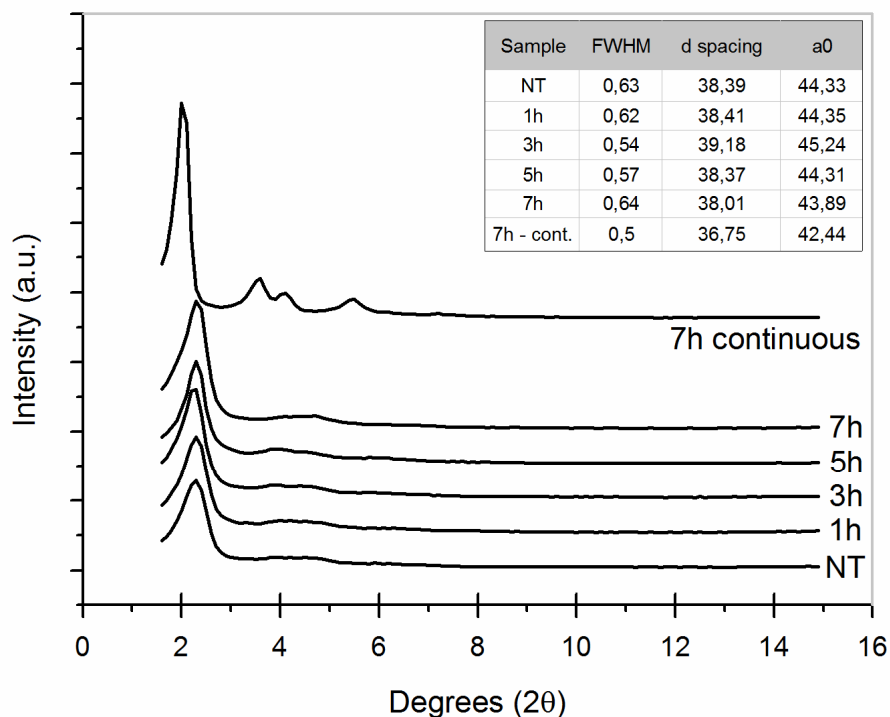
*Figure 7. Evaluation of the morphological properties related with the microwave-assisted hydrothermal treatment.*

When the silicate-based samples were compared in terms of different hydrothermal treatments, as reported on Figure 8, some interesting differences were highlighted. Indeed, the small angle diffraction pattern did not reveal enormous differences, but relevant. The microwave treated sample (MW) has the same reflections enlargement and intensity, but the (100) reflection was centered in a higher $d_{100}$ spacing (lower degrees) and observing the secondary reflections, generally seems to have higher long-range order. On the others hand, the greater sensibility of the $N_2$-adsorption analysis evidences great difference between these materials. In fact, the microwave treated one, have reported an adsorption/desorption isotherms with a capillary condensation step at higher values of $p/p^0$ than the traditionally treated material. Moreover, the isotherm slope, in the capillary condensation step is higher for the MW-sample, highlighting a narrower pore size distribution for this last sample. Finally, it must be remarked how the total amount of $N_2$

adsorbed, and also the total pore volume, increase introducing the microwave-assisted hydrothermal treatment (Table 3).

Taking into account all the previous consideration, the silicate-based synthesis, due to its sodium silicate-mediated mechanism to form the rod-micelle of template, has reported interesting effects on the morphological properties changing the hydrothermal treatment method.
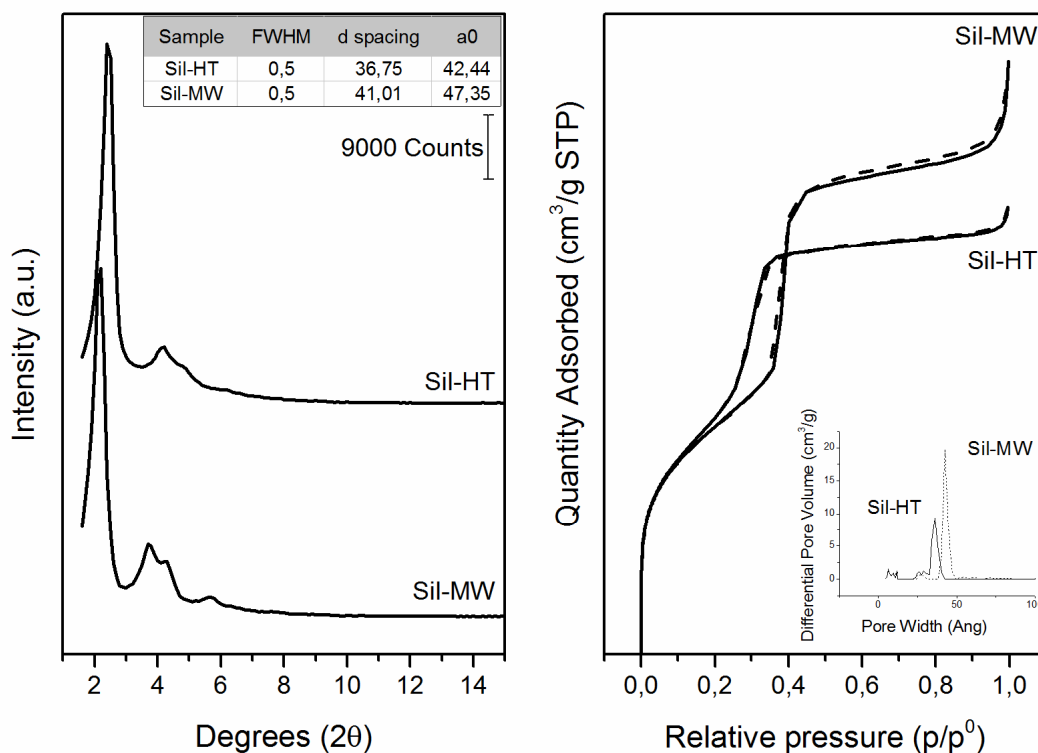


*Figure 8. XRPD pattern (left-side) N2 adsorption/desorption isotherms and pore size distribution curves calculated through the NLDFT method (right-side) of pure MCM-41 prepared using sodium silicate as silica source and performing different hydrothermal treatment.*

Concluding this evaluation of the microwave-assisted hydrothermal treatment in the silicate-based MCM-41, in the following Table 3 are reported and summarized some interesting parameters suggested by the $N_2$-adsorption analysis. In fact, the introduction of this treatment method did not lead to a general improvement of the obtained material, but to a morphologically different framework, characterized by the presence of larger mesopores, with higher pore volume but maintaining the exceptionally high value of specific surface area, common to the MCM-41 structure.

# 5. Mesoporous silicate supported catalysts

| Sample | SSA BET [sqm/g] | t-Plot mesopore area [sqm/g] | t-Plot mesopore volume [mL/g] | Total Vp [mL/g] | NLDFT diameter [Å] |
|--------|-----------------|------------------------------|-------------------------------|-----------------|---------------------|
| Sil-HT | 1131 | 690 | 0,802 | 0,956 | 36 |
| Sil-MW | 1109 | 639 | 1,125 | 1,234 | 42 |

*Table 3. $N_2$ adsorption/desorption isotherms elaboration through BET, t-Plot and NLDFT methods.*

Finally, an explanation for the observed higher amount of nitrogen adsorbed when $p/p^0 \sim 1$ on Figure 8, was suggested by SEM analysis on Figure 9, where is evident a more fine aggregation of the particles leading to an increased formation of secondary mesopores for the MW sample.
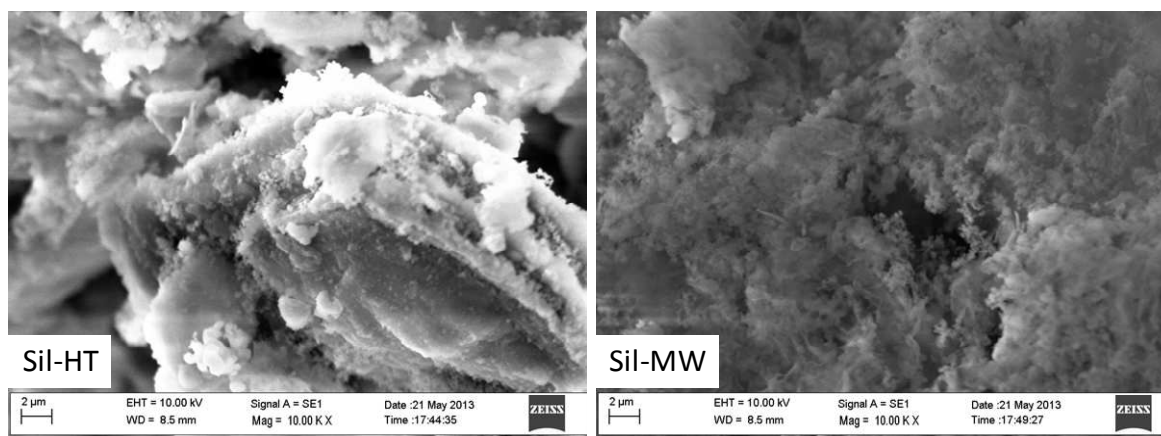


*Figure 9. SEM imaging of MCM-41 prepared performing different hydrothermal treatment.*

Following the same survey methodology, TEOS-based samples are compared in terms of hydrothermal treatment, between traditional and microwave-assisted method (Figure 10). In order to carefully evaluate these samples, it must be remarked that the synthesis reported by Cassiers, and used for preparing the precursor (gel), includes two different ageing procedures, at different temperature, during 24 hours, before performing the traditional hydrothermal treatment. Obviously, during these ageing steps the micelle reached a stable condition, thus limiting the effect of the hydrothermal treatment on the micelle's sizes. This observation, is in agreement with the obtained results carrying out XRPD and $N_2$-adsorption analysis. Indeed, the x-ray diffraction pattern obtained for TEOS-HT and TEOS-MW substantially have evidenced the same spacing between the planes and, clearly, more or less the same values for the cell parameter $a_0$. However, the microwave treated

78

sample, has reported a lower intensity on the principal reflection, suggesting a lower regularity of this material and probably the presence of amorphous areas. Paying attention on the adsorption analysis, as in the case of silicate-based materials, noticeable difference has reported, in particular on the total amount of adsorbed nitrogen, due to a higher pore volume. Differently from the silicate-based MW-sample, the positions and the slopes of the capillary condensation steps are the same with respect to the traditionally heated sample, in agreement with the reported NLDFT elaboration, where the distribution of the pore sizes are totally overlapped.
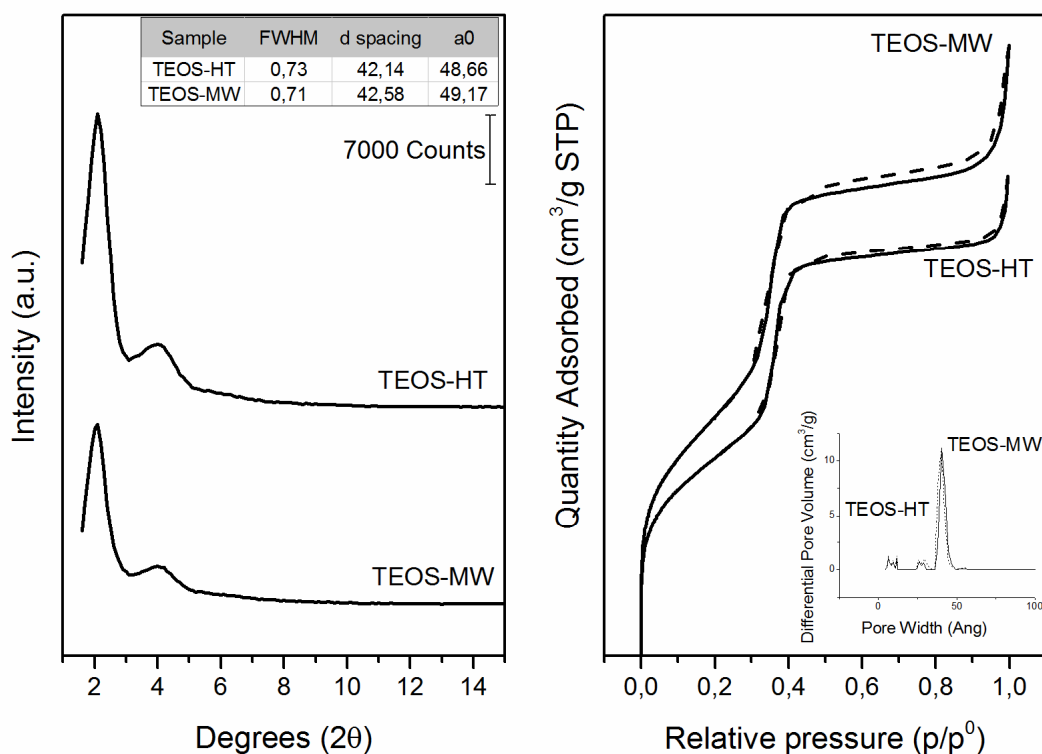


*Figure 10. XRPD pattern (left-side) $N_2$ adsorption/desorption isotherms and pore size distribution curves calculated through the NLDFT method (right-side) of pure MCM-41 prepared using TEOS as silica source and performing different hydrothermal treatment.*

Summarizing the observed results, in the case of TEOS-based materials, diffraction and adsorptive analysis were not in complete agreement (Table 4). In fact, the $N_2$-adsorption analysis revealed higher pore volume and specific surface area for the MW-sample, unlike from what has been shown performing the XRPD analysis where the MW-sample was appeared less structured and ordered, because of its lower reflections intensity.

| Sample | SSA BET [sqm/g] | t-Plot mesopore area [sqm/g] | t-Plot mesopore volume [mL/g] | Total Vp [mL/g] | NLDFT diameter [Å] |
|---|---|---|---|---|---|
| TEOS-HT | 861 | 504 | 0,807 | 0,899 | 41 |
| TEOS-MW | 1018 | 634 | 1,02 | 1,129 | 40 |

*Table 4. N₂ adsorption/desorption isotherms elaboration through BET, t-Plot and NLDFT methods.*

Concluding, the fast volumetric microwave heating decreases the ageing time required to obtain the ordered MCM-41 structure. Furthermore, as suggested by $N_2$ adsorption/desorption data, the microwave treatment modifies the formation of secondary mesopores, influencing the formation of particle agglomerates as reported previously on Figure 9 for the silicate-based sample and on Figure 11 for the TEOS-based material.
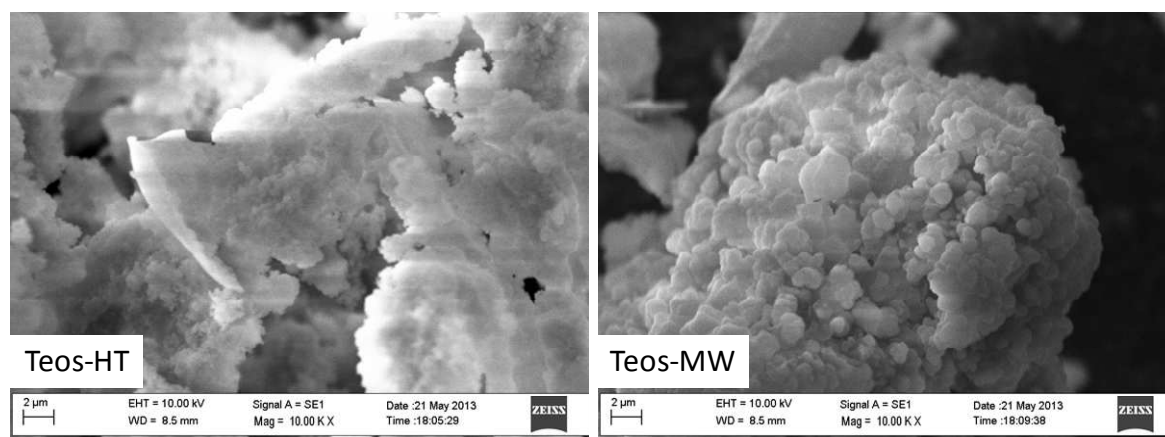


*Figure 11. SEM imaging of MCM-41 prepared performing different hydrothermal treatment.*

Silica wall thickness are reported on Table 5. All the prepared supports have values of wall-thickness in agreement with those reported in the literature, moreover, taking into account how reported by Tuel and co-workers, the explanations of different wall-thickness, different shrinkage of the arrangement spacing (due to template removal) and probably different aggregation behaviors of particles, arise from different framework cross-linking density influenced by different synthesis conditions and thus, in conclusion by different synthetic methodologies [13].

| Sample | XPRD cell parameter $a_0$ [Å] | NLDFT diameter [Å] | Silica wall [Å] |
|--------|------------------------------|--------------------|-----------------|
| Sil-HT | 42,4 | 36 | 6,4 |
| Sil-MW | 47,3 | 42 | 5,3 |
| TEOS-HT | 48,7 | 41 | 7,7 |
| TEOS-MW | 49,2 | 40 | 9,2 |

*Table 5. Pore wall thickness calculation varying silica source and hydrothermal method.*

### 5.2.3 Effect of the metal introduction

The development of the synthetic methodology used for preparing the MCM-41, and the morphological modifications related, must be added to a specific study with the goal of minimize the possible negative effect due to the introduction of the active phase.

In our case, the active phase is constituted by metallic palladium and copper, obtained by reducing chlorinated inorganic precursors like $PdCl_2$ and $CuCl_2$. The most widely used method to introduce inorganic precursors on a selected support, is to prepare a solution of the involved metal salts, and then, deposits it by incipient impregnation.

In order to give a list of the precursors introduction methods, the nature of the used MCM-41 as support and the respective metal content, a short table is reported below.

| Sample | Description | Metal Content [%wt] | Precursors |
|--------|-------------|--------------------|------------|
| i-PdCu-SHT | IWI[a] on Sil-HT MCM-41, molar ratio 1:1 | 1,0 Pd - 0,6 Cu | $PdCl_2$ - $CuCl_2$ |
| i-PdCu-THT | IWI[a] on TEOS-HT MCM-41, molar ratio 1:1 | 1,0 Pd - 0,6 Cu | $PdCl_2$ - $CuCl_2$ |

[a] Incipient Wetness Impregnation

*Table 6. Procedures and composition of the characterized catalysts.*

Figure 12 reports the small angle diffraction patterns and the $N_2$-adsorption isotherms of the incipient impregnation-prepared PdCu containing MCM-41. The impregnation procedures (referred as IWI) have evidenced, as expected, an issue of pore channel occlusion, clearly shown by the relevant decrease of the (100) reflection. In fact, as reported by Chakarova and co-workers [7], the metal deposition decrease the electron density contrast between the pore wall and the empty space of the pores, resulting in a significant decrease of reflections intensity. $N_2$-adsorption/desorption analysis, on the right side of the Figure 12, increases the consciousness of the reported XRPD evidence, by revealing a capillary condensation lacking, and by suggesting a total mesopore occlusion for the silicate-based materials Sil-HT used for prepare the catalyst labelled i-PdCu-SHT.

## 5. Mesoporous silicate supported catalysts

With respect to the other, the TEOS-HT support used for prepare the i-PdCu-THT, presents a decreased capillary condensation confirming that most of, but not all, the mesopore channel are occluded.



| Sample | FWHM | d spacing | a0 |
|---|---|---|---|
| Sil-HT | 0,5 | 36,75 | 42,44 |
| i-PdCu-SHT | 0,63 | 36,88 | 42,59 |
| TEOS-HT | 0,73 | 42,14 | 48,66 |
| i-PdCu-THT | 0,62 | 40,5 | 46,77 |
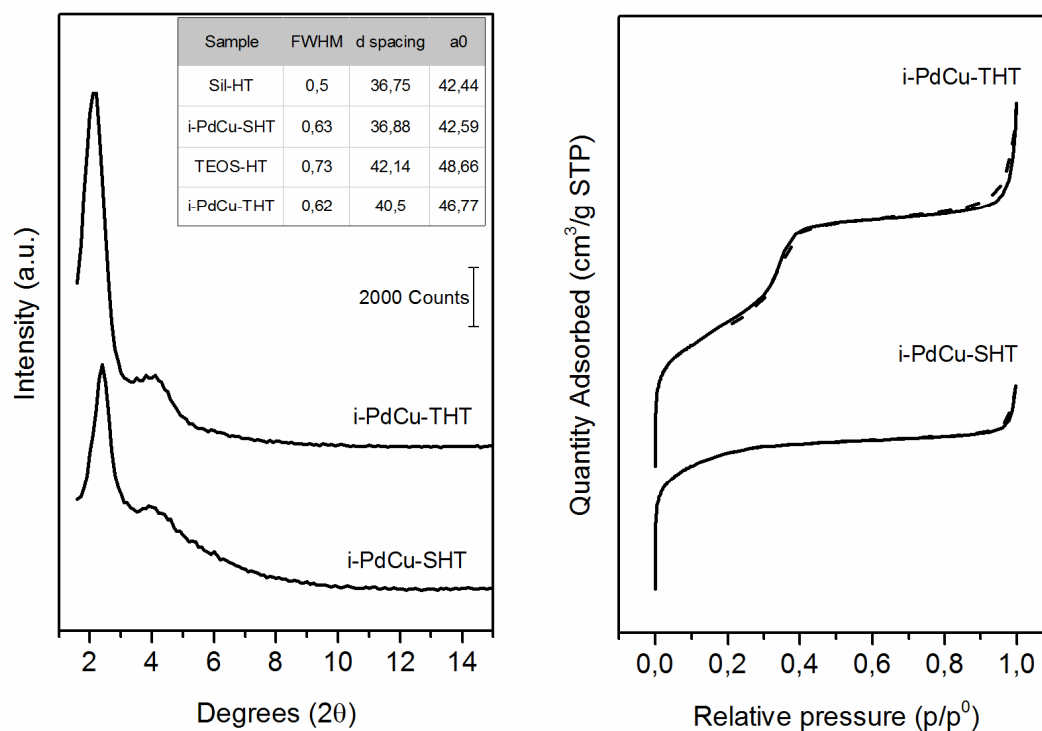
*Figure 12. XRPD pattern, cell parameters(left-side) and $N_2$ adsorption/desorption isotherms (right-side) of impregnated PdCu containing MCM-41 prepared using TEOS and sodium silicate as silica source and performing microwave-assisted hydrothermal treatment.*

Taking into account all the previous consideration, on Figure 13 are reported the NLDFT-calculated distribution of the pore sizes, where is clearly observable the total occlusion of the Sil-HT support mesopores, while in the case of the TEOS-HT support the occlusion emerges as partial. Furthermore, the occlusion phenomena explains the displacement of the distribution maximum down to lower value of about 39 (Table 7). However, in respect of these results is not yet possible to explain why the spacing between the planes (Figure 12, inlay table) for the sample i-PdCu-THT has resulted lower than the starting bare support TEOS-HT.
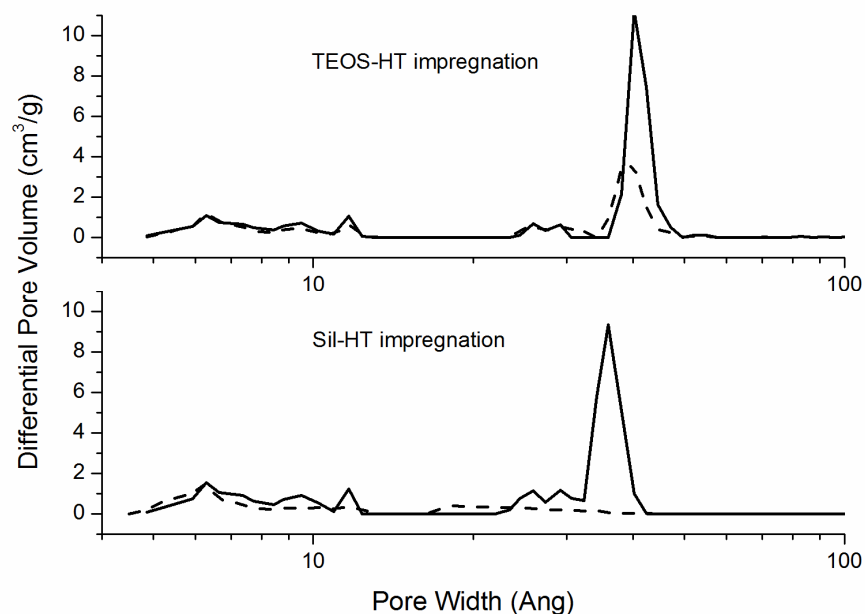
*Figure 13. Pore size distribution curves calculated through the NLDFT method for the impregnated catalysts.*

From the surface point of view, the specific surface areas measured by $N_2$-adsorption analysis are shown in Table 7, where the pore occlusion phenomena above observed, causes a significant decrease in the IWI samples. Moreover, in agreement with XRPD analysis, is possible to observe the almost completed lack of mesopore area, reporting a decrease from 690 to 32 sqm/g caused by the impregnation procedure for the Sil-HT based sample.

On the other hand, the TEOS-HT based sample has highlighted a partial occlusion of the mesopores, maintaining more than the half of the mesoporous specific surface area.

| Sample | SSA BET [sqm/g] | t-Plot mesopore area [sqm/g] | t-Plot mesopore volume [mL/g] | Total Vp [mL/g] | NLDFT diameter [Å] |
|---|---|---|---|---|---|
| Sil-HT | 1131 | 690 | 0,802 | 0,956 | 36 |
| i-PdCu-SHT | 618 | 32 | 0,259 | 0,366 | 6,3 |
| TEOS-HT | 861 | 504 | 0,807 | 0,899 | 41 |
| i-PdCu-THT | 609 | 281 | 0,537 | 0,645 | 39 |

*Table 7. $N_2$ adsorption/desorption isotherms elaboration through BET, t-Plot and NLDFT methods.*

Especially considering the "source sensitive" occlusion phenomena, this evidence could be explained taking into account the higher starting size of the mesopores with respect to the

silicate-based support. Furthermore, an alternative explanation of this observation could be referred to an intrinsic difference between the sources of silica, sodium silicate and tetraethyl orthosilicate, in terms of surface charge of the resulting materials. Indeed, starting from the hypothesis that the (ionic) sodium silicate could lead to a more hydrophilic materials with respect to tetraethyl orthosilicate based materials, an effect in influencing the deposition phenomena could be considered.

With the aim of overcoming the observed issues caused by the IWI method, an alternative method for introducing the metal precursors were developed and applied as explained in the Methods and Materials chapter. Table 8 shows the list of samples prepared by "direct introduction" synthesis, which consists in introduce the metal precursors during the formation of the silica framework.

| Sample | Description | Metal Content [%wt] | Precursors |
|--------|-------------|--------------------|------------|
| d-PdCu-SHT | Direct Introduction, Sil-based, HT | 1,0 Pd - 0,6 Cu | $PdCl_2$ - $CuCl_2$ |
| d-PdCu-SMW | Direct Introduction, Sil-based, MW | 1,0 Pd - 0,6 Cu | $PdCl_2$ - $CuCl_2$ |

*Table 8. Procedures and composition of the characterized catalysts.*

The characterization results in terms of XRPD and $N_2$-adsorption analysis are shown in Figure 14. The reflection patterns and the adsorption isotherms obtained for d-PdCu-SHT and d-PdCu-SMW are mostly similar to the equivalent patterns recorded for the bare MCM-41. Taking into account these evidences, the inclusion of these metal precursors during the framework formation seems to have no effect on structure order and feasibility. However, regarding the morphological properties of the final materials, the introduction of metals seems to lead to higher cell parameters, highlighting a significant increase mainly in the case of sample treated by traditional hydrothermal heating. In particular, the introduction of metal, increasing the spacing between the planes, makes it more difficult to be analyze for goniometric limitation, and makes it less suitable in FWHM evaluation. Nevertheless, the primary (100) reflection appears narrow and intense, for each sample.

All of the prepared samples show secondary reflections resolved and intense, indicating a well-built long-range ordered structure, but combining these observations with those obtained by $N_2$-adsorption/desorption analysis, from a morphological point of view, a great nitrogen adsorption at high $p/p^0$ indicates a relevant formation of particles aggregates and thus, secondary mesopores.

| Sample | FWHM | d spacing | a0 |
|---|---|---|---|
| Sil-HT | 0,5 | 36,75 | 42,44 |
| d-PdCu-SHT | 0,4 | 42,75 | 49,36 |
| Sil-MW | 0,5 | 41,01 | 47,35 |
| d-PdCu-SMW | 0,44 | 42,1 | 48,61 |
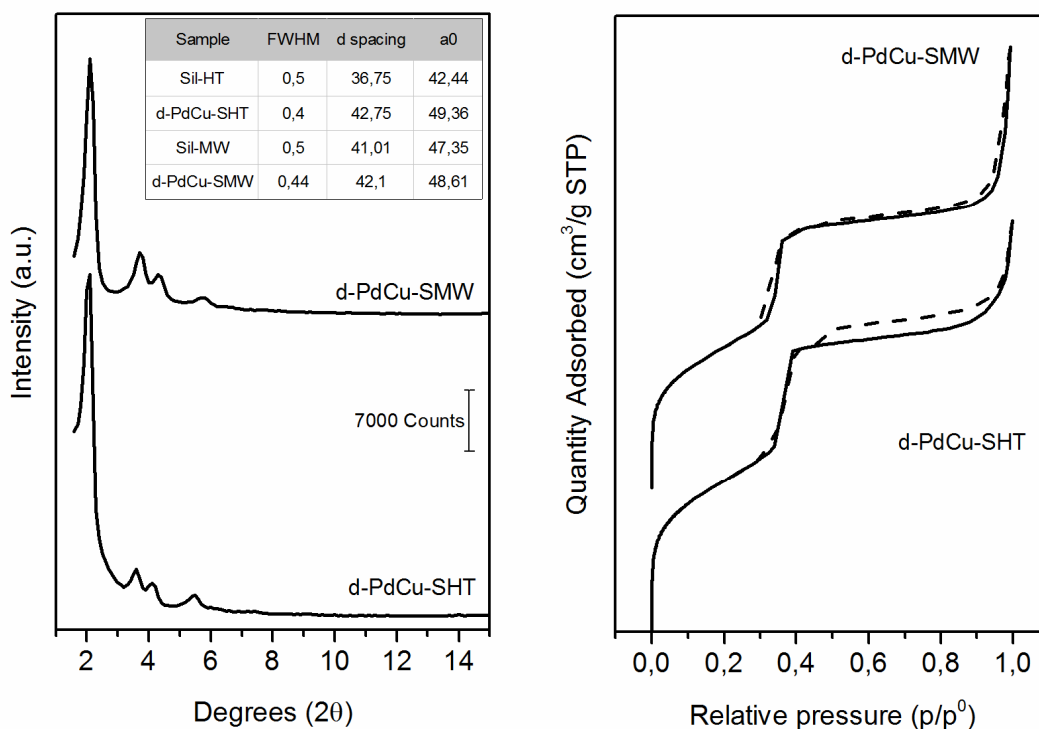
*Figure 14. XRPD pattern, cell parameters(left-side) and N₂ adsorption/desorption isotherms (right-side) of PdCu containing MCM-41 obtained by "direct introduction", prepared using sodium silicate as silica source and performing different hydrothermal treatment.*

Differently from the previously reported comparison, between silicate-base MCM-41 treated by traditional or microwave heating method, the adsorption isotherms are not so different each other, and thus, also the NLDFT-calculated distributions appear almost overlapped (Figure 15).

However, as previously observed on TEOS-MW sample, the desorption isotherm of d-PdCu-SHT not fully reflects the shaped of the adsorption isotherms, probably due to an aggregation that produces a secondary porosity and its relative small hysteresis.

## 5. Mesoporous silicate supported catalysts
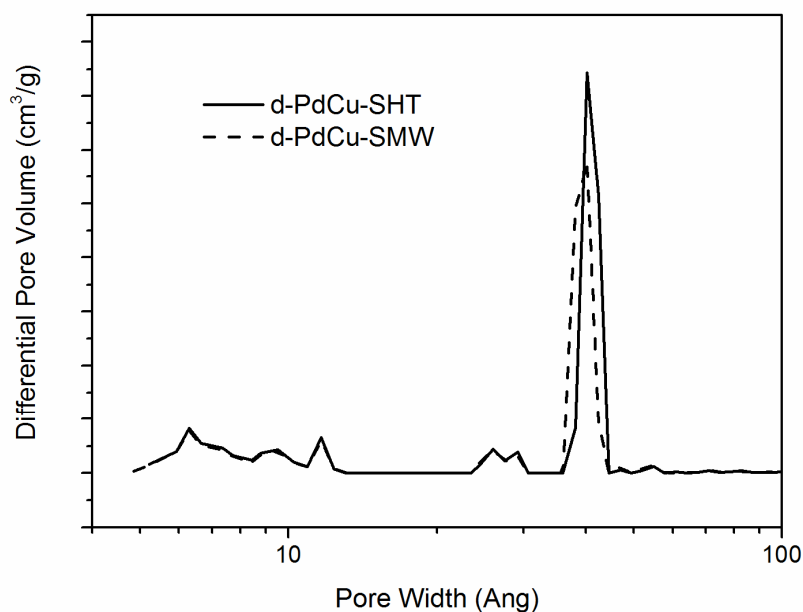


*Figure 15. Pore size distribution curves calculated through the NLDFT method for the sodium silicate catalysts prepared through "direct introduction" and treated with different hydrothermal treatment..*

With the aim of underlining the morphological properties guaranteed by the use of the "direct introduction", the following Table 9 reports a comparison between the MCM-41 supports prepared using sodium silicate or tetraethyl orthosilicate and the metal-charged MCM-41, prepared using the respective silica source. As above mentioned in terms of structure order, is possible to evidence the high values of pure MCM-41 regarding to the specific surface area, with the values of the metal-containing samples (of about 1000 sqm/g), also evidencing that the inclusion of the metal precursors during the framework formation seems to have no effect on the synthesis feasibility and on the material quality.

The reported values for the Sil-HT samples underlines the differences between this sample and all the others, particularly in the size of the mesoporous channels. However, the different values of channels size must be attributed to the digestion conditions, as well as previously reported, considering the hydrothermal treatment methodologies.

86

| Sample | SSA BET [sqm/g] | t-Plot mesopore area [sqm/g] | t-Plot mesopore volume [mL/g] | Total Vp [mL/g] | NLDFT diameter [Å] |
|---|---|---|---|---|---|
| Sil-HT | 1131 | 690 | 0,802 | 0,956 | 36 |
| d-PdCu-SHT | 1105 | 630 | 1,143 | 1,282 | 41 |
| Sil-MW | 1109 | 639 | 1,125 | 1,234 | 42 |
| d-PdCu-SMW | 1041 | 593 | 1,249 | 1,381 | 40 |

*Table 9. N$_2$ adsorption/desorption isotherms elaboration through BET, t-Plot and NLDFT methods.*

Returning to the preparation considerations, performing the previously explained calculation (pore wall = XRPD cell parameter - NLDFT mesopore diameter), is possible to observe how the metal introduction affect the pore wall dimension, leading to thicker walls (Table 10).

| Sample | XPRD cell parameter a$_0$ [Å] | NLDFT mesopore diameter [Å] | Silica wall [Å] |
|---|---|---|---|
| Sil-HT | 42,4 | 36 | 6,4 |
| d-PdCu-SHT | 49,4 | 41 | 8,4 |
| Sil-MW | 47,3 | 42 | 5,3 |
| d-PdCu-SMW | 48,6 | 40 | 8,6 |

*Table 10. Pore wall thickness calculation varying the hydrothermal method.*

### 5.2.4 Effect of the metal content

In order to investigate further the "direct introduction" of the metal precursors into the silica framework, a series of catalysts were prepared including an increased metal content.

#### 5.2.4.1 Sodium silicate -based catalysts

On Table 11 are reported the respectively metal content of Pd and Cu, the preparation condition in terms of precursors introduction, the silica source and the hydrothermal treatment methodology.

## 5. Mesoporous silicate supported catalysts

| Sample | Description | Metal Content [%wt] | Precursors |
|---|---|---|---|
| 1 (PdCu) | Direct Introduction, Sil-based, MW | 1,0 Pd - 0,6 Cu | $PdCl_2$ - $CuCl_2$ |
| 1,5 (PdCu) | Direct Introduction, Sil-based, MW | 1,5 Pd - 0,9 Cu | $PdCl_2$ - $CuCl_2$ |
| 2 (PdCu) | Direct Introduction, Sil-based, MW | 2,0 Pd - 1,2 Cu | $PdCl_2$ - $CuCl_2$ |
| 2,5 (PdCu) | Direct Introduction, Sil-based, MW | 2,5 Pd - 1,5 Cu | $PdCl_2$ - $CuCl_2$ |

*Table 11. Procedures and composition of the characterized catalysts.*

All the prepared samples have shown intense and well-defined x-ray diffraction patterns, on Figure 16, together with a well-developed capillary condensation in the $N_2$-adsorption/desorption analysis.

From a morphological point of view, all the samples appear well-developed and basically constituted by MCM-41, reporting a series of differences in the XRPD patterns and adsorption/desorption isotherms that are difficult to correlate with the increased metal content.

Firstly, the 1(PdCu) and the 2(PdCu) present a different maximum in the (100) reflections with respect to the other synthesis, together with a higher resolution of the secondary reflections (110) and (200). Furthermore, these samples present a large difference in the final range of the $N_2$-adsorption/desorption isotherms, suggesting a different behavior in aggregating particles.

In particular, the 2(PdCu) sample has shown a great adsorption (more or less the 50%) in the final range of the isotherm, suggesting a large presence of secondary mesopores, but without indications of trends with the metal content.
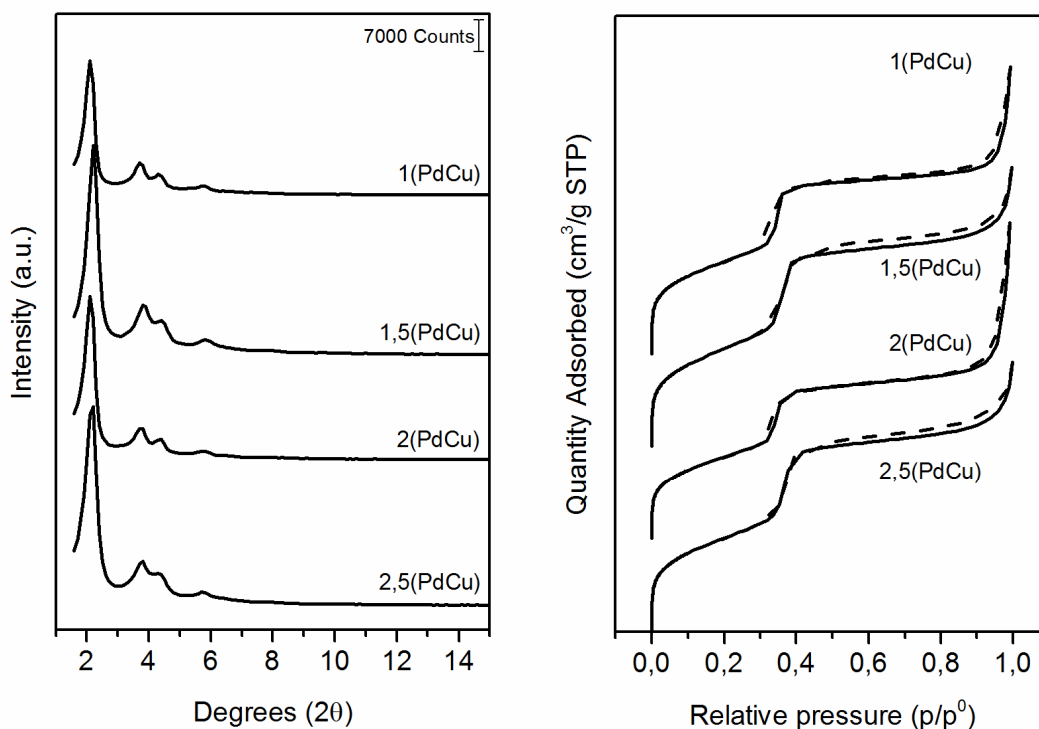
*Figure 16. XRPD pattern, (left-side) and N$_2$ adsorption/desorption isotherms (right-side) of different PdCu containing MCM-41 obtained by "direct introduction", prepared using sodium silicate as silica source and performing microwave hydrothermal treatment.*

Obviously, the NLDFT calculation, depending on the adsorption/desorption isotherms, is not able to highlight other differences between the samples. Observing these reported calculation (Figure 17) is possible to underlines that there is not a trend between metal content and the channels size. Moreover, the pores are preferentially mesoporous, in agreement with those has been shown in the pure MCM-41 supports.
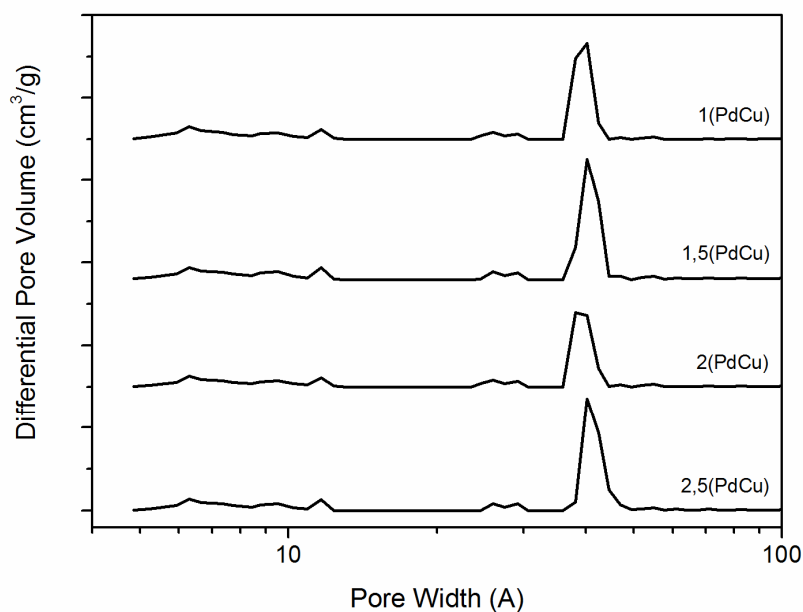
*Figure 17. Pore size distribution curves calculated through the NLDFT method for various sodium silicate catalysts prepared through "direct introduction".*

The specific surface area, measured for these samples (Table 12) is in agreement with the previously reported samples, generally of about 1000 sqm/g, constituted of about 60% from the mesoporous channels area.

| Sample | SSA BET [sqm/g] | t-Plot mesopore area [sqm/g] | t-Plot mesopore volume [mL/g] | Total Vp [mL/g] | NLDFT diameter [Å] |
|---|---|---|---|---|---|
| 1(PdCu) | 1041 | 593 | 1,249 | 1,381 | 40 |
| 1,5(PdCu) | 1097 | 656 | 1,239 | 1,347 | 40 |
| 2(PdCu) | 952 | 572 | 1,558 | 1,672 | 39 |
| 2,5(PdCu) | 1046 | 618 | 1,192 | 1,296 | 41 |

*Table 12. $N_2$ adsorption/desorption isotherms elaboration through BET, t-Plot and NLDFT methods.*

However, considering the wall thickness calculation on Table 13, no trend was found between thickness and metal content. Because of this, and previous reported considerations in terms of XRPD patterns, it must be paid attention in the catalysts synthesis which are observed as difficult to reproduce.

| Sample | XPRD cell parameter $a_0$ [Å] | NLDFT mesopore diameter [Å] | Silica wall [Å] |
|---|---|---|---|
| 1(PdCu) | 48,61 | 40 | 8,6 |
| 1,5(PdCu) | 46,15 | 40 | 6,2 |
| 2(PdCu) | 48,0 | 39 | 9,0 |
| 2,5(PdCu) | 47,0 | 41 | 6,0 |

*Table 13. Pore wall thickness calculation varying the amount of metals introduced.*

### 5.2.4.2 Tetraethyl orthosilicate -based catalysts

With the aim of observing the role of different silica source in influencing the resulting properties, a similar series of catalysts were prepared using TEOS as silica source and increasing the metal content, summarized on Table 14.

| Sample | Description | Metal Content [%wt] | Precursors |
|---|---|---|---|
| 1 (PdCu)T | Direct Introduction, Teos-based, MW | 1,0 Pd - 0,6 Cu | $PdCl_2 - CuCl_2$ |
| 1,5 (PdCu)T | Direct Introduction, Teos-based, MW | 1,5 Pd - 0,9 Cu | $PdCl_2 - CuCl_2$ |
| 2 (PdCu)T | Direct Introduction, Teos-based, MW | 2,0 Pd - 1,2 Cu | $PdCl_2 - CuCl_2$ |
| 2,5 (PdCu)T | Direct Introduction, Teos-based, MW | 2,5 Pd - 1,5 Cu | $PdCl_2 - CuCl_2$ |

*Table 14. Procedures and composition of the characterized catalysts.*

All the catalysts prepared, basically show the known properties repeatedly observed in terms of x-ray diffraction reflections pattern and on the $N_2$-adsorption/desorption analysis (Figure 18). However, despite of the good correlation between the first three materials, 1(PdCu)T, 1.5(PdCu)T and 2(PdCu)T samples, it must be remarked that something has changed on performing the last preparation. Indeed, the sample with the higher metal content shows an x-ray diffraction pattern with very low intensity of the reflections, leading to serious issues on measuring the crystallographic parameters generally observed. On the other hand, the capillary condensation stair generally observed in the $N_2$ adsorption/desorption analysis has been interrupted by an additional hysteresis, attributable to higher diameter pores.

Moreover, with respect to the sodium silicate - based samples, the final nitrogen adsorption at higher values of $p/p^0$, were less evident, suggesting a lower presence of secondary pores, indicating a lower aggregation of particles.
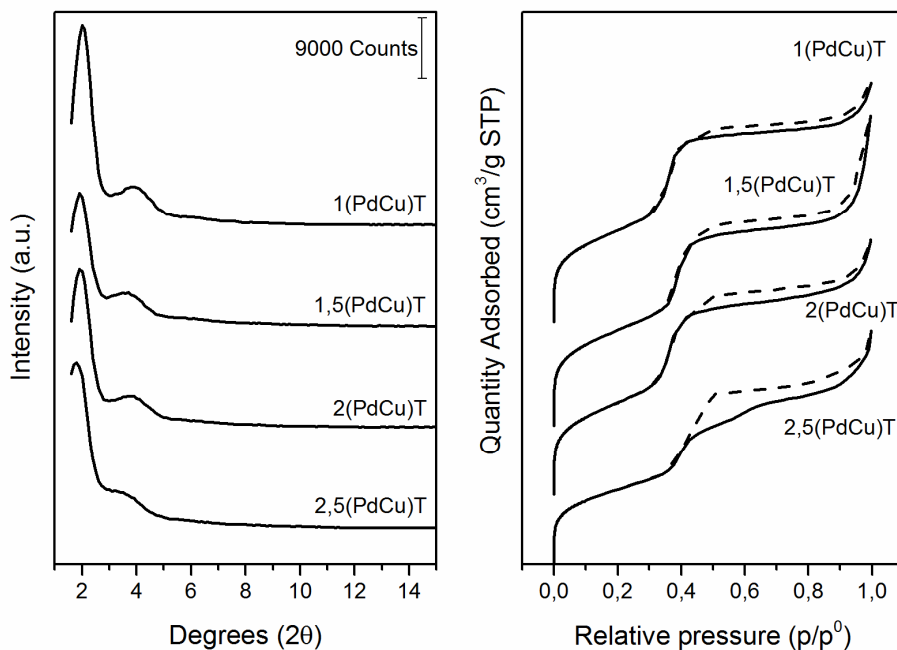
*Figure 18. XRPD pattern (left-side) and N₂ adsorption/desorption isotherms (right-side) of different PdCu containing MCM-41 obtained by "direct introduction", prepared using TEOS as silica source and performing microwave-assisted hydrothermal treatment.*

The observed evidences in the adsorption isotherms are extremely confirmed by observing the NLDFT calculation of the pore sizes distribution reported on Figure 19. In fact, differently with respect to the other sample, the catalyst with the higher metal content shows adsorption within pores of dimension up to 80-90 angstrom, also explaining the significant separation between the isotherms of adsorption and desorption on Figure 18.
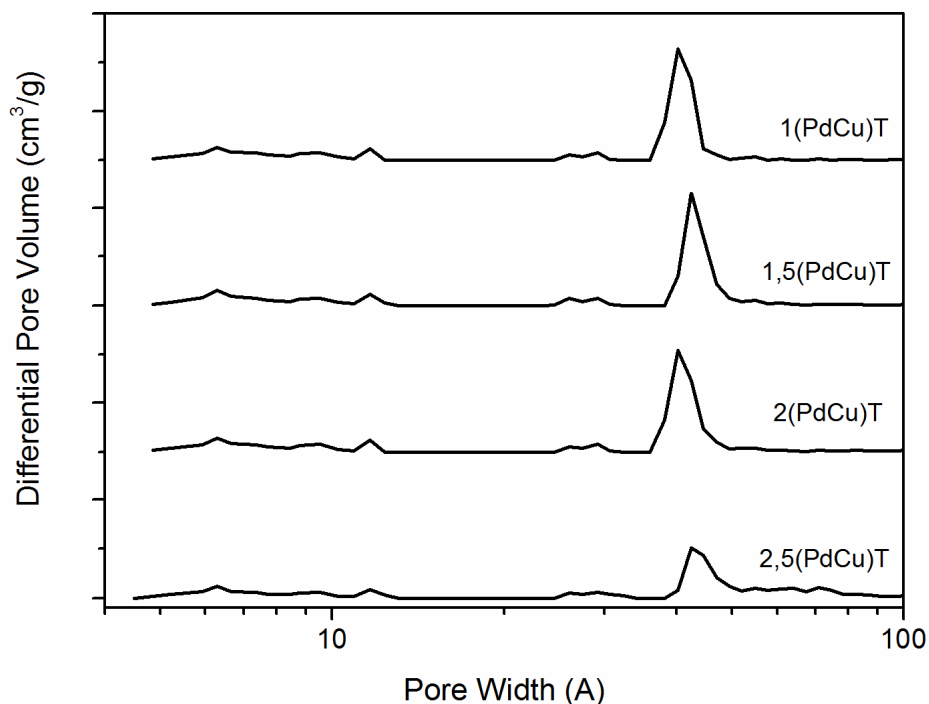
*Figure 19. Pore size distribution curves calculated through the NLDFT method for the TEOS catalysts, prepared through "direct introduction" method.*

Furthermore, observing the pore diameter and the silica wall thickness, is not obvious any trend, leading to consider this synthetic method much more difficult to be reproduced in the morphological properties than the sodium silicate -based catalysts (Table 15).

| Sample | XPRD cell parameter $a_0$ [Å] | NLDFT diameter [Å] | Silica wall [Å] |
|---|---|---|---|
| 1(PdCu)T | 48,8 | 41 | 7,8 |
| 1,5(PdCu)T | 49,9 | 43 | 6,9 |
| 2(PdCu)T | 49,6 | 41 | 8,6 |
| 2,5(PdCu)T | 49,1 | 43 | 6,1 |

*Table 15. Pore wall thickness calculation varying the total metal content.*

Regarding this series of samples, the positive aspect is that in the case of the lower metal content, no substantial differences compared to the bare-MCM-41 were found. On the contrary, the sample with the higher metal content, has shown a significant loss of ordered structure, indicating a limit in the content of metals that can be introduced in the structure.

# 5. Mesoporous silicate supported catalysts

Concluding, in this work, a series of supports and Pd/Cu containing catalysts were prepared, performing a large number of bare-MCM-41 synthesis, carrying out several alternative treatment and finally verifying different metal precursors introduction, a series of catalysts were obtained in order to study the catalytic performance in the hydrogen assisted dechlorination of $CF_3OCFClCF_2Cl$ to $CF_3OCF=CF_2$.

With the aim of summarizing this discussion focused on the chemical-physical properties behaviors of these materials, some interesting observation can be reported:

- the use of microwave-assisted hydrothermal treatment leads to faster synthesis, maintaining the structural properties of the traditional-treated MCM-41. Crystallinity and structural order of the obtained materials were comparable, or even better, with respect to those prepared by the traditional heating method.

- according to the expectations, is possible to design each step of the synthesis and all the following treatment (silica source and hydrothermal treatment) in order to obtain different materials with different morphological properties.

- the introduction of the active phase precursors could be performed by various methodologies.

- the MCM-41 prepared using TEOS as silica source seems to be more sensitive to the introduction of metals, significantly worsening the morphological properties of the resulting materials.

However, in order to complete the characterization of the catalytic system, the resulting active phase properties must be carefully evaluated. Indeed, investigating in detail the behaviors and the deposition of metals during the methodology of direct introduction, with the help of TEM/EDS analysis it was possible to highlight substantial differences between the samples prepared by incipient wetness impregnation and those prepared by direct introduction method. The sizes of the metal particles were around 10 and 60 nm, with a mean size of 30 nm, for the samples prepared by direct introduction, with respect to the surprising narrower particle size distribution of around 3-13 nm evidenced for the impregnated samples. In fact, the thermal treatment required for removing the organic template from the MCM-41 pores (at about 540-550°C) may cause sintering of the active phase particles leading to larger aggregate in the direct-introduction samples. On the other hand, the impregnated samples were treated at 330°C performing the reduction to metallic phase, which could cause a lower sintering of particles.

Taking into account the previously discussed properties in the hydrodechlorination reaction, and its structure sensitive character toward the active phase, is clearly considerable that the catalytic performance can be significantly affected by the variation of particle sizes and composition. Because of this, the investigation focused on verifying the properties of the formed particles was continued by performing an XRPD study of the previously evaluated catalysts.

### 5.2.5 XRPD survey of the segregated phases composition.

Considering the structure sensitive behavior of the hydrodechlorination reaction has assumed a significant importance the composition of the metal particle formed with different preparation method.

Regarding the sodium silicate -based catalysts, on Figure 20 are reported the XRPD pattern obtained performing a wide range analysis, between 34 and 50 °2θ, interesting for the purpose of this investigation, due to the presence of the elemental reflection for Pd and Cu particles. According to the previously reported publications by Kariuki and Ma, Pd and Cu are used to form various solid mixtures and alloys observable in the chosen range, between 34 and 50 °2θ (Table 16) [14,15].

| Compound | Reference | 2Theta [deg] | Intensity [%] |
|---|---|---|---|
| Pd | 00-046-1043 | 40.119 | 100 |
| | | 46.659 | 60 |
| Cu | 00-004-0836 | 43.298 | 100 |
| | | 50.434 | 46 |
| Cu$_3$Pd | 00-007-0138 | 34.129 | 40 |
| | | 36.373 | 50 |
| | | 42.319 | 100 |
| | | 49.015 | 90 |
| | | 49.699 | 80 |
| CuPd | 00-048-1551 | 41.424 | 100 |
| | | 48.213 | 65 |

*Table 16.XRPD references and reflections placement about Pd, Cu and PdCu alloys.*

When the crystalline unit cell of palladium is inserted by few copper atoms, the distortion of the crystalline planes caused a displacement of the reflection towards lower degrees. On the contrary, when the crystalline unit cell of copper is inserted by palladium atoms, the displacement was found to be towards higher degrees, due to an enlargement of the crystalline planes. Taking into account this considerations and the observation that, to the

increase of the metal content loaded on the silica framework corresponds an increased displacement of the phase reflections, the formation of a mixed metallic phase was considered, in some case indicated by TEM/EDS analysis as a non-stoichometric mixed oxide.

In order to maximize the number of information, was introduced the use of the Vegard's Law to estimate the composition of phases that match the revealed reflections. In fact, all the possible alloy phases between Pd and Cu ($Cu_3Pd$ *bct*, $CuPd$ *fcc*) have not given positive response comparing the calculate spacing between the planes and the calculate unit cell parameters, leading to an unique classification as Pd-rich phase (at about 41°2θ) and Cu-rich phase (at about 43°2θ). Despite of the extended commitment, the information provide by this survey are purely qualitative, indicating a possible effect of the increased metal content in the particle composition, as well as a greater intensity in the reflection of the copper-rich phase with the total metal content increase.
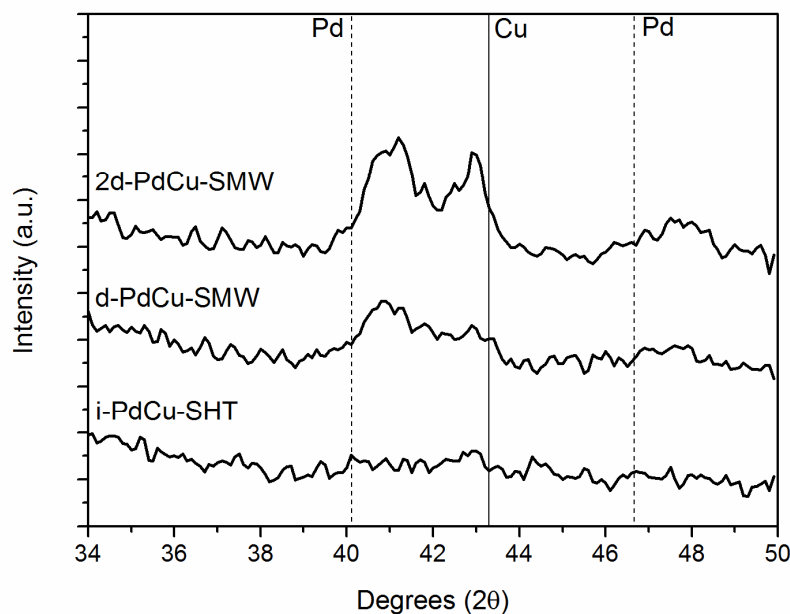


*Figure 20. XRPD comparison between catalysts prepared by impregnation or by direct introduction using sodium silicate as silica source.*

According to the previous considered survey, investigating further the phases composition of the TEOS-based catalysts, the observations differ only for the different placement of the observed reflections, which suggest a Pd-rich phase composition very close to the pure-Pd in terms of unit cell parameters and thus, composition. Furthermore, in this case as in the

previous, the increased content of metal into the framework corresponds to an increased displacement of the mixed phases reflections (Figure 21).
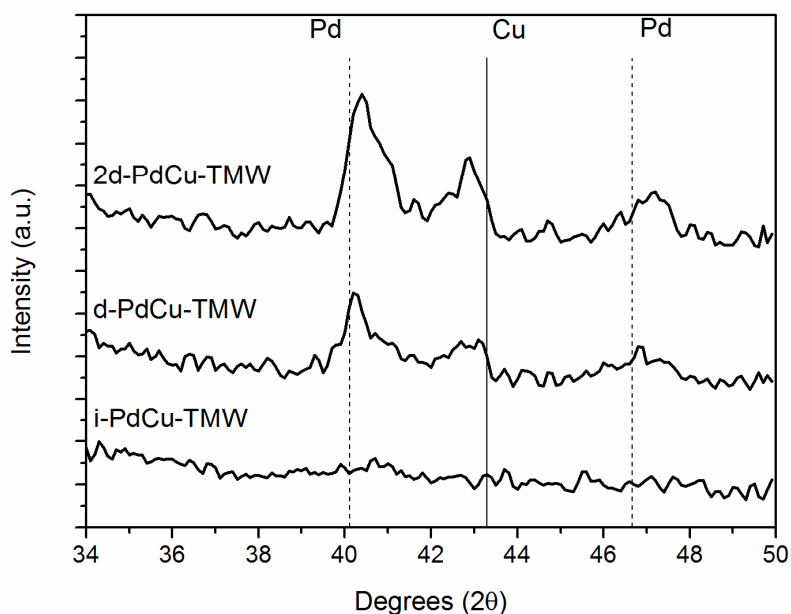


*Figure 21. XRPD comparison between catalysts prepared by impregnation or by direct introduction using TEOS as silica source.*

Due to an unforeseen changes in the synthetic procedure, the samples prepared using TEOS as silica source, and intermediate metal content have reported a completely different phase reflections and thus different distributions, with respect to the other samples.

Thus, investigating further this observation, and the complete lack of Cu-rich phase reflections, a possible match with a non-stoichometric CuPd fcc alloy phase was found, considering the addition of other copper atoms to the CuPd lattice.

Furthermore, observing the reflection placement at about 41°2θ, differently with respect to the other catalysts, the increase in metal content does not correspond to a shift of the phases reflections (Figure 22).
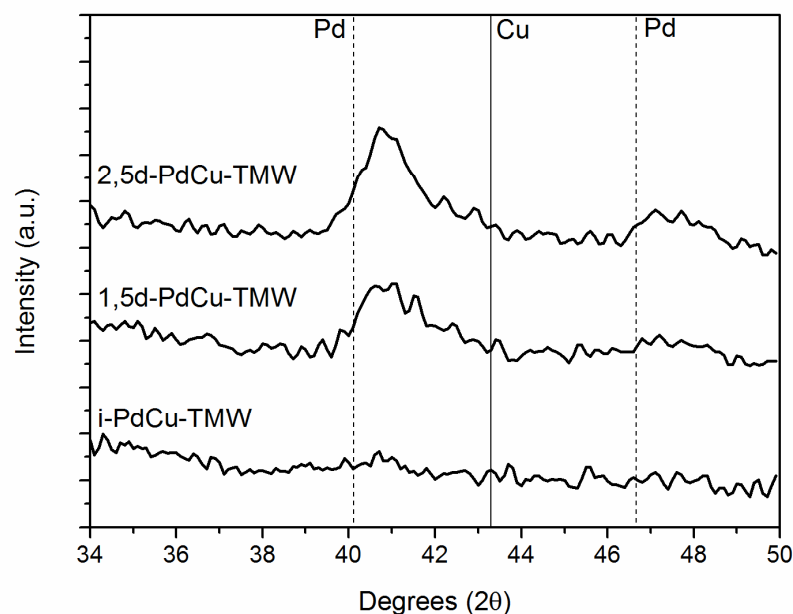
*Figure 22. XRPD comparison between catalysts prepared by impregnation or by direct introduction using TEOS as silica source, reporting different phases.*

With the aim of concluding this discussion, it certainly seems important to emphasize that, to different synthetic methodologies often correspond different phases, compounds and species formed. The correlation between this different observed active phase and the catalytic properties, especially in gas-phase reactions, may be difficult to be observed because of reduced mass transfer or diffusion issues.

### 5.2.6  Effect of the method utilized for template removal

In order to overcome the evidenced issues in metal particle sizes, the ability to remove the organic template by washing was evaluated following an alternative method previous reported by Lang and co-workers, fundamentally based on the ionic exchange between the organic template and the ammonium nitrate [13]. Using this method is possible to avoid the conventional thermal degradation of the organic template, and thus, avoid the high temperatures which can cause a sintering of the active phase. The obtained material from the hydrothermal procedure, was treated refluxing an ethanolic solution of ammonium nitrate at 60°C for three times, with an overall ammonium/template molar ratio of 2. As suggested by FT-IR analysis shown an Figure 23, the recovered and ethanol-washed materials have shown a gradual and total decrease into the infrared absorption bands attributed to the template, in particular to the alkylic substituent of the quaternary

ammonium (cetyltrimethylammonium bromide). Taking into account this success in removing the organic template, the material obtained was further investigated to evaluate the resulted morphological characteristics.
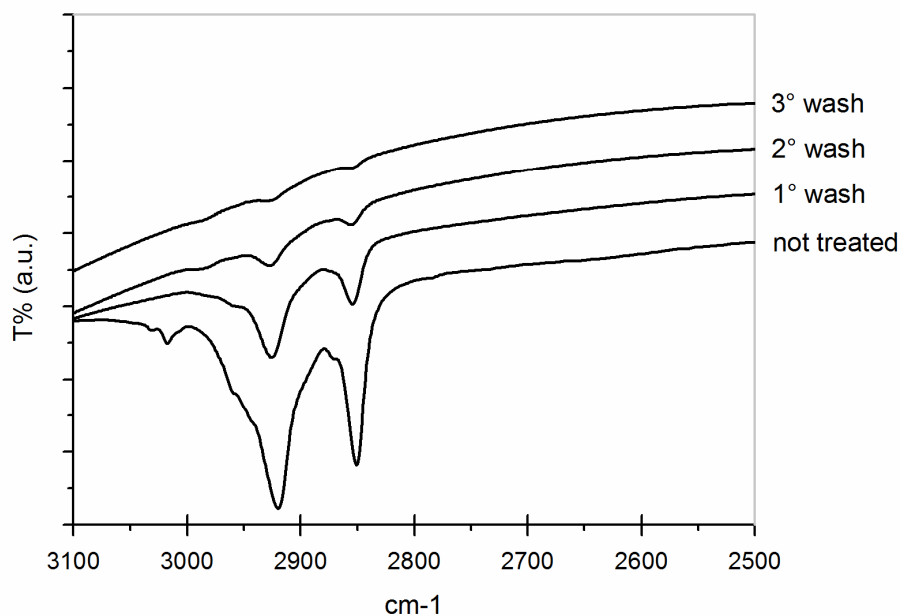


*Figure 23.Successfull organic template removal performed by ion-exchange and followed through FT-IR analysis.*

When the ion exchanged meso-phase was analyzed by XRPD, the result clearly showed that the framework formed was poorly crystallized, revealing only the (100) reflection and the secondary reflections due to the long-range order are lacking. However, this procedure has been useful for evaluate, through this indirect proof, the importance of the heating treatment in consolidating the mesoporous structure and obtain an extremely ordered hexagonal pores arrangement (Figure 24).
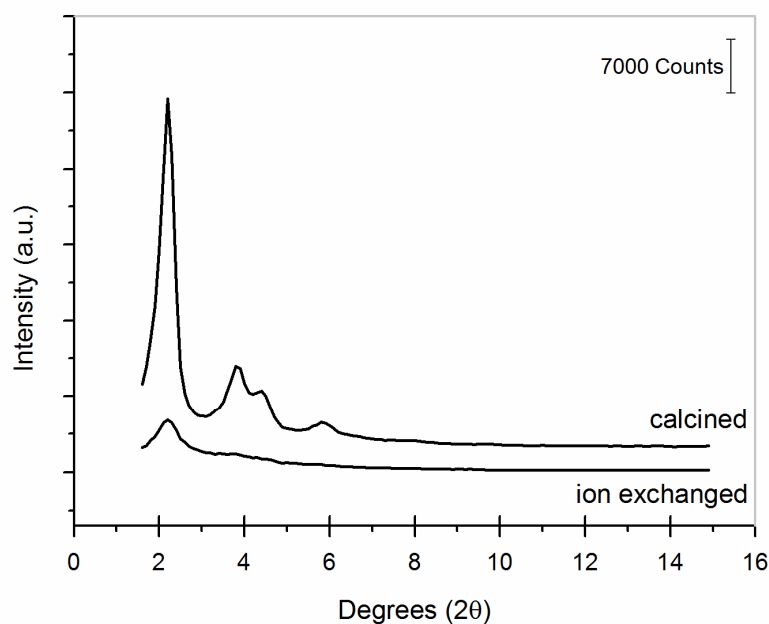
*Figure 24. XRPD comparison between conventional calcined and ion-exchanged PdCu containing samples.*

With the aim of investigating the metal particle sizes, transmission electronic microscope analysis were carried out over ion-exchanged catalysts, also in the $H_2$ reduced form.

EDS mapping of the sample obtained by ionic exchange evidenced a homogeneous dispersion of Cu in the MCM-41 framework, while Pd was segregated forming agglomerates of about 15 nm, due to their different electronic configuration and affinity to the MCM-41 tetrahedral structure (Figure 25). The particle sizes were similar for the observed PdCu particle formed in consequence to the reduction treatment. In fact, when the catalyst reduction was conducted, copper was reduced and aggregate to the outer palladium particles, and then, migrate to the particle core.
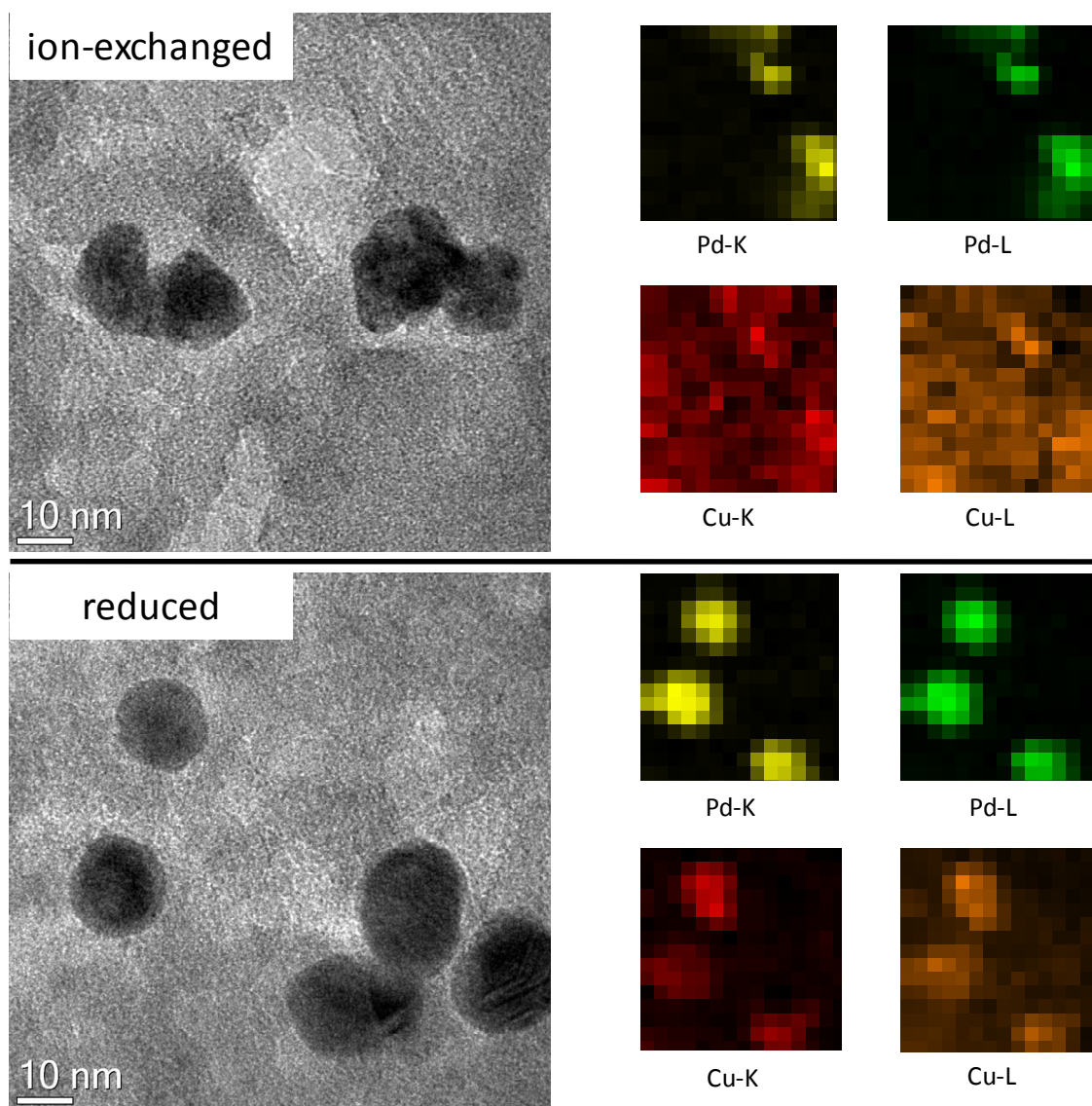
*Figure 25. HR-TEM and EDS mapping performed over ion-exchanged and calcined PdCu-MCM-41.*

In conclusion, the removal of the template by ionic exchange could be considered as a viable alternative to the conventional thermal treatment, allowing to obtain particles with lower sizes avoiding the sintering previously reported.

On the other hand, it must be remarked that the ionic exchange procedures, generate a large amount of waste ethanol, polluted by quaternary ammonium residue. The environmental problem of this procedure is the poor ammonium nitrate solubility in ethanol, which joint to the large amount of template to be removed, considerably increases the volume of ethanol to be used and then disposed of.

Because of this, so far the catalytic system prepared by ionic exchange has not been produced in sufficient quantity to be used in a catalytic test.

## 5.3 Catalytic performance in hydrodechlorination of the prepared Pd/Cu/MCM-41

Several heterogeneous Pd/Cu catalysts supported on mesoporous silicates were prepared as previously explained, thoroughly studied in the morphological properties and then on the hydrodechlorination of $CF_3OCFClCF_2Cl$ (ADM) in the presence of hydrogen. The hydrodechlorination activities of catalysts were investigated according to different silica source, different hydrothermal treatment, different methodology of deposition of metals and different metal content. The main purpose of this part of the survey was to correlate the best morphological properties with the catalytic performance on the hydrodechlorination of $CF_3OCFClCF_2Cl$ (ADM) in the presence of hydrogen.

In order to clearly discuss the catalytic performance, as in the previous chapter, all the possible products were reported on the following scheme [16].
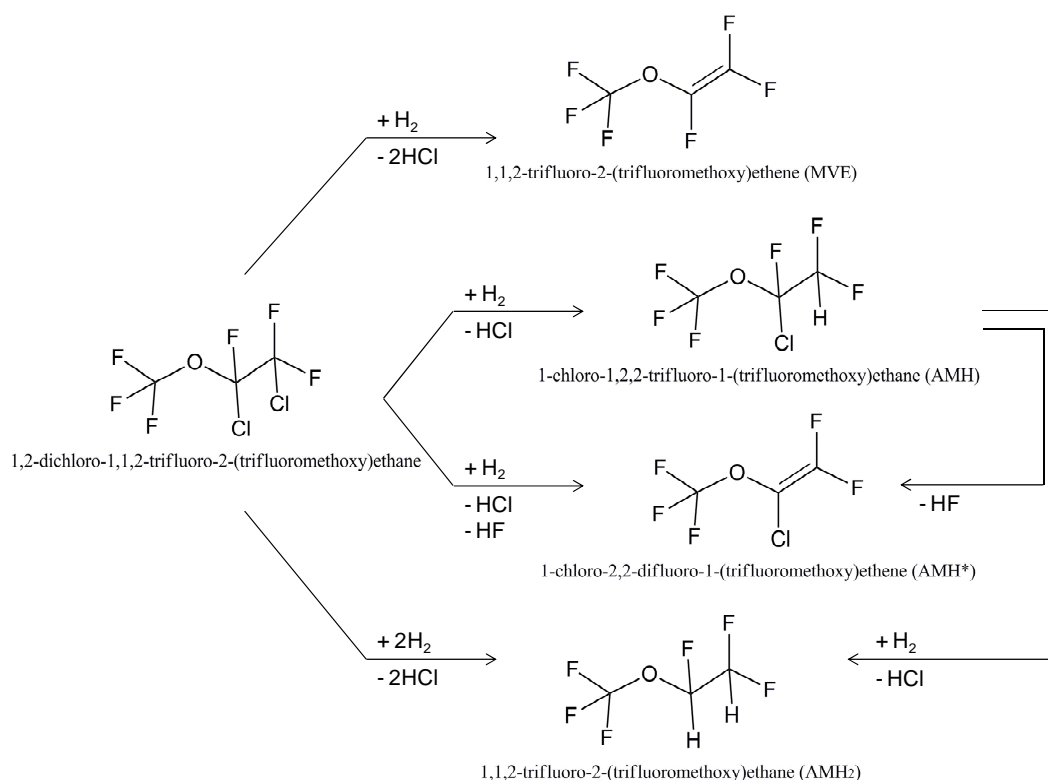


*Scheme 1. Reaction pathway proposed for the hydrodechlorination of $CF_3OCFClCF_2Cl$ [16].*

### 5.3.1 Effect of the preparation route on catalytic performance

With the aim to further investigate the effect on the catalytic activity of metal introduction by impregnation catalysts, prepared by incipient wetness impregnation both over sodium

silicate and TEOS obtained MCM-41, were tested in the hydrodechlorination reaction (Table 17).

| Sample | Description | Metal Content [%] | Precursors |
|--------|-------------|-------------------|------------|
| i-PdCu-SHT | IWI[a] on Sil-HT MCM-41, molar ratio 1:1 | 1,0 Pd - 0,6 Cu | $PdCl_2$ - $CuCl_2$ |
| i-PdCu-THT | IWI[a] on TEOS-HT MCM-41, molar ratio 1:1 | 1,0 Pd - 0,6 Cu | $PdCl_2$ - $CuCl_2$ |

[a] Incipient Wetness Impregnation

*Table 17. Materials and composition of the catalysts involved in the hydrodechlorination study.*

In Figure 26 are reported the obtained data, which highlight relevant difference between samples, both in terms of ADM conversion and MVE selectivity. The activity of the sodium silicate-based catalyst, i-PdCu-SHT, is largely affected by pore occlusion, in fact as explained above the mesoporous specific surface area is lacking and this condition adversely affects the performance. From a mechanistic point of view, these evidences, at least for the ADM conversion, could be explain in terms of reduced available area but also in terms of metallic particle agglomeration (lower specific surface area of metals).
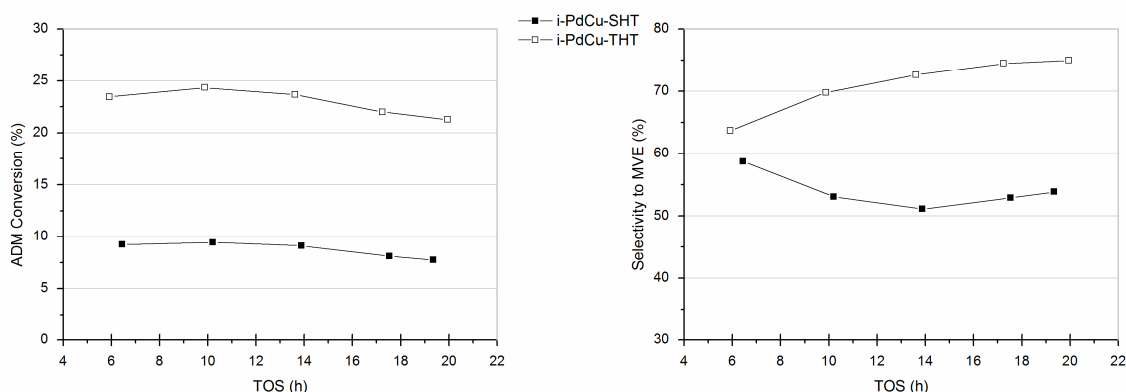


*Figure 26. Catalytic performance over impregnated sodium silicate and TEOS-based MCM-41. Reaction conditions: ADM = 16%v/v, contact time 10s, ADM/$H_2$ molar ratio = 1, reaction temperature 250°C.*

Taking into account all the previous consideration, on Figure 27 are reported the by-products distribution for i-PdCu-SHT (on the left side) and i-PdCu-THT (on the right side) with the aim of investigating the observed difference in terms of selectivity to the target product, MVE. Both the catalysts show as main by-product HMVE ($CF_3OCHF=CF_2$) which reach, in the case of i-PdCu-SHT sample, particularly high values of about the 25%. Following as close as possible, the criteria developed observing the activated-carbon supported catalysts, at the beginning of the reaction, due to the reduction treatment, the hydrogen coverage of the catalysts surface is high. In this situation, the selectivity to MVE is lowered by a favorite formation of hydrogenated products like AMH ($CF_3OCFHCF_2Cl$

or $CF_3OCFClCF_2H$) and the de-fluorinated product AMH* ($CF_3OCCl=CF_2$) in which case the formation is favored by the presence of hydrogen that plays a role in the intermediate desorption. In particular, observing these catalytic trials on Figure 27, is possible to expose some arguments.

- the AMH* product formation is quite small, indicating a relatively weak interaction between active phase and organic substrate (ADM), unable to induce a C-F cleavage.

- the AMH products formation highlights different behavior with respect to the time on stream (TOS), revealing a decreased formation with TOS in the case of i-PdCu-THT sample, probably due to a gradual decrease of the hydrogen coverage for competitive adsorption of halogens.

- the by-products, summarized and indicated as "others", contain chloro-trifluoroethylene (CTFE) and halogenated $C_2$ species, all derived from cracking reaction.
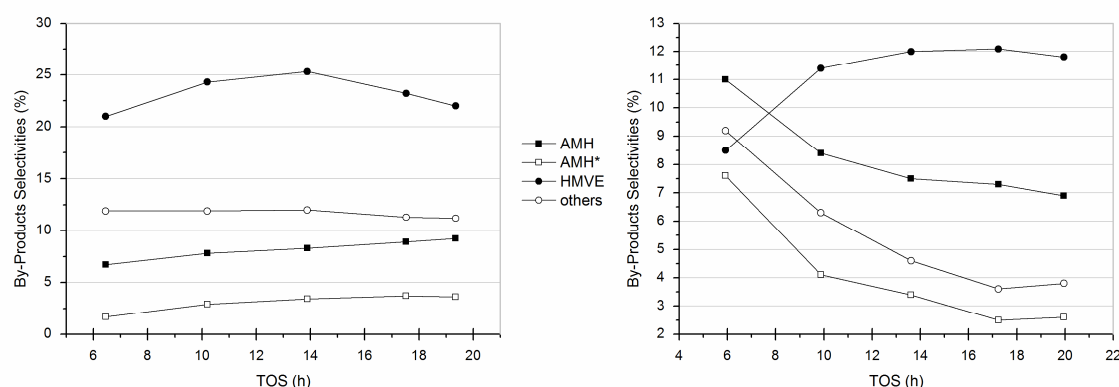


*Figure 27. By-products formation over impregnated sodium silicate (on the left side) and TEOS-based MCM-41(on the right side). Reaction conditions: ADM = 16%v/v, contact time 10s, ADM/$H_2$ molar ratio = 1, reaction temperature 250°C.*

Investigating further the effects on the catalytic performance, a comparison between sodium silicate- based samples, treated with different hydrothermal ageing, is proposed. These samples, were loaded with Pd and Cu following the developed method called "direct introduction", during the silica framework formation and thus, reduced in flowing $H_2$ to obtain metallic active phase (Table 18).

| Sample | Description | Metal Content [%] | Precursors |
|---|---|---|---|
| d-PdCu-SHT | Direct Introduction, Sil-based, HT | 1,0 Pd - 0,6 Cu | $PdCl_2$ - $CuCl_2$ |
| d-PdCu-SMW | Direct Introduction, Sil-based, MW | 1,0 Pd - 0,6 Cu | $PdCl_2$ - $CuCl_2$ |

*Table 18. Materials and composition of the catalysts involved in the hydrodechlorination study.*

When d-PdCu-SHT and d-PdCu-SMW samples were used on the hydrodechlorination of ADM, the observed conversion was very low, ranging between 1.5 and 3.0%. Because of this, all the arguments, in terms of selectivity, could be affected by a significant uncertainty, due to the small amount of products considered. However, all the samples yield the expected as main product, with values of about 60-65%, showing a gradual increase in formation with time on stream (Figure 28).
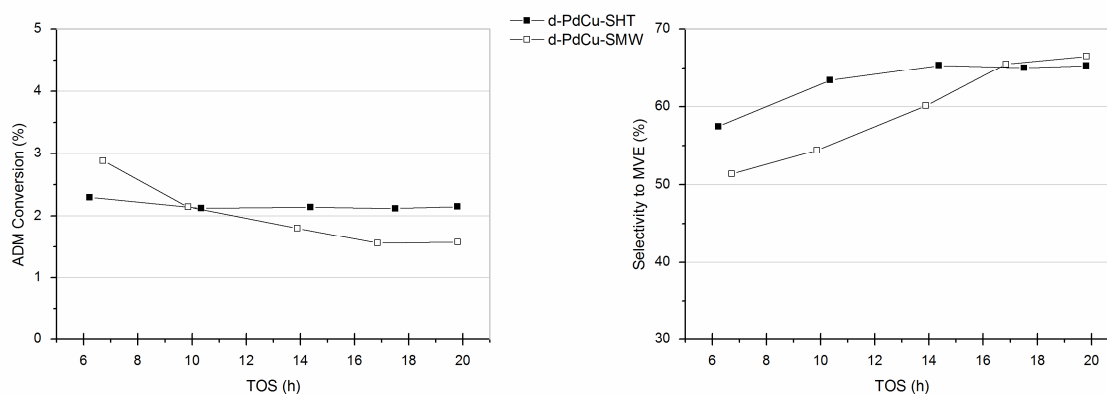


*Figure 28. Catalytic performance over sodium silicate-based MCM-41, prepared by "direct introduction" method and treated with microwave heating. Reaction conditions: ADM = 16%v/v, contact time 10s, ADM/H$_2$ molar ratio = 1, reaction temperature 250°C.*

Taking into account the previous opinion about the uncertainly, two objective consideration are proposed. The product labeled HMVE, considered as a consecutive de-halogenation of MVE or AMH\*, is formed in relevant amount and decrease with time on stream. Obviously, as a consecutive formation, this reaction strongly depends on the first step, but also depends on the amount of activated hydrogen over the catalyst surface, in fact explaining the decrease with time on stream.

From a strict point of view, a consecutive product could be characterized by an initial formation close to zero, and a maximum value place after the maximum formation of the primary product which is transformed into the secondary (consecutive) when its amount over the catalyst surface is relevant. In this case the possible reaction pathway suggest that the HMVE is formed due to an accumulation (or a non-desorption) of the MVE intermediate on the surface of the catalyst, and the absence of an MVE production maximum is probably due to the effect of decreased hydrogen coverage on the secondary reaction feasibility (Scheme 2).
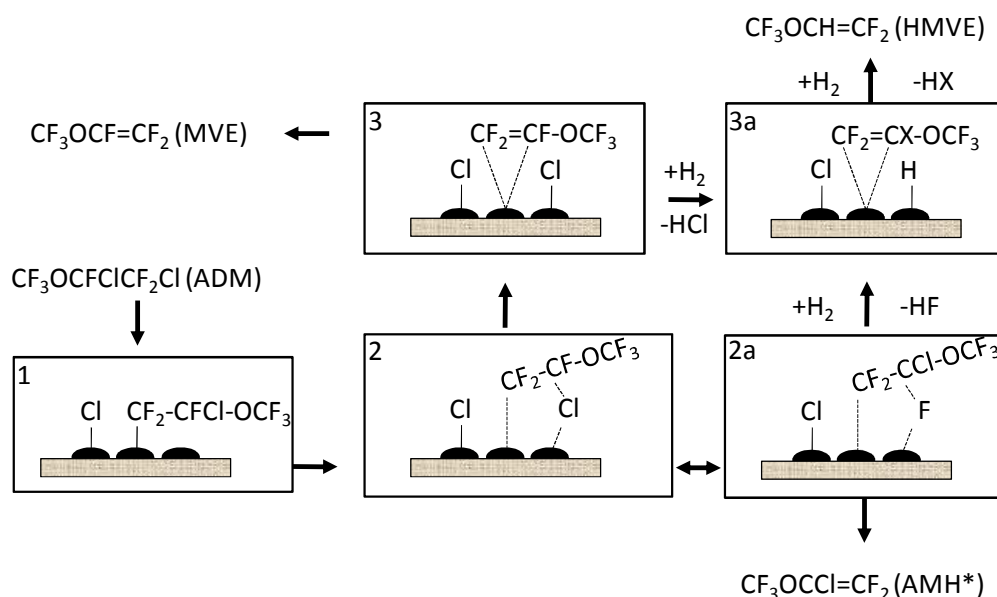
*Scheme 2. Reaction pathway proposed for the hydrodechlorination of CF₃OCFClCF₂Cl.*

On the other hand it must be highlighted the increase of cracking products (others) with the time on stream (Figure 29). In order to give an explanation about these observations, could be proposed, that the interaction between active phase and substrate seems to be not so strong, avoiding phenomena of C-F cleavage, even if fairly stable to allow a consecutive, and several cracking reaction. These last one (cracking) could be favorite to a general surface acidity, but in this case most probably from structural framework defects caused by metal insertion, and from Lewis acids (as $PdCl_2$).
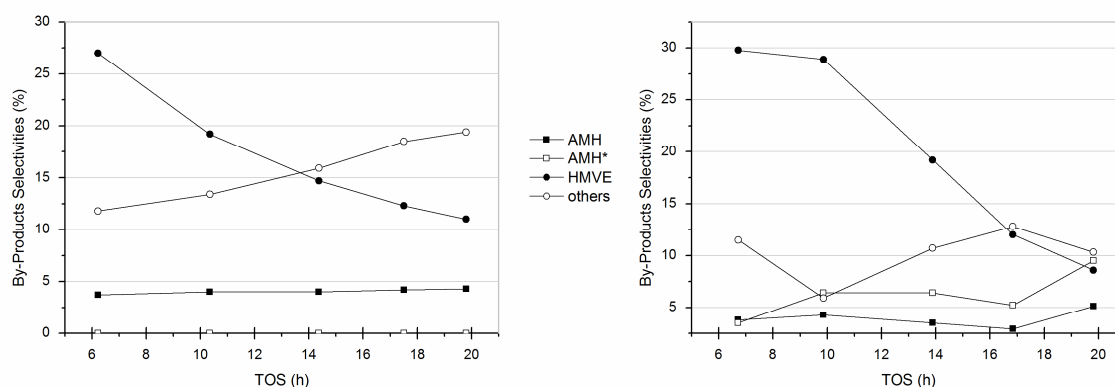


*Figure 29. By-products formation over impregnated sodium silicate-based MCM-41 treated by conventional (on the left side) and microwave heating (on the right side). Reaction conditions: ADM = 16%v/v, contact time 10s, ADM/H₂ molar ratio = 1, reaction temperature 250°C.*

In order to investigate possible variation in the active phase, between the impregnation method and the direct introduction method, several reduction in programmed temperature and HR-TEM were performed.

Observing the obtained data, from programmed reduction analysis (TPR) shown on Figure 30, a different active phase formation appears clearly, showing reduction peaks different in the $T_{max}$ of the profile. Taking into account the impregnated samples, the catalyst based on THT support, has a second peak at a higher temperature, attributable to a copper-rich phase, while the sample based on SHT support, presents reductions generally more favored (lower temperature) that may indicate a greater propensity in activate hydrogen. In fact, the reduction of the copper, would occur at much higher temperature, between 250 and 350°C, while the presence of palladium makes the system more reducible by increasing the availability of activated hydrogen (spillover). This evidence is in agreement with the catalytic performance observed, where the i-PdCu-SHT has been revealed as less selective to MVE due to a particularly high formation of HMVE (Figures 26 and 27).

Regarding the "direct introduction" samples, the reduction profiles have evidenced higher temperature with respect to the impregnated sample and much more symmetry, whereby the distribution of phase seems to be more homogeneous, despite of a small shoulder at about 160°C for the silicate-based sample. This observation is in agreement with the reported low conversion value of ADM (Figure 28). Moreover, considering the higher reduction temperature as an indicator of the interaction strength between active phase and supports, this evidence could be considered as an explanation of higher formation of cracking products on Figure 29, because the more the metal are inserted in the silica framework, the more defects are produced in the supports structure, leading to a higher surface acidity, and thus, a higher occurring of cracking reactions [17].
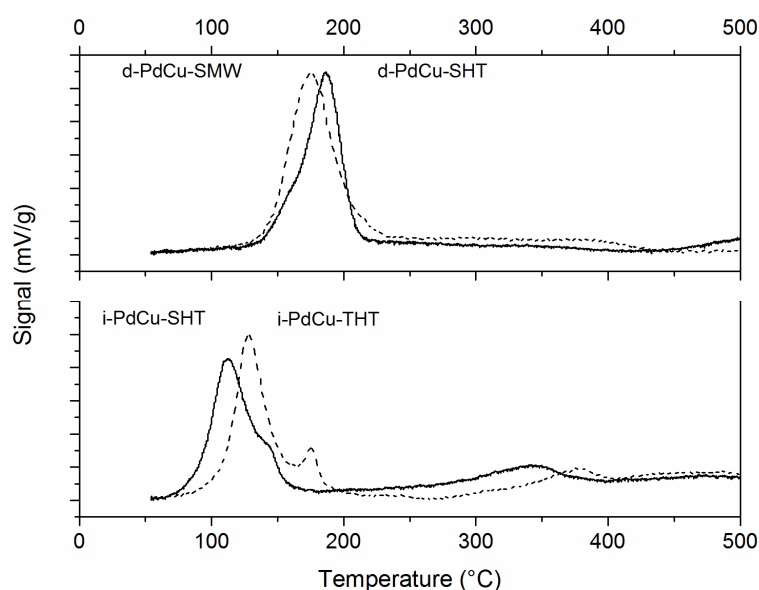


Figure 30. $H_2$-TPR investigation over impregnated and incorporated PdCu active phase.

5. Mesoporous silicate supported catalysts

All the reported programmed reduction were carried out over PdCu containing catalysts, where is not possible to determine the mechanism of reduction, and then, the particle size corresponding to the different reduction peaks in the profile. Thus, in order to obtain information about the particle size distribution, several studies by electronic microscope TEM were carried out. The obtained results highlight a relevant difference in particle size distribution, as summarized on Figure 31. Because of these evidences, is possible to attribute the observed difference in reduction temperature profile, also to different particles diameter, and different composition (evidenced by EDS elemental mapping), which can also explain the different catalytic properties observed above.
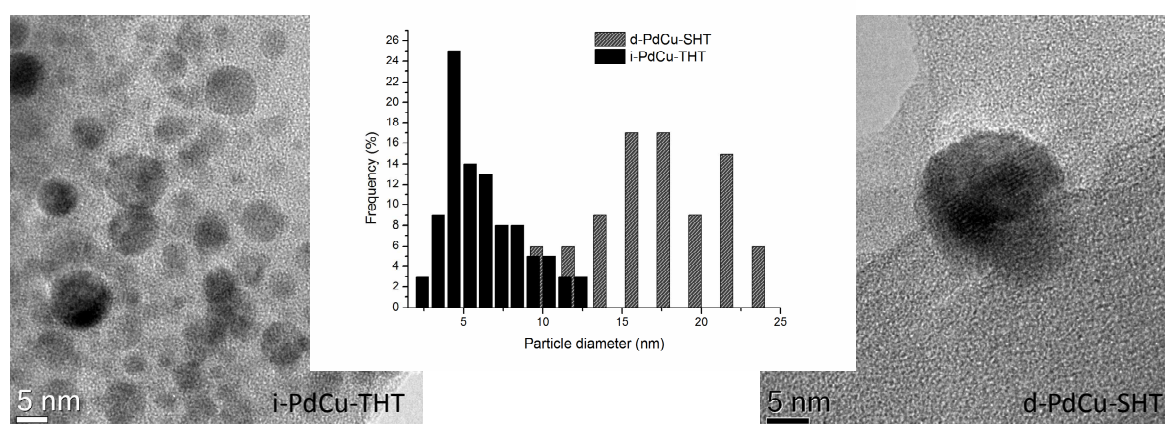


*Figure 31. HR-TEM images and particle sizes distribution for impregnated and incorporated PdCu active phases.*

The reported results, that evidence the presence of particles with different composition are totally in agreement with the observed XRPD, characterized by the presence of different mixed metal phases for the sample prepared by direct introduction of metal precursors. In fact, in the case of impregnated sample, there were no diffraction reflection due to the particularly small particle dimension.

## 5.3.2 Effect of the total metal loading on catalytic performance

With the aim of concluding this study and the catalyst optimization, considering the poor performance in ADM conversion of Pd/Cu-MCM-41 samples prepared by direct introduction of metals during the synthesis, a series of catalysts with different metal loading were prepared (Table 19).

| Sample | Description | Metal Content [%] | Precursors |
|---|---|---|---|
| 1 (PdCu) | Direct Introduction, Sil-based, MW | 1,0 Pd - 0,6 Cu | $PdCl_2$ - $CuCl_2$ |
| 1,5 (PdCu) | Direct Introduction, Sil-based, MW | 1,5 Pd - 0,9 Cu | $PdCl_2$ - $CuCl_2$ |
| 2 (PdCu) | Direct Introduction, Sil-based, MW | 2,0 Pd - 1,2 Cu | $PdCl_2$ - $CuCl_2$ |
| 2,5 (PdCu) | Direct Introduction, Sil-based, MW | 2,5 Pd - 1,5 Cu | $PdCl_2$ - $CuCl_2$ |

*Table 19. Materials and composition of the catalysts involved in the hydrodechlorination study.*

As expected, the catalytic performance in terms of ADM conversion were strongly dependant from the amount of metals loaded in the catalyst (Figure 32). In fact, the catalyst with the higher metal content has the higher ADM conversion, but in terms of selectivity to MVE none clear trend is in the obtained values (Figure 33). Furthermore, all the prepared catalysts display significant deactivation with time on stream, simultaneously to an increase in selectivity to MVE.

Considering the observed values of ADM conversion, it is possible to hypothesize that the hydrpdechlorination reaction, causes by itself catalyst degradation or modification in the active phase, leading to a decreased value of conversion. On the other hand, the simultaneous increase in selectivity to MVE, may indicate a focusing of the deactivation phenomena onto active sites different to those responsible for MVE production, favoring the formation of MVE as main product.
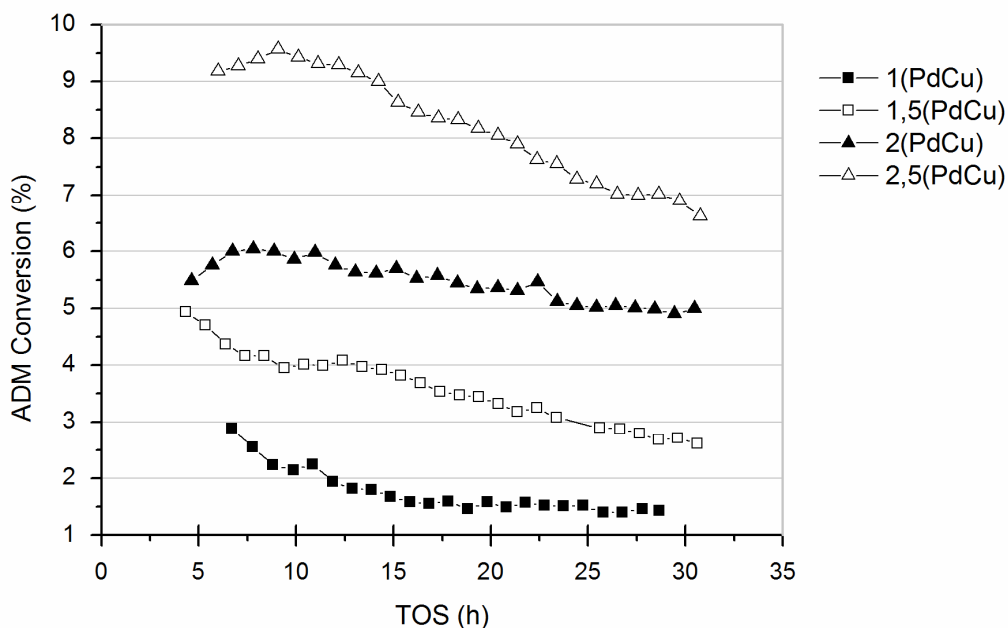


*Figure 32. Catalytic performance in terms of $CF_3OCFClCF_2Cl$ conversion over sodium silicate-based MCM-41 prepared with different metal content. Reaction conditions: ADM = 16%v/v, contact time 10s, ADM/$H_2$ molar ratio = 1, reaction temperature 250°C.*
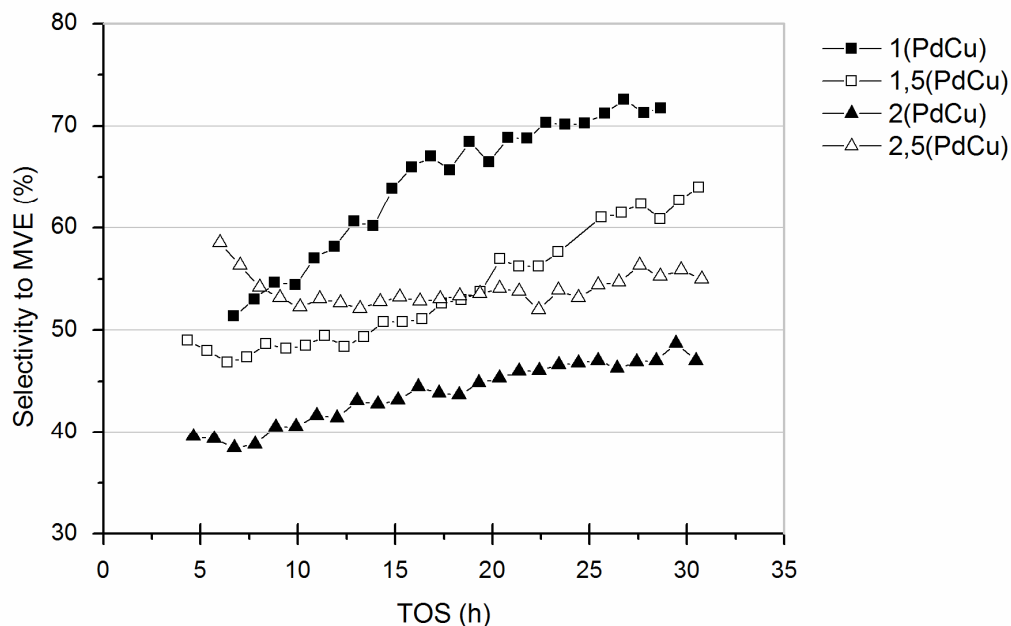
*Figure 33. Catalytic performance in terms of CF₃OCF=CF₂ selectivity over sodium silicate-based MCM-41 prepared with different metal content. Reaction conditions: ADM = 16%v/v, contact time 10s, ADM/H₂ molar ratio = 1, reaction temperature 250°C.*

In order to understand the reason of the increased selectivity to MVE, the values of selectivity relative to the main by-product (CF₃OCH=CF₂, HMVE) are reported on Figure 34. Indeed, this comparison indicate a quite similar trend respect to MVE selectivity (but in a reversed form). The catalyst with the lower metal content, 1(PdCu) shows the higher value of selectivity to MVE and consequently the lower value in HMVE formation. Increasing the metal content, increases HMVE formation leading to lower MVE selectivity. Thus the formation of CF₃OCH=CF₂ molecule could be correlate with the segregated metal presence, in particular with Pd segregated species that could increase the quantity of activated hydrogen able to be inserted in the product.
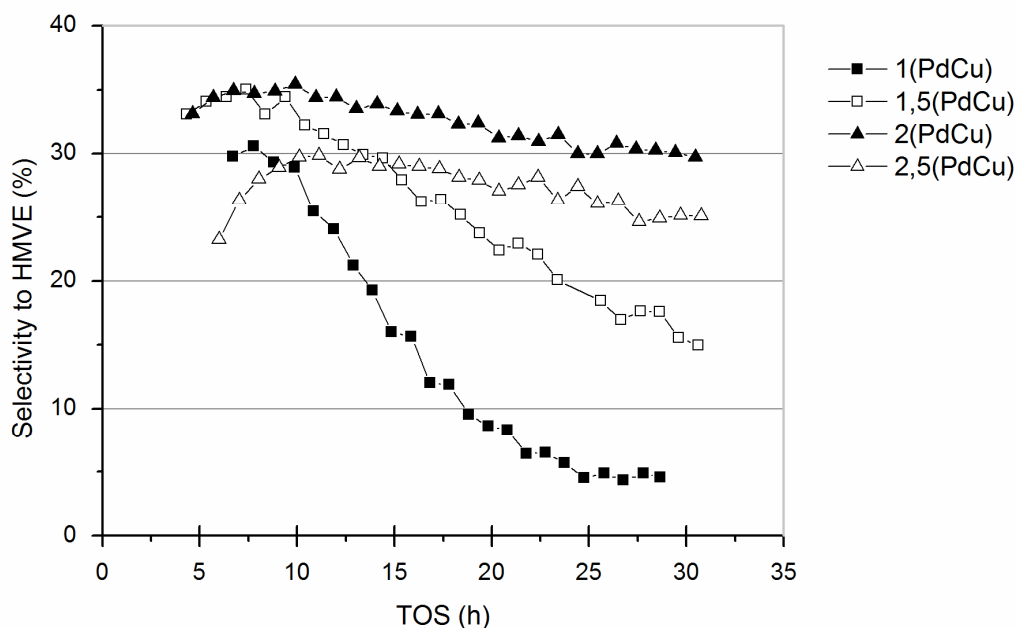
*Figure 34.Observed formation for CF$_3$OCH=CF$_2$ by product.*

At the same way, one more time, it is observed that the hydrogen coverage of catalysts surface and its decrease during the reaction is directly correlated with catalytic performance. Thus, focusing the attention to catalysts design, it is important to underline that not only the composition of active phase is important, but also the catalyst capability of maintaining the optimal value of activated hydrogen over the surface of catalysts versus the competitive absorption of chlorine and fluorine atoms.

On the other hand, it must be remarked that these observed catalytic performances are not in agreement with the suggested (by XRPD) major interaction between Pd and Cu, increasing the total metal content. In fact, a greater interaction between Cu and Pd should decrease the hydrogenation properties of the catalytic system, increasing the selectivity to MVE. Obviously, the studies must be continued in order to identify the correct explanations for the observed catalytic performance.

Another key factor for the catalytic stability has been found carrying out some x-ray diffraction analysis on used catalysts. The obtained diffraction pattern, reported in Figure 35, clearly highlights the great increase in the Cu-rich reflection intensity, probably due to an extended sintering phenomena which could be considered responsible for the catalytic performance variation with time on stream. Furthermore, it appears evident the effect of increased metal content in the importance of the sintering phenomena.

## 5. Mesoporous silicate supported catalysts

Taking into account all previous considerations, it must be remarked that none shift toward lower degrees was observed for the Cu-rich reflection, for both catalysts. On the contrary, Pd-rich phases appear to be subject to redispersion phenomena [18] leading to a partial removal of the Cu atoms from the Pd lattice.
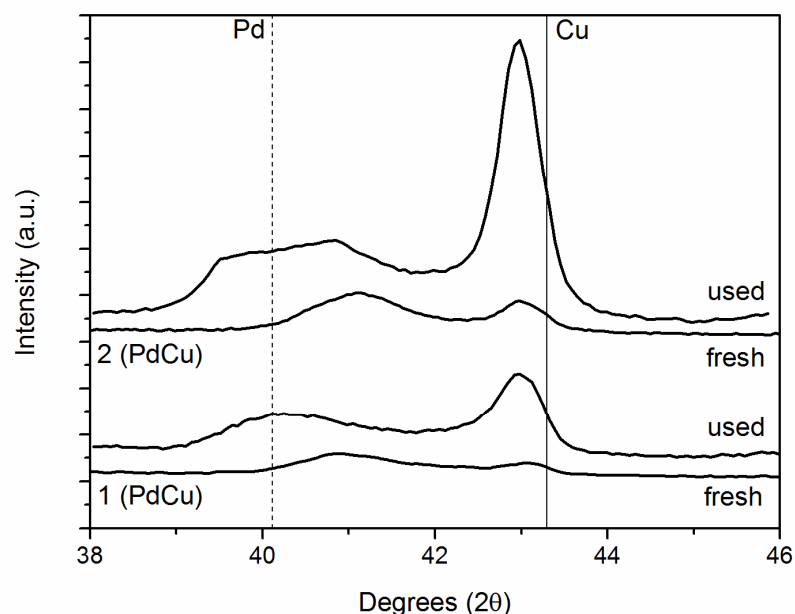


*Figure 35. XRPD investigation over fresh and spent catalysts.*

The study was continued with another series of catalysts, prepared with different metal content, by direct introduction of metal during Teos-based MCM-41 framework formation (Table 20).

| Sample | Description | Metal Content [%] | Precursors |
|---|---|---|---|
| 1 (PdCu)T | Direct Introduction, Teos-based, MW | 1,0 Pd - 0,6 Cu | $PdCl_2$ - $CuCl_2$ |
| 1,5 (PdCu)T | Direct Introduction, Teos-based, MW | 1,5 Pd - 0,9 Cu | $PdCl_2$ - $CuCl_2$ |
| 2 (PdCu)T | Direct Introduction, Teos-based, MW | 2,0 Pd - 1,2 Cu | $PdCl_2$ - $CuCl_2$ |
| 2,5 (PdCu)T | Direct Introduction, Teos-based, MW | 2,5 Pd - 1,5 Cu | $PdCl_2$ - $CuCl_2$ |

*Table 20. Materials and composition of the catalysts involved in the hydrodechlorination study.*

The use of this method of synthesis leads to catalyst with performance in terms of conversion and selectivity to MVE difficult to be explained. In fact, differently from the previously reported silicate-based series, none clear trend in ADM conversion with the total metal content was observed (Figure 36).
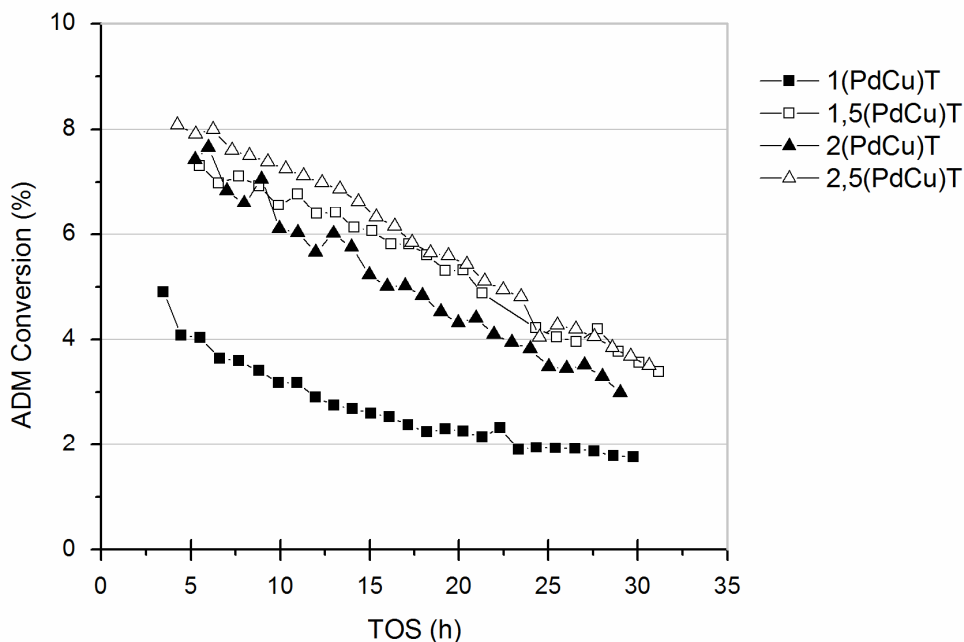
*Figure 36. Catalytic performance in terms of CF$_3$OCFClCF$_2$Cl conversion over TEOS-based MCM-41 prepared with different metal content. Reaction conditions: ADM = 16%v/v, contact time 10s, ADM/H$_2$ molar ratio = 1, reaction temperature 250°C.*

Focusing the attention on the catalytic performance in terms of selectivity to MVE, differently respect to the silicate-based samples, indicated that the catalyst with the higher metal content has the higher selectivity to MVE (Figure 37).

Furthermore, it must be highlight that all the samples, except the lower metal content catalyst showed an increase in the selectivity to MVE during the reaction. Using these samples the selectivity to the expected product was lowered by an increased formation of the Cl/H mono-substituted product, labeled AMH (CF$_3$OCFClCF$_2$H or CF$_3$OCFHCF$_2$Cl) Nevertheless, also in this case, in agreement with the previously reported data, the main by-product, with the greater effect in lowering the selectivity to MVE, is HMVE.

With the goal of observe the main by-product trends, a complete comparison is shown on Figure 38. Obviously, regarding this series of samples, another breaking point is originated in the obtained values of HMVE selectivity, which appears divided in two distinct trend, not related with the metal content, increasing the attention into the difficult synthesis reproducibility.

## 5. Mesoporous silicate supported catalysts
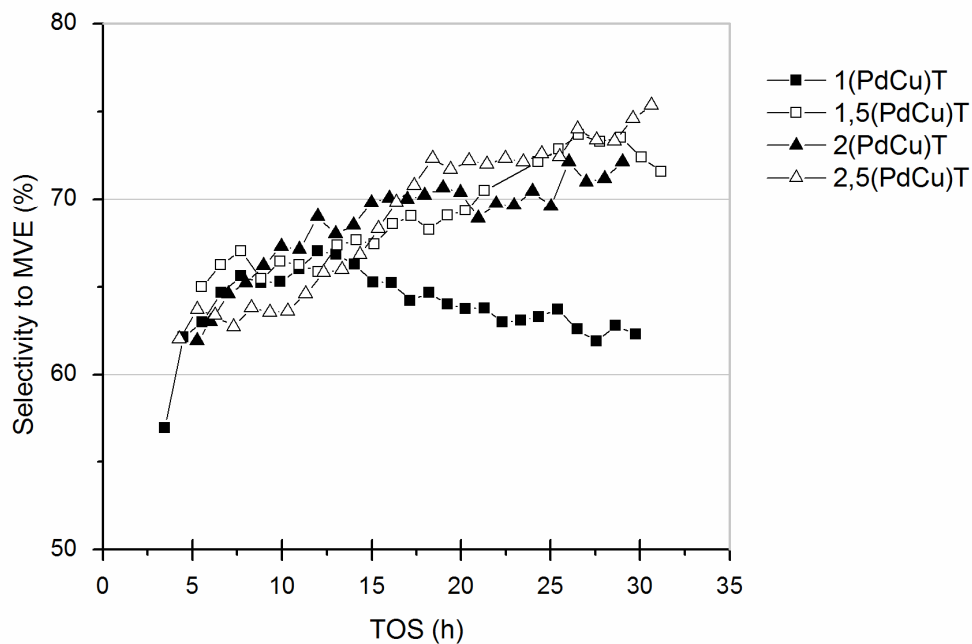


*Figure 37. Catalytic performance in terms of CF<sub>3</sub>OCF=CF<sub>2</sub> selectivity over TEOS-based MCM-41 prepared with different metal content. Reaction conditions: ADM = 16%v/v, contact time 10s, ADM/H<sub>2</sub> molar ratio = 1, reaction temperature 250°C.*
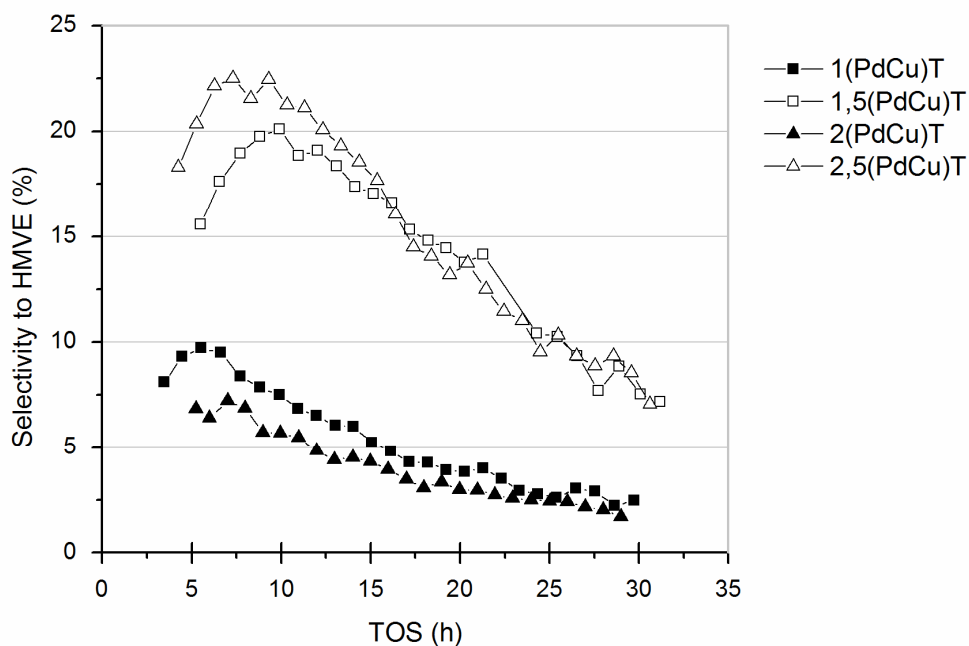


*Figure 38. Observed formation for CF<sub>3</sub>OCH=CF<sub>2</sub> by product.*

The previously reported difference in XRPD analysis, revealing in some sample a possible Cu-rich CuPd alloys, are in agreement with the observed "disordered" catalytic performance reported by this TEOS-based materials.

114

It seems from the above that there is the need for improving the preparation methods in order to ensure effective and reproducible incorporation of the metallic active species in the support.

## 5.4 Conclusion

In conclusion, MCM-41 mesoporous silicate were widely studied in order to investigate the relationship between each preparation steps and the morphological properties of the final material, afterwards used as support for the preparation of the metal containing catalysts. Furthermore, observing that the deposition of Pd and Cu by incipient wet impregnation has caused pores occlusion, an alternative synthetic methods were developed with the aim of introducing the metal precursors during the MCM-41 framework formation. The so called "direct introduction" catalysts prepared, both by the conventional and microwave treatment, keep the structural and textural properties of bare supports, but larger bimetallic particles are formed during template removal, with respect to the impregnated catalysts, also reporting different particle compositions.

PdCu-based catalysts, supported over MCM41, were studied on the dechlorination of $CF_3OCFClCF_2Cl$ to $CF_3OCF=CF_2$ in the presence of hydrogen, where all studied catalysts yielded the target product as main product, and the MCM-41 support obtained from TEOS leads to a more efficient catalyst, nevertheless with lower morphological properties. The metallic particle size and composition, strongly dependant from the synthesis conditions, influence the activity in the hydrodechlorination of $CF_3OCFClCF_2Cl$ to $CF_3OCF=CF_2$ and finally concluding,  it must be considered more important for the catalytic purpose, with respect to the structural and textural properties of MCM-41-based materials.

**References**

[1] J.S. Beck, J.C. Vartuli, W.J. Roth, M.E. Leonowicz, C.T. Kresge, K.D. Schmitt, C.T-W. Chu, D.H. Olson, E.W. Sheppard, S.B. McCullen, J.B. Higgins and J.L. Schlenker, *J. Am. Chem. Soc.* **114** (1992) 10834-10843.

[2] K. Cassiers, T. Linssen, M. Mathieu, M. Benjelloun, K. Schrijnemakers, P. Van Der Voort, P. Cool and E.F. Vansant, *Chem. Mater.* **14** (2002) 2317-2324.

[3] J.Y. Ying, C.P. Mehnert and M.S. Wong, *Angew. Chem. Int. Ed.* **38** (1999) 56-77.

[4] X.S. Zhao, G.Q.(Max) Lu, G.J. Millar, *Ind. Eng. Chem. Res.* **35** (1996) 2075-2090.

[5] F. Kleitz, W. Schmidt, F. Schüth, *Micropor. Mesopor. Materials* **65** (2003) 1-29.

5. Mesoporous silicate supported catalysts

[6] I. García-Mateos, M.M. Velázquez and L.J. Rodríguez, *Langmuir* **6** (1990) 1078-1083.

[7] K. Chakarova, G. Petrova, M. Dimitrov, L. Dimitrov, G. Vayssilov, T. Tsoncheva, K. Hadjiivanov, *Appl. Catal. B: Env*. **106** (2011) 186– 194.

[8] C-F Cheng, D. H. Park and J. Klinowski, *J. Chem. Soc., Faraday Trans.* **93** (1997) 193-197.

[9] M. Kruk, M. Jaroniec, Y. Sakamoto, O. Terasaki, R, Ryoo, C.H. Ko, *J. Phys. Chem. B* **104** (2000) 292-301.

[10] R. Ravikovitch, S.C.O. Domhnail, A.V. Neimark, F. Schuth and K.K. Unger, *Langmuir* **11** (1995) 4765-4772.

[11] M. Thommes, *CHemie Ingenieur Technik* **82** (2010) 1059-1073.

[12] A.N. Ergun, Z.O. Kocabas, M. Baysal, A. Yurum, and Y.Yurum, *Chem. Eng. Comm.* **200** (2013) 1057-1070.

[13] N. Lang and A. Tuel, *Chem. Mater.* **16** (2004) 1961-1966.

[14] N.N. Kariuki, X. Wang, J.R. Mawdsley, M.S. Ferrandon, S.G. Niyogi, J.T. Vaughey, D.J. Myers, *Chem. Mater.* **22** (2010) 4144-4152.

[15] N. Pomerantz, Y.H. Ma, E.A. Payzant, *AlChE* **56** (2010) 3062-3073.

[16] M. Gregori, G. Fornasari, G. Marchionni, V. Tortelli, S. Millefanti, S. Albonetti, *Appl. Catal. A: General* **470** (2014) 123-131.

[17] C.M. Chanquía, E.L. Winkler, M.T. Causa, G.A. Eimer, *J. Phys. Chem. C* **116** (2012) 5376-5382.

[18] K. Foger, D. Hay, H. Jaeger, *J. Catal.* **96** (1985) 170-181.

# Chapter 6

## 6   Conclusion

In this work, the hydrodechlorination of $CF_3OCFClCF_2Cl$ to $CF_3OCF=CF_2$ was studied, focusing our interest basically on catalyst design. The first part of the research, was mainly focused on evaluating the different catalytic performance of various active phases, mono- and bi- metallic, and allowed to evidence the key factors that the catalyst must possess to be active and stable. The second part of this work was mainly focused in optimizing the MCM-41 synthesis, also incorporating the active phase during the framework synthesis, and allowed to observe correlation between the metal particles shape, composition and size, and the catalytic performance in the hydrodechlorination of $CF_3OCFClCF_2Cl$ to $CF_3OCF=CF_2$.

The evaluation of various active phases was performed over activated carbon supported catalysts, which yielded as main product the expected perfluoromethylvinylether. The best performing in terms of selectivity to expected product resulted to be the Ru-based catalysts; however, factors including hydrogen coverage of the catalyst surface, stability and deactivation of the catalyst are to be considered in the catalyst's choice. Indeed, Ru-based catalysts showed poor stability regardless of the content of active phase present over the support, indicating that the deposition of heavy halogenated compounds could block the active sites.

Contrarily, Pd-based catalysts showed high stability in terms of $CF_3OCFClCF_2Cl$ conversion, and seem not to be affected by desorption problems, and as a consequence, by active sites blocking. The exhibited performance for the Pd-based catalyst, in terms of selectivity to $CF_3OCF=CF_2$, was lowered by the high Pd hydrogenation properties, which mainly lead to hydrogenated products. On the other hand, carrying out a series of catalytic trials over Pd/Ru and Pd/IB elements, the long-term selectivity and stability of Pd/Ru and Pd/Cu bimetallic catalysts were observed. The observed catalytic properties suggests that the introduction of a second metal induce a modification in the interaction between substrates and Pd-based active phase, lowering its hydrogenation properties. Pd/Ru and Pd/Cu bimetallic catalysts could be employed in the gas-phase hydrodechlorination of $CF_3OCFClCF_2Cl$ to $CF_3OCF=CF_2$ with high selectivity and high conversion.

# 6. Conclusion

During the second part of this work, a series of bimetallic mesostructured Pd/Cu MCM-41 catalysts were obtained by incipient wetness impregnation and direct hydrothermal synthesis using different silica sources, different metal loadings and performing various synthetic procedures.

Obtained data, in the hydrodechlorination of $CF_3OCFClCF_2Cl$ to $CF_3OCF=CF_2$, indicated that the use of microwave-hydrothermal method leads to shorter synthesis times and the MCM-41 supports prepared with this option showed textural properties, long-range order and distribution of the pore sizes, similar or even better to those prepared by the conventional method. The deposition of Pd and Cu by incipient wet impregnation blocks the pores, a behavior more remarkable when the support is obtained from silicates. On the contrary, the "direct-introduction" preparation, both by the conventional and microwave treatment, keeps the structural and textural properties of bare supports, but larger bimetallic particles are formed during template removal performed by calcination at high temperature (540°C). The template removal performed by ion-exchange has been performed, allowing the formation of smaller metal particles, but negatively affecting the MCM-41 structure. The differences in the metallic particle size and environment of metallic species determine the activity in the hydrodechlorination of $CF_3OCFClCF_2Cl$ to $CF_3OCF=CF_2$. In particular, so far the incipient wetness impregnation route using the MCM-41 support obtained from TEOS leads to a more efficient catalyst.

Nevertheless further studies are required to optimize catalysts thermal treatments, in order to improve the reproducibility of the synthesized materials, the distribution of metal particle sizes and their composition.

# Acknowledgement